

POLITECNICO DI TORINO

CORSO DI LAUREA MAGISTRALE IN INGEGNERIA ENERGETICA E NUCLEARE
Innovazione nella Produzione di Energia

TESI DI LAUREA MAGISTRALE



**Heat Pump system control strategies:
comparison of two system layouts and evaluation
of the energy saving potential from
human behaviour and weather information**

Relatori

Prof. Marco Carlo MASOERO

Prof. Hatef MADANI

Correlatore

Dott. Ing. Davide ROLANDO

Candidato

Marius SHTEMBARI

Marius Shtembari: *Heat Pump system control strategies: comparison of two system layouts and evaluation of the energy saving potential from human behaviour and weather information* | Tesi di Laurea Magistrale in Ingegneria Energetica e Nucleare, Politecnico di Torino.

© Copyright October 2018.

Politecnico di Torino:

www.polito.it

Dipartimento ENERGIA:

www.polito.it/ricerca/dipartimenti/denerg/

to my brother

Acknowledgements

I would like to thank my supervisor Prof. Hatef Madani and my co-supervisor Dr. Davide Rolando of the KTH Royal Institute of Technology in Stockholm, for their continuous support during the work of my master thesis and for having allowed me the opportunity to carry it out in such a stimulating environment as the Department of Energy Technology.

I would also like to thank my Italian supervisor Prof. Marco Carlo Masoero for his constant guide throughout the thesis project and for providing me with all the essential computer equipment to accomplish my work.

The present study is related to the project “Smart Control Strategies for Heat Pump Systems” within the EffSys Expand program, co-funded by the Swedish Energy Agency together with several industrial project partners. I would like to thank Danfoss Heat Pumps AB, IVT-Bosch, Nibe, Bengt Dahlgren, Nowab AB, ETM Kylteknik AB, Hesh Automation and ElectroTest AB for the support to this project.

Turin, October 2018

M. S.

Abstract

The present work is focused on the implementation of smart control strategies applied to a Ground-Source Heat Pump system (GSHP), for Space Heating (SH) and Domestic Hot Water (DHW) needs, in a Swedish single-family house. In particular, the developed rule-based control logics, using both a predictive and non-predictive approach, take into account human behaviour and weather information, such as the profiles of the DHW consumption and of the internal heat gains, and the solar radiation data.

The study is carried out by means of TRNSYS[®] numerical simulations. An existing system model (Layout A), developed by Braida and Tomasetig from Polytechnic University of Milan [1], which includes a typical Swedish building, a single-speed GSHP unit, an auxiliary heater and a stratified storage tank, has been adapted to a different system layout (Layout B). The main difference is represented by the direct connection between the heating generation and distribution loops, since the storage tank is used for DHW purposes only. A comparison of the two layouts reveals an energy consumption reduction and an increased thermal comfort for the DHW, in the latter configuration, but with a lower indoor temperature stability.

In order to evaluate the performance of the developed control logics applied to Layout B, a basic degree-minute on/off controller has been adopted as a benchmark. Considering the DHW consumption over the summer season, a potential energy saving is achievable thanks to the improved control logic. With reference to the Swedish heating season, the thermal comfort enhancement, deriving from the use of the internal gains profile and already shown in [1], is more consistent when a non-predictive approach is adopted. The highest potential in terms of energy saving and thermal comfort improvement is given by the simultaneous implementation of all the developed control logics, including the exploitation of the solar radiation data.

Keywords: heat pump system control, HVAC predictive rule-based control, weather forecast, occupancy behaviour, internal gains

Sommario

Il presente lavoro è incentrato sull'implementazione di strategie di controllo innovative applicate a un sistema basato su una pompa di calore a risorsa geotermica, per il riscaldamento di ambienti e la produzione di acqua calda sanitaria (ACS), in un'abitazione monofamiliare svedese. In particolare, le logiche di controllo sviluppate, basate su un sistema di regole e facendo uso di un approccio sia predittivo che non predittivo, prendono in considerazione il comportamento umano e le informazioni sulle condizioni meteorologiche come, ad esempio, il profilo del consumo di ACS e del carico termico interno e i dati sulla radiazione solare.

Lo studio è stato condotto utilizzando il software di simulazione TRNSYS®. Un modello esistente (Layout A), sviluppato da Braida e Tomasetig del Politecnico di Milano [1], che include una tipica abitazione svedese, una pompa di calore geotermica a velocità costante, un riscaldatore ausiliario e un serbatoio di accumulo stratificato, è stato adattato a una nuova configurazione (Layout B). La differenza principale consiste nel collegamento diretto tra il circuito di produzione e quello di distribuzione del calore, impiegando il serbatoio di accumulo esclusivamente per l'ACS. Un confronto tra i due layout rivela una riduzione dei consumi energetici e un aumento del comfort termico per l'ACS, nella seconda configurazione, ma con una minore stabilità della temperatura interna.

Al fine di valutare le prestazioni delle logiche di controllo sviluppate e applicate al Layout B, è stato assunto come riferimento un controllore "on/off" basato sul metodo "degree-minute". Considerando i consumi di ACS durante la stagione estiva, è possibile ottenere un potenziale di risparmio energetico grazie alla logica di controllo migliorata. Facendo riferimento alla stagione di riscaldamento svedese, l'aumento del comfort termico, derivante dall'uso del profilo degli apporti interni e già dimostrato in [1], risulta essere più consistente quando viene adottato un approccio non predittivo. Il più alto potenziale in termini di risparmio energetico e miglioramento del comfort termico viene raggiunto tramite l'implementazione simultanea di tutte le logiche di controllo sviluppate, includendo l'utilizzo dei dati sulla radiazione solare.

Parole chiave: sistemi di controllo per pompe di calore, controllo per sistemi HVAC basato su regole predittive, previsioni meteorologiche, comportamento degli abitanti dell'edificio, apporti interni di calore

Table of Contents

Acknowledgements	VII
Abstract	IX
Sommario	XI
List of Figures	XV
List of Tables	XIX
List of Abbreviations	XXI
List of Scripts	XXIII
Introduction	1
1 Literature review	5
1.1 Energy consumption in buildings	5
1.2 State of the art of heat pump systems	8
1.2.1 Performance indicators	10
1.2.2 Types of heat pumps	12
1.2.3 Ground-source heat pumps	12
1.2.4 Building heating demand and heat pump sizing	15
1.3 State of the art of heat pump control systems	17
1.3.1 Control techniques for on/off controlled heat pumps	19
1.3.2 Improved control techniques	20
1.4 Weather information	21
1.5 Human behaviour information	22
1.6 Thermal comfort assessment	23
2 System modelling	25
2.1 Methodology	25
2.2 Model elements	26
2.2.1 Building	26
2.2.2 System disturbances: weather and human behaviour	27
2.2.3 Heating generation loop	31
2.2.4 Stratified storage tank	36
2.2.5 Heating distribution loop	38

2.2.6	Control system	40
3	Layout comparison and improved control strategies	45
3.1	Overview	45
3.1.1	Heating curve modulation and performance evaluation	45
3.2	Improved control logic for the DHW heating	47
3.2.1	DHW schedule and “three set-points” configuration	48
3.2.2	TRNSYS [®] implementation	49
3.3	Comparison between Layout A and Layout B	51
3.3.1	Combined operating modes during the heating season	52
3.3.2	Methodology and adopted parameters	53
3.4	HC modulation based on the internal gains	55
3.4.1	Creation of the internal gains profile	55
3.4.2	TRNSYS [®] implementation	56
3.5	HC modulation based on the solar radiation	58
3.5.1	Working principle of the control strategy	58
3.5.2	TRNSYS [®] implementation	59
3.6	Complete system model	61
4	Results	63
4.1	DHW heating over the summer season	63
4.2	Layout comparison over the heating season	68
4.3	Internal gains	76
4.4	Solar radiation and complete system model	82
	Conclusions	87
A	Adopted scripts	91
A.1	VBA [®] scripts	91
A.2	Matlab [®] scripts	94
	Bibliography	99

List of Figures

1	World energy consumption (1990–2040). Source: IEO 2017 [3].	1
1.1	Final energy consumption and CO ₂ emissions in IEA countries, 2014. Source: IEA [5].	5
1.2	World residential and commercial sector energy consumption by fuel. Source: IEO 2017 [3].	6
1.3	Residential energy consumption and intensity in IEA countries, 2014. Source: IEA [5].	7
1.4	Aerothermal and geothermal heat pump park in operation in EU countries in 2015 (installed units). Source: EurObserv'ER 2016 [7].	8
1.5	Schematic representation of a reverse Carnot machine (heat pump).	9
1.6	Illustration of a vapour-compression cycle.	9
1.7	T - s and p - h diagrams of an ideal vapour-compression cycle.	10
1.8	Working principle of a heat pump.	10
1.9	COP values for GSHPs at given outlet temperatures. Source: [8].	11
1.10	Ground temperature over the year at different depths.	13
1.11	Different configurations of ground-source heat pumps.	14
1.12	Sketch of a U-tube borehole heat exchanger.	15
1.13	Building heating demand at different ambient temperatures. Source: [10].	15
1.14	Bivalent temperature position. Source: [11].	16
1.15	Bivalent temperature depending on the heating capacity of the heat pump. Source: [11].	16
1.16	Examples of heating curves.	17
1.17	Building heating demand at different ambient temperatures for on/off controlled and modulating heat pumps. Source: [10].	18
1.18	Basic principle of MPC for buildings. Source: [16].	21
1.19	Diagram of the DHW consumption profile integration in the MPC controller. Source: [20].	23
2.1	Weekly occupancy profile (time resolution: 5 minutes). Source: [18].	28
2.2	Activity signal and metabolic rate during the weekdays and the weekend.	29
2.3	Weekly DHW consumption profile (time resolution: 3 minutes).	30
2.4	TRNSYS [®] components for the human behaviour modelling.	31
2.5	TRNSYS [®] heating generation loop: Layout A.	32
2.6	TRNSYS [®] heating generation loop: Layout B.	32

2.7	Heat pump block diagram.	33
2.8	Temperature stratification of the storage tank.	37
2.9	DHW consumption in the TRNSYS [®] model.	38
2.10	TRNSYS [®] heating distribution loop: Layout A.	39
2.11	TRNSYS [®] heating distribution loop: Layout B.	39
2.12	Block diagram of the basic control logic.	41
2.13	TRNSYS [®] model for the basic control logic system.	41
2.14	Example of heating curve adopted in the simulations.	42
3.1	DHW schedule profile during the weekdays and the weekend.	48
3.2	Weekly profile of the DHW schedule (time resolution: 5 minutes).	49
3.3	TRNSYS [®] model of the HUB component in the improved control logic.	50
3.4	Block diagram of the improved control logic for the DHW heating.	51
3.5	TRNSYS [®] model of Layout A.	52
3.6	TRNSYS [®] model of Layout B.	52
3.7	TRNSYS [®] equation block for constant solar radiation values.	54
3.8	TRNSYS [®] equation block for the internal gains-based HC modulation.	55
3.9	Original and filtered weekly profile of the internal heat gains.	56
3.10	HC correction according to the internal heat release, in the performed tests for the month of January.	57
3.11	HC correction according to the internal heat release, in the performed tests for the month of April.	57
3.12	Total solar radiation averaged on the building surfaces, over a day period in March, with the green area representing the complementary integral CI in the time interval Δt	60
3.13	TRNSYS [®] model for the solar radiation-based HC modulation.	60
3.14	Complete TRNSYS [®] system model of Layout B: combination of all the developed control strategies.	62
4.1	SPF values obtained with the basic controller and with the improved control logic, adopting different prediction horizons of the DHW schedule, over the test month of June.	64
4.2	Condenser thermal energy, compressor electrical energy and corresponding average COP variations with respect to the base case, obtained adopting different prediction horizons of the DHW schedule, over the test month of June.	65
4.3	Operating time of the HP, on the left-hand side of the y -axis, and DBD_{DHW} parameter, on the right-hand side of the y -axis, in the base case and with the improved control logic, adopting different prediction horizons of the DHW schedule, over the test month of June.	65
4.4	Tank temperatures, on the left-hand side of the y -axis, and control signals of the heat pump and of the normal schedule, together with the COP and the draw-offs power, on the right-hand side of the y -axis, over a day period of the weekend, during the test month of June.	66

List of Figures

4.5	Tank temperatures, on the left-hand side of the y -axis, and control signals of the heat pump and of the slide schedule (prediction horizon: 3 h), together with the COP and the draw-offs power, on the right-hand side of the y -axis, over a day period of the weekend, during the test month of June.	66
4.6	SPF comparison between Layout A and Layout B, over the test months of the heating season.	68
4.7	Performance variation observed in Layout B with respect to Layout A, over the test months of the heating season.	69
4.8	Comparison of the indoor temperature observed in Layout A and in Layout B, over a day period in April.	70
4.9	Comparison of the HP control signal observed in Layout A and in Layout B, over a day period in April.	70
4.10	Comparison of the required supply temperature observed in Layout A and in Layout B, over a day period in April.	71
4.11	Comparison of the DHW supply temperature observed in Layout A and in Layout B, on the left-hand side of the y -axis, and draw-offs power, on the right-hand side of the y -axis, over a three days period in April.	71
4.12	Tank temperatures observed in Layout A, over a three days period in April.	72
4.13	Tank temperatures observed in Layout B, over a three days period in April.	72
4.14	Comparison of the required supply temperature observed in Layout A and in Layout B, over a three days period in April.	73
4.15	Comparison of the load temperature observed in Layout A and in Layout B, over a three days period in April.	73
4.16	SPF comparison between Layout A and Layout B, over the test months of the heating season, with real solar radiation values.	75
4.17	Performance variation observed in Layout B with respect to Layout A, over the test months of the heating season, with real solar radiation values.	75
4.18	Solar radiation influence on the heating system performance, observed in Layout A, over the test months of the heating season.	75
4.19	Solar radiation influence on the heating system performance, observed in Layout B, over the test months of the heating season.	76
4.20	Comparison of the SPF values obtained in the base case and in the performed tests, over the month of January. The best performing tests, for the Energy mode and for the Comfort mode, are highlighted.	76
4.21	Comparison of the SPF values obtained in the base case and in the performed tests, over the month of April. The best performing tests, for the Energy mode and for the Comfort mode, are highlighted.	77
4.22	Comparison of the performed tests in terms of energy saving and indoor thermal comfort variation, with respect to the base case, over the month of January. The best performing tests, for the Energy mode and for the Comfort mode, are highlighted.	77

4.23 Comparison of the performed tests in terms of energy saving and indoor thermal comfort variation, with respect to the base case, over the month of April. The best performing tests, for the Energy mode and for the Comfort mode, are highlighted.	78
4.24 Energy saving obtained in the performed tests, with respect to the base case, adopting different prediction horizons of the internal gains profile, over the month of January. The selected test for the Energy mode is highlighted.	79
4.25 Indoor thermal comfort variation obtained in the performed tests, with respect to the base case, adopting different prediction horizons of the internal gains profile, over the month of January. The selected test for the Comfort mode is highlighted.	80
4.26 Energy saving obtained in the performed tests, with respect to the base case, adopting different prediction horizons of the internal gains profile, over the month of April. The selected test for the Energy mode is highlighted.	80
4.27 Indoor thermal comfort variation obtained in the performed tests, with respect to the base case, adopting different prediction horizons of the internal gains profile, over the month of April. The selected test for the Comfort mode is highlighted.	81
4.28 Original and filtered profiles of the internal heat gains, adopting different prediction horizons, over a day period in April.	81
4.29 Comparison of the indoor temperature observed in the base case and with the improved control logic, adopting a non-predictive approach, over a day period in April.	82
4.30 Energy saving and indoor thermal comfort variation obtained with the HC correction after sunset, adopting different values of Δt_+ , over the test month of March.	83
4.31 On the left-hand side of the y -axis: comparison of the indoor temperature observed in the base case, with the improved control logics and when also the HC correction after sunset is applied. On the right-hand side of the y -axis: total irradiance averaged on the building surfaces, over a day period in March.	84
4.32 On the left-hand side of the y -axis: comparison of the required supply temperature for the space heating, observed in the base case, with the improved control logics and when also the HC correction after sunset is applied. On the right-hand side of the y -axis: total irradiance averaged on the building surfaces, over a day period in March.	85

List of Tables

2.1	Building properties and parameters.	27
2.2	Metabolic rate values according to the type of activity.	28
2.3	Main parameters and settings of the BHE component.	35
2.4	Geometrical parameters for the pipes modelling.	35
2.5	Ports configuration of the tank in Layout A and Layout B.	37
2.6	Main parameters of the coiled heat exchanger.	38
2.7	Adopted parameters for the radiator model.	40
2.8	Threshold values for turning on or off the HP and the AH for the SH demand.	44
3.1	Adopted parameters/indicators for the layout comparison and the performance evaluation of the developed control logics.	46
3.2	DHW set-point temperature according to the schedule value.	48
3.3	HC parameters for three test months of the heating season (constant solar radiation).	54
3.4	HC parameters for two test months of the heating season (real solar radiation).	54
3.5	Adopted corrective coefficients in the performed tests for the months of January and April.	57
3.6	HC parameters for the test month of March.	61
3.7	Adopted parameters and corrective coefficients, for the combined control strategies, in the complete system model.	62
4.1	Comparison of the simulation results obtained with the basic controller and with the improved control logic, over the whole summer season.	67
4.2	Performance comparison between Layout A and Layout B, over the test months of the heating season.	69
4.3	Average <i>COP</i> comparison between Layout A and Layout B, over the test months of the heating season, according to the operating mode of the heating system.	74
4.4	Obtained performance variation with respect to the base case, with the selected tests for the Energy mode and the Comfort mode, for the month of January.	78
4.5	Obtained performance variation with respect to the base case, with the selected tests for the Energy mode and the Comfort mode, for the month of April.	79

4.6	Comparison of the simulation results obtained with the basic controller and with the combined improved control logics, over the test month of March.	83
4.7	Comparison of the average <i>COP</i> values obtained with the basic controller and with the combined improved control logics, over the test month of March, according to the operating mode of the heating system.	84

List of Abbreviations

ACH	Air Change per Hour
AH	Auxiliary Heater
ANN	Artificial Neural Network
ASHRAE	American Society of Heating, Refrigerating and Air-Conditioning Engineers
BHE	Borehole Heat Exchanger
COP	Coefficient Of Performance
DBD	Dead-band Deviation
DHW	Domestic Hot Water
DM	Degree-minute
DMPC	Deterministic Model Predictive Control
DOT	Design Outdoor Temperature
EEA	European Environment Agency
EER	Energy Efficiency Ratio
EIA	U.S. Energy Information Administration
GCHP	Ground-coupled Heat Pump
GHE	Ground Heat Exchanger
GSHP	Ground-source Heat Pump
GWHP	Groundwater Heat Pump
HC	Heating Curve
HP	Heat Pump
HX	Heat Exchanger
IEA	International Energy Agency

IEO	International Energy Outlook
MPC	Model Predictive Control
MSE	Mean Square Error
NWP	Numerical Weather Prediction
OECD	Organization for Economic Co-operation and Development
PI	Proportional-Integral
PIR	Passive InfraRed
PM	Persistence Method
PMV	Predicted Mean Vote
RBC	Rule-based Control
SH	Space Heating
SMPC	Stochastic Model Predictive Control
SPF	Seasonal Performance Factor
SWHP	Surface Water Heat Pump
TABULA	Typology Approach for BUilding stock energy Assessment

List of Scripts

A.1	Creation of the occupancy profile.	91
A.2	Creation of the DHW schedule.	92
A.3	Generation of the water draw-offs profile.	93
A.4	Writing of the water draw-offs profile into an output data file.	93
A.5	Analysis of the simulation results over the summer season.	94
A.6	Creation of the smooth profile of the internal heat gains.	97
A.7	Creation of the hourly average profile of the solar radiation.	98

Introduction

The impacts of global climate change have become increasingly concerning in the last decades: a recent assessment of the European Environment Agency (EEA) shows that Europe’s regions as well are facing the effects of global warming, such as rising sea levels, more extreme weather, flooding, droughts and storms. Therefore, the key challenges of the 21st century are the mitigation and adaptation to climate change: at the core of these challenges is our overall energy consumption and our dependence on fossil fuels, which represent by far the largest source of greenhouse gas emissions from human activities [2].

As reported by the U.S. Energy Information Administration (EIA), in the “International Energy Outlook 2017”, the energy consumption has been increasing in the last decades. Furthermore, the modelled projections show that the world energy consumption is expected to rise by 28% between 2015 and 2040. Most of the increase in energy needs is represented by the non-OECD countries, where strong economic development and population growth lead to rising demand for energy. In particular, an increase of 41% between 2015 and 2040 is expected in non-OECD countries, in contrast to a 9% increase in OECD countries, due to the trade-off between technology development and higher standards of living [3].

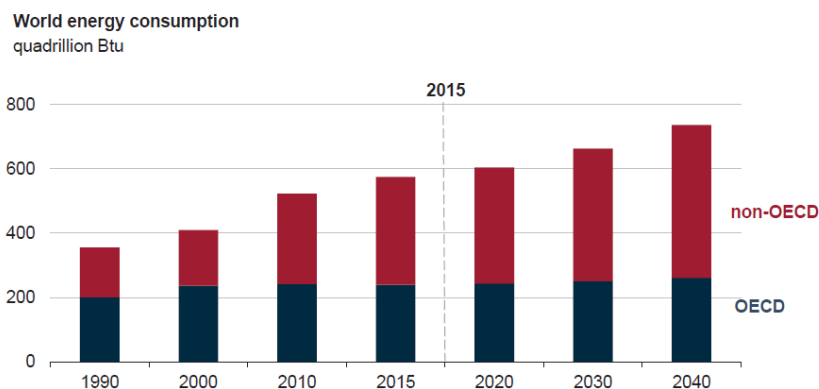


Figure 1: World energy consumption (1990–2040). Source: IEO 2017 [3].

According to EIA, the buildings sector, which includes residential and commercial structures, accounts for approximately 20% of the total delivered¹ energy consumed worldwide. Therefore, any improvement effort in the space heating sector represents

¹Consumption of delivered energy contrasts with the use of the primary energy that also includes the energy used to generate and deliver electricity to individual sites such as homes, offices, or industrial plants (1 Btu = 1.055 kJ).

an important energy saving potential, as long as a good life quality is assured. Similarly to the other available heating systems, the technology of the heat pump (HP) systems has reached maturity over the last twenty years, and thus they can be considered a valid alternative to the fossil fuel-based systems, contributing to the reduction of the greenhouse gas emissions to a large extent. In particular, the exploitation of geothermal energy, through the ground-source heat pumps, reveals higher energy performances if compared to the air or water source systems. Moreover, in literature can be found that an improvement in the control system is more cost-effective than a technology enhancement of the system equipment.

The present work starts from the results achieved by G. Braida and R. Tomasetig in their “Preliminary analysis of the potential energy saving achievable with a predictive control strategy of a heat pump for a single-family house” [1]. In particular, in the environment of the TRNSYS[®] simulation software, they modelled a typical Swedish single-family house, with a 6.5 kW GSHP unit, an auxiliary heater to cover the peak demand by providing an additional power up to 9 kW, and a 300 litres storage tank, used for both SH and DHW purposes. They adopted a short response model to represent the borehole heat exchanger (BHE), with a depth of 125 m and a water-ethanol mixture as working fluid. Finally, they used the described model to test several improved control logics, with a deterministic approach based on perfect predictions of weather conditions, such as solar radiation and outdoor temperature, and of human behaviour – i.e. internal heat gains and DHW consumption. The improved control logics, implemented and applied in separate system models, revealed an energy saving potential of about 6–7%, with a considerable decrease of the indoor temperature deviation from the set-point value and a significant reduction of the auxiliary heater usage [4].

The same model has been used, in the present work, to better investigate the improvement potential given by the combination of the above-mentioned control logics, with some variations and further improvements in their implementation, and with the adoption of a different system layout (Layout B), in which the storage tank is used for DHW purposes only. At first, a comparison between the two layouts is carried out, in terms of energy saving and thermal comfort. Then, three different improved control logics are implemented, taking into account the information about the DHW consumption, the internal gains and the solar radiation, and eventually their combination is applied within Layout B. The obtained results show that it is possible to achieve a potential energy saving and a thermal comfort enhancement, with respect to a basic on/off controller, despite a lower indoor temperature stability is observed in Layout B, if compared to that of the original configuration (Layout A).

The work is organized according to the following structure:

Chapter 1 shows the literature review on the state of the art of heat pumps and of their control systems.

Chapter 2 describes the system modelling and the adopted methodology.

Chapter 3 provides the details of the proposed control strategies and of their implementation, after having performed the layout comparison.

Chapter 4 presents the obtained results and their discussion.

The last chapter reports the conclusions about the achieved results.

Chapter 1

Literature review

1.1 Energy consumption in buildings

The world energy consumption can be divided in three main categories: industrial, transportation and buildings. According to IEA [5], as shown in Fig. 1.1a, the transport sector accounted for the highest share of final energy consumption in 2014, followed by manufacturing and residential sector². Moreover, in almost all the IEA countries, CO₂ emissions for both residential space heating and appliances were larger than those of any manufacturing sub-sector (see Fig. 1.1b).

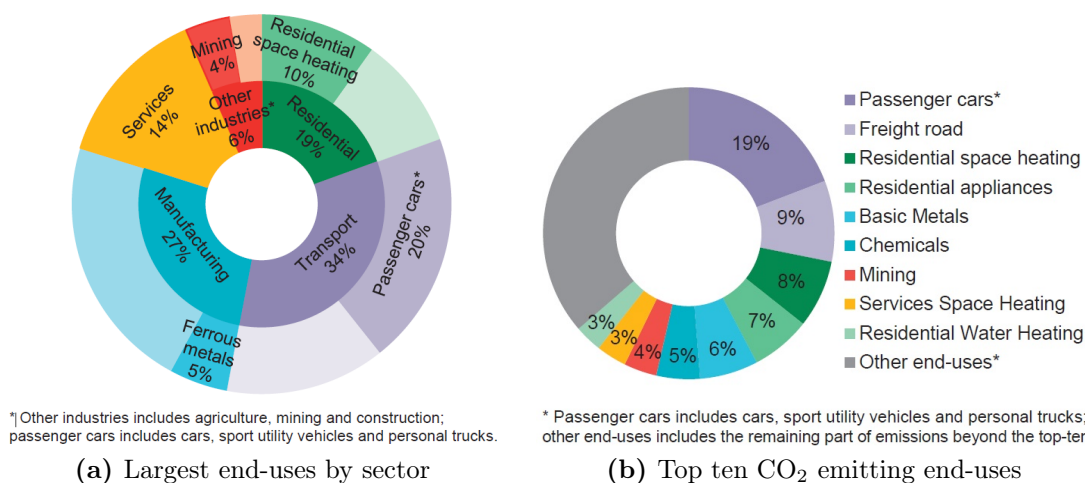


Figure 1.1: Final energy consumption and CO₂ emissions in IEA countries, 2014. Source: IEA [5].

At a more global level, as reported in the IEO 2017, the buildings sector, which consists of residential and commercial end users, accounts for almost 21% of the total delivered energy consumed worldwide in 2040, about the same as its share in 2015. In fact, energy use in buildings is projected to increase by 32% between

²The IEA aggregate refers to the nineteen out of thirty IEA member countries for which energy efficiency data, covering most of the end-uses, are available: Australia, Austria, Canada, Czech Republic, Finland, France, Germany, Greece, Ireland, Italy, Japan, Korea, New Zealand, The Netherlands, Spain, Sweden, Switzerland, the United Kingdom and the United States. These countries represented about 95% of the total IEA final energy consumption for 2014.

2015 and 2040, following the same trend of the global energy consumption, with an average increase of 1.5%/year (see Fig. 1.2). Most of the increase (2.1%/year, nearly three times the growth rate of the OECD countries) occurs in large, emerging non-OECD nations, where population continues to shift from rural to urban areas. In particular, electricity use in buildings grows by 2%/year in the considered period of the projections, considering rising standards of living in non-OECD countries with a consequent increase in the demand for appliances, personal equipment, and commercial services. Whereas natural gas consumption in buildings grows by 20% over the same period, as increased demand in non-OECD countries is partially offset by improvements in space heating equipment [3].

The energy delivered to buildings is used for heating, cooling, lighting, water heating and many other appliances. Size and location of the structure are key factors for the energy consumption. For instance, small flats require less energy and less occupation than big accommodations. Moreover, the amount and type of energy consumed are mainly related to weather conditions, architectural design, energy systems and economic level of the occupants.

According to IEA [5], space heating and sanitary water heating accounted for almost 70% of the energy consumption of the IEA member countries in the residential sector in 2014 (see Fig. 1.3a on the next page). Therefore, any improvement in the heating systems of buildings would represent a high potential for energy saving. In this regard, energy efficiency improvements for space heating have occurred across IEA countries, mostly in the form of better insulation of new buildings, improvements in heating equipment and renovation of old buildings. The effects can be seen by the trends of the residential space heating energy intensity – defined as energy consumption per floor area – which significantly decreased in many IEA countries in the period 2000–2014 (see Fig. 1.3b on the facing page). For instance, Austria, France, Germany, Ireland, Korea, Netherlands and Spain have experienced reductions of more than 30% since 2000 (as one would expect, warmer countries generally have lower space heating intensities, since less energy is required on average to keep the indoor temperature at comfort level). Furthermore, according to the 2010 European Performance of Building Directive [6], the member countries shall guarantee that all new buildings constructed after 2020 will be “nearly zero-energy”.

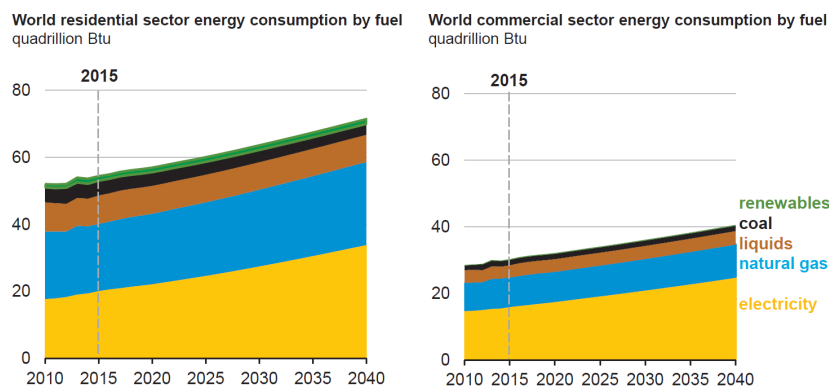


Figure 1.2: World residential and commercial sector energy consumption by fuel. Source: IEO 2017 [3].

1.1. Energy consumption in buildings

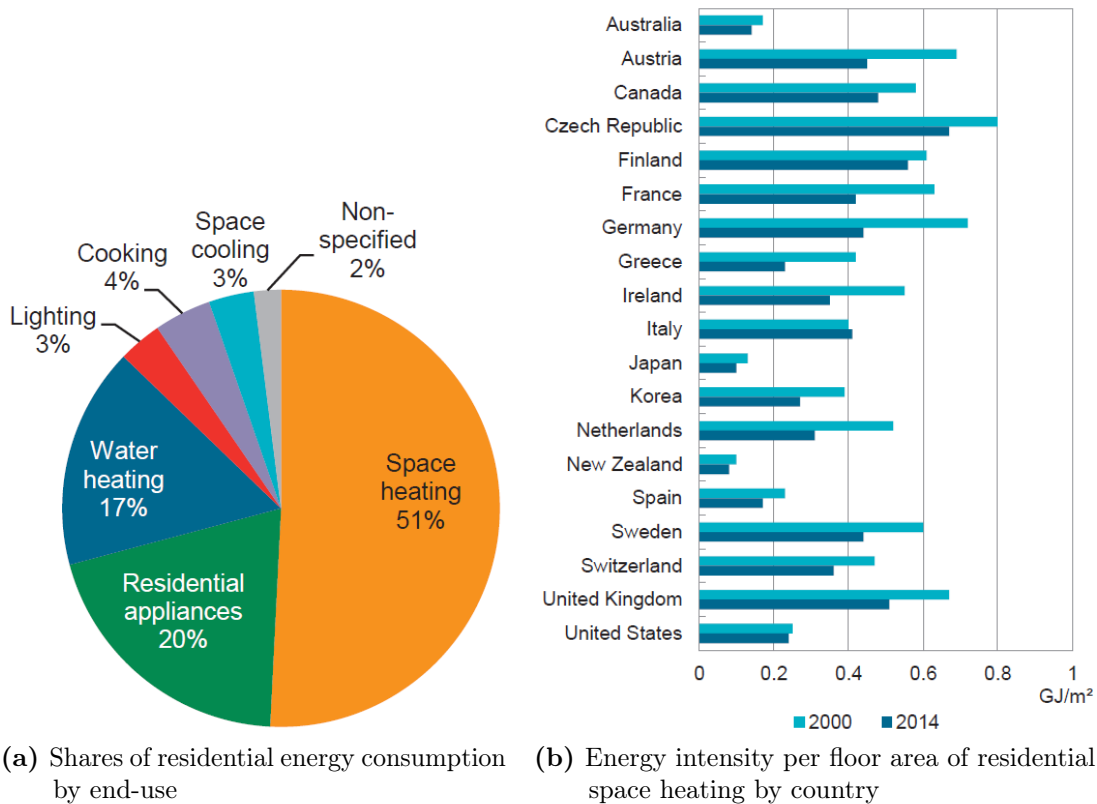


Figure 1.3: Residential energy consumption and intensity in IEA countries, 2014. Source: IEA [5].

As concerns the available heating systems, the heat pump (HP) technology has become a valid alternative for heating and cooling needs. According to the study carried out by the EurObserv'ER [7], the heat pump sector had an excellent year in 2015. Appliance sales, considering all heating and cooling market technologies, increased by 20% from 2 212 898 units in 2014 to 2 655 331 units in 2015, reaching a total number of 29.5 million HPs in operation, with an estimated renewable energy provided in the European Union of 8.8 Mtoe in 2015. Regarding the installed capacity, the most recent data covers 2014 and indicates 194.3 GW capacity to date, including 178.4 GW from air-source heat pumps and 15.9 GW from ground-source heat pumps. The spreading of this latter technology is more consistent in the North-Central European countries, with Sweden being the leader of this market segment, followed by Germany and Finland (see Fig. 1.4 on the next page).

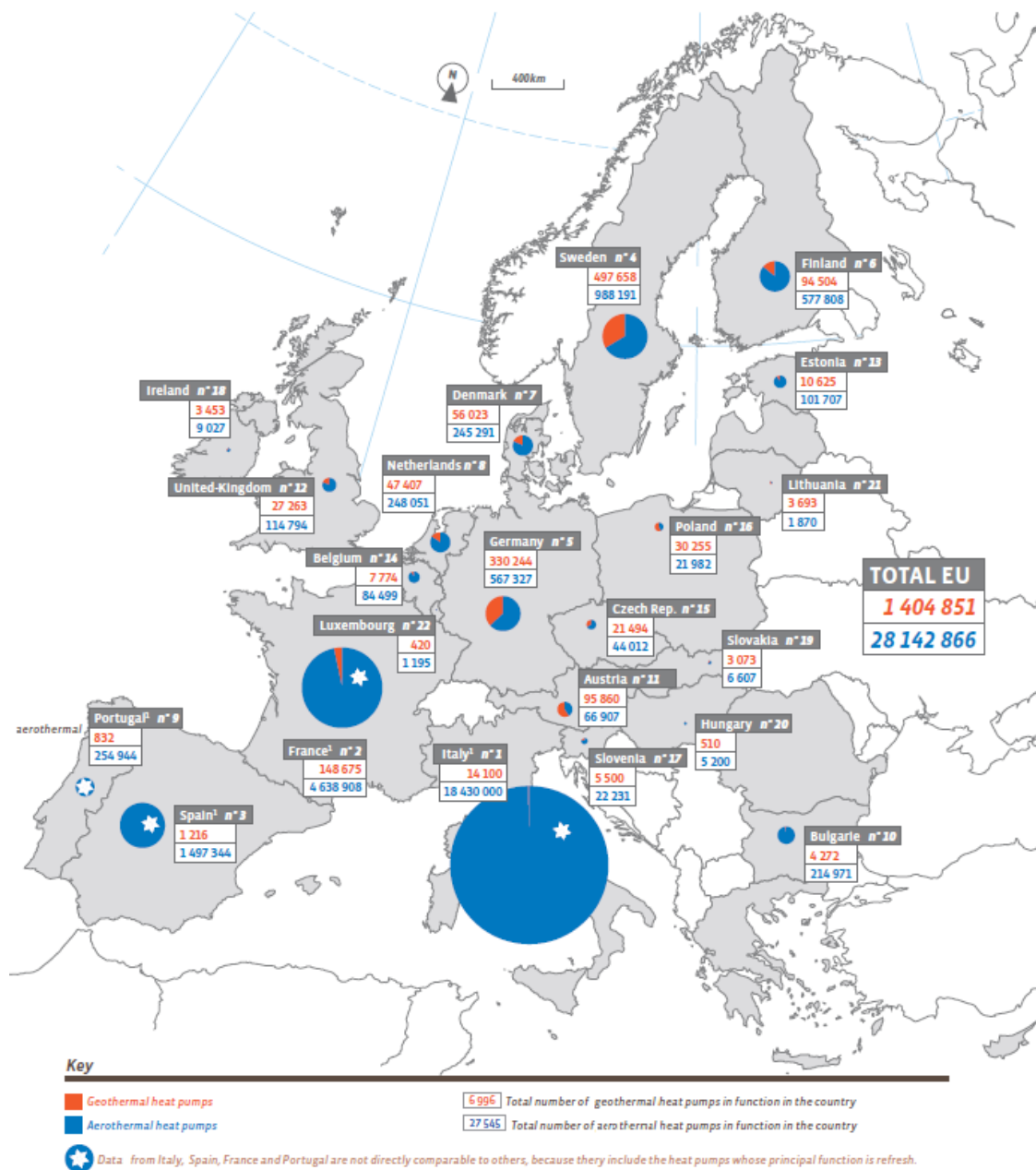


Figure 1.4: Aérothermal and geothermal heat pump park in operation in EU countries in 2015 (installed units). Source: EurObserv'ER 2016 [7].

1.2 State of the art of heat pump systems

A heat pump is a thermal installation based on a reverse Carnot thermodynamic cycle, which transfers thermal energy in the opposite direction of spontaneous heat transfer. In fact, by means of external power, heat is moved from a lower temperature heat reservoir (cold source) to a higher temperature one (hot sink), as illustrated in Fig. 1.5 on the facing page.

In particular, in a heat pump, a vapour-compression cycle (or reverse Rankine cycle) is accomplished. Following the scheme in Fig. 1.6 on the next page, in the

1.2. State of the art of heat pump systems

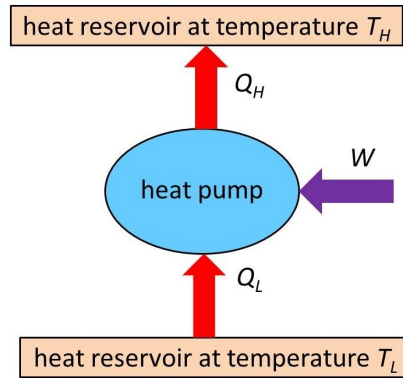


Figure 1.5: Schematic representation of a reverse Carnot machine (heat pump).

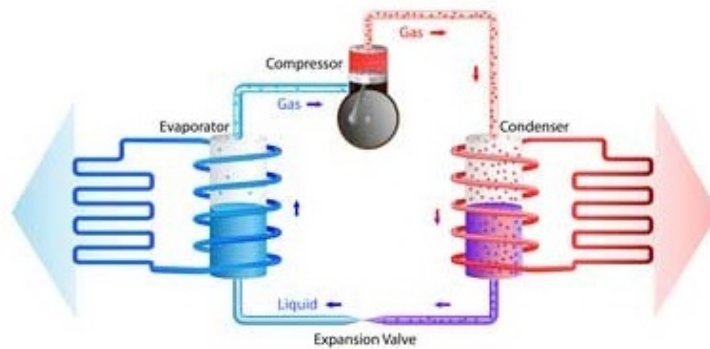


Figure 1.6: Illustration of a vapour-compression cycle.

evaporator, the working fluid evaporates absorbing heat from the cold source and then the vapour pressure is raised by means of a compressor, which consumes drive energy (for instance, electrical converted into mechanical energy). Subsequently, the vapour releases its thermal energy in the condenser by exchanging heat with the hot sink, and finally, the thermodynamic cycle is closed by means of an expansion valve, where the working fluid pressure is reduced to its original value. A graphic representation of an ideal vapour-compression cycle, in the $T-s$ (temperature-entropy) and $p-h$ (pressure-enthalpy) diagrams, is shown in Fig. 1.7 on the following page.

Considering the useful effect of the machine, two different operating modes can be identified, as illustrated in Fig. 1.8 on the next page. When the user needs a cooling effect (summer), the heat pump works in “cooling mode” and the useful effect is provided by the evaporator, whereas it works in “heating mode” when the user needs a heating effect (winter), which is provided by the condenser of the heat pump.

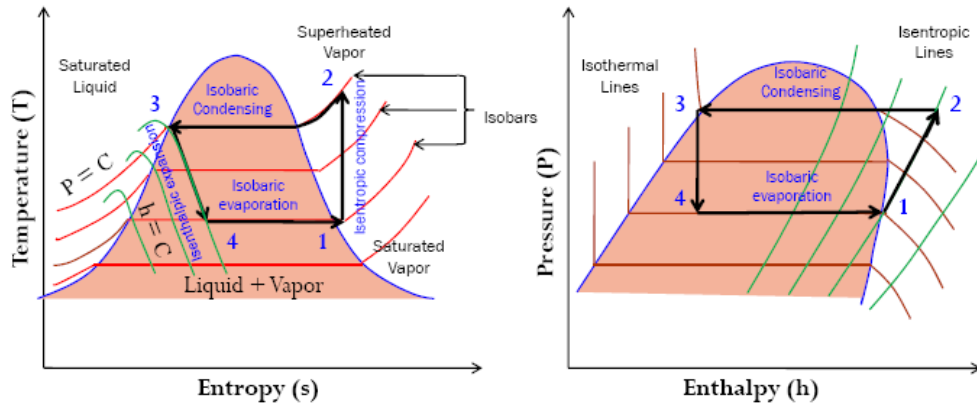


Figure 1.7: T - s and p - h diagrams of an ideal vapour-compression cycle.

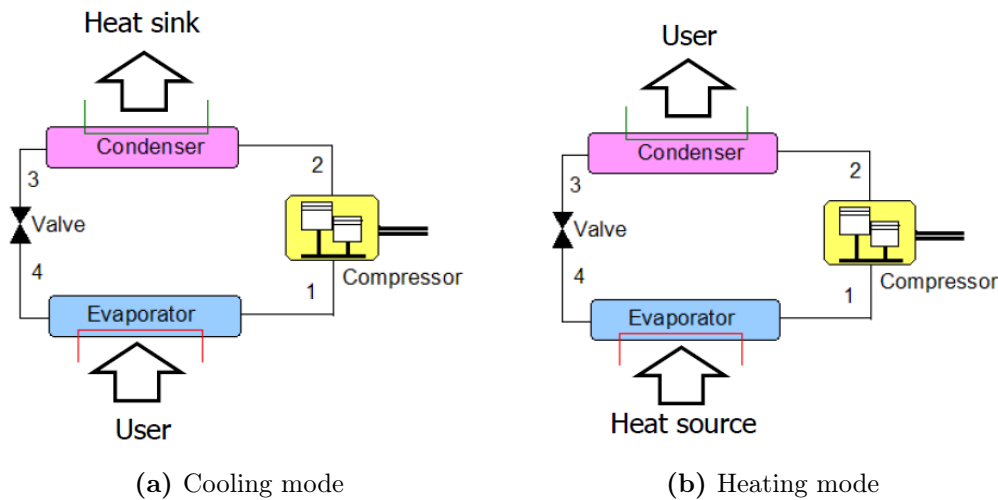


Figure 1.8: Working principle of a heat pump.

1.2.1 Performance indicators

The energy efficiency of a heat pump in heating mode can be expressed by the coefficient of performance (COP), defined as the ratio between the useful effect and the power consumed to drive the compressor:

$$COP = \frac{\dot{Q}_{\text{cond}}}{P_{\text{compr}}} \quad (1.1)$$

where \dot{Q}_{cond} is the condenser heat rate and P_{compr} is the electrical power absorbed by the compressor.

When the useful thermal power and the consumed electrical one are considered over a given period – e.g. the heating season – it is possible to obtain the seasonal performance factor (SPF), which also includes the thermal energy released and the

1.2. State of the art of heat pump systems

electrical energy consumed by the auxiliary – or back-up – heating system, if any:

$$SPF = \frac{Q_{\text{cond}} + Q_{AH}}{E_{\text{compr}} + E_{AH}} \quad (1.2)$$

where Q_{cond} and Q_{AH} are respectively the heat released in the condenser and in the auxiliary heater (AH), and E_{compr} and E_{AH} are respectively the electrical energy consumed by the compressor of the HP and by the back-up system.

Considering a heat pump working in cooling mode, its performance can be determined by means of the energy efficiency ratio (EER), defined analogously to the COP, as the ratio between the useful effect and the power consumed by the compressor:

$$EER = \frac{\dot{Q}_{\text{eva}}}{P_{\text{compr}}} \quad (1.3)$$

where \dot{Q}_{eva} is the evaporator heat rate.

The maximum theoretical efficiency – i.e. the Carnot efficiency – of a heat pump depends on the source and sink temperatures: the higher their difference, the lower the efficiency. In particular, as reported in [8], for a GSHP, the COP depends on the temperature of the water entering the evaporator from the ground circuit, on the heating/cooling load, on the type of building heating/cooling system and on the supply temperature – i.e. the outlet temperature of supply water from the condenser (see Fig. 1.9). According to [8], the maximum COP of existing GSHPs is around 4.5, however their mean COP during operation is lower. Hence, the SPF should be considered for more reliable data. In general, the SPF values vary between 3.0 and 3.8, and they can reach 4.0 if high quality components of the GSHP unit and an optimum building system heating are adopted.

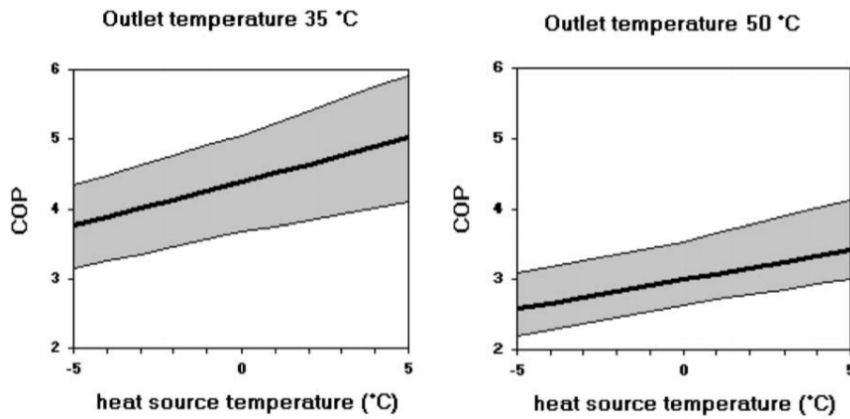


Figure 1.9: COP values for GSHPs at given outlet temperatures. Source: [8].

1.2.2 Types of heat pumps

A first classification of heat pumps can be made considering the different heat sources:

- *Water*: since it is one of the most spread elements, it can be easily used as a heat source (river, lake, pond or sea). For instance, the water temperature of natural ponds is often limited in between 8 °C and 16 °C, allowing an efficient usage of the machine.
- *Air*: it has a lower heat transfer coefficient, thus larger surfaces must be used with a consequent increase of costs and space. Moreover, air is subjected to variable weather conditions that strongly affects the heat pump performances.
- *Ground*: see the following section [1.2.3](#).

Taking into account the useful effect of the machine, the fluid that contributes to this effect is called *primary fluid*: for instance, in heating mode, it is the one that exchanges heat with the working fluid in the condenser (load side). While the fluid necessary for the correct operation of the machine is called *secondary fluid*: for instance, in heating mode, it is the one that exchanges heat with the working fluid in the evaporator (source side). Therefore, a second classification of heat pumps can be made according to the different configurations of primary and secondary fluids (water or air), as reported below, where the first element represents the secondary fluid and the second element corresponds to the primary one:

- *Air-to-air*
- *Water-to-air*
- *Water-to-water*

1.2.3 Ground-source heat pumps

As explained in [\[8\]](#), a factor that affects the water temperature in the ground circuit, and therefore the COP of the heat pump, is represented by the geological conditions, such as the thermal and hydraulic properties of the underground, and by technical parameters (for instance, length and type of ground heat exchanger, material, etc.). As shown in [Fig. 1.10 on the next page](#), the temperature of the ground is still influenced by the external environment until around 10 m of depth, whereas for lower depths it can be considered constant throughout the year, in the range of 10÷15 °C.

1.2. State of the art of heat pump systems

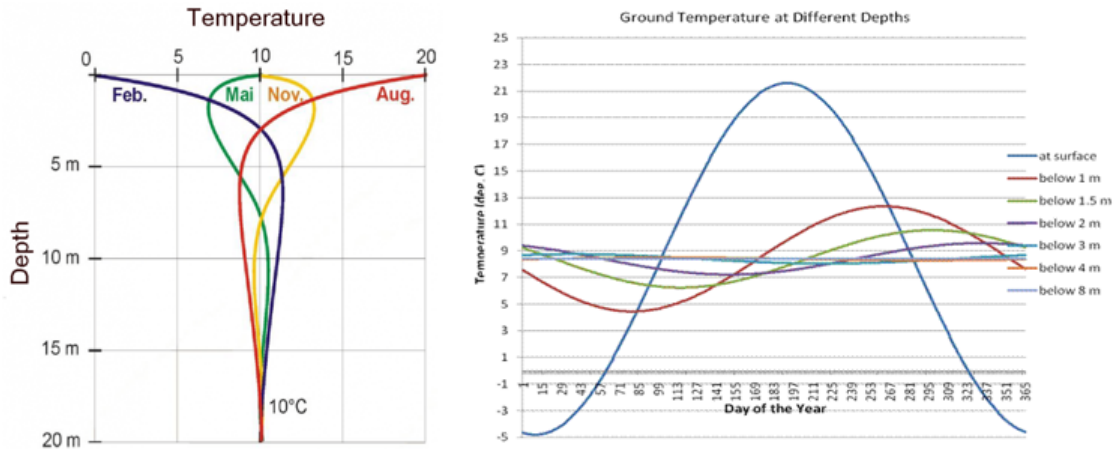


Figure 1.10: Ground temperature over the year at different depths.

Considering the annual operation of a GSHP system, the ground is used as a source during the heating season, while it can be used as a thermal sink throughout the cooling season: therefore, temperature variations of the ground can be detected during the years, if the relative durations of these seasons are much different.

A classification of ground-source heat pumps can be made according to the type of configuration in which the heat exchange with the heat source (ground or water) occurs, as depicted in Fig. 1.11 on the following page.

- *Surface Water Heat Pumps* (SWHP): if a nearby water body (pond, lake) is available, heat is exchanged either in an open or in a closed piping loop, which can be submerged under the surface.
- *Groundwater Heat Pumps* (GWHP): in the presence of an aquifer with adequate hydraulic properties, groundwater can be physically abstracted from an abstraction well and dumped into a re-injection one or directly into a lake, river or pond (therefore such a configuration is an open loop).
- *Ground-coupled Heat Pumps* (GCHP): heat is extracted from or rejected to the ground by means of a closed piping loop, where usually a mixture of pure water and antifreeze (often referred to as brine) circulates.

As concerns the GCHP systems, there are two main configurations for the ground heat exchangers (GHE): vertical or horizontal. In the latter, the pipes are buried in trenches ranging from 1 m to 2 m deep, and they are arranged either in a parallel or in a series connection or, when available land area is limited, a coiled pipe, called “slinky” or spiral, can be used. On the other hand, the vertical configuration consists of a set of one or more boreholes, where typically a “U-tube” closed loop is emplaced, as shown in Fig. 1.12 on page 15.

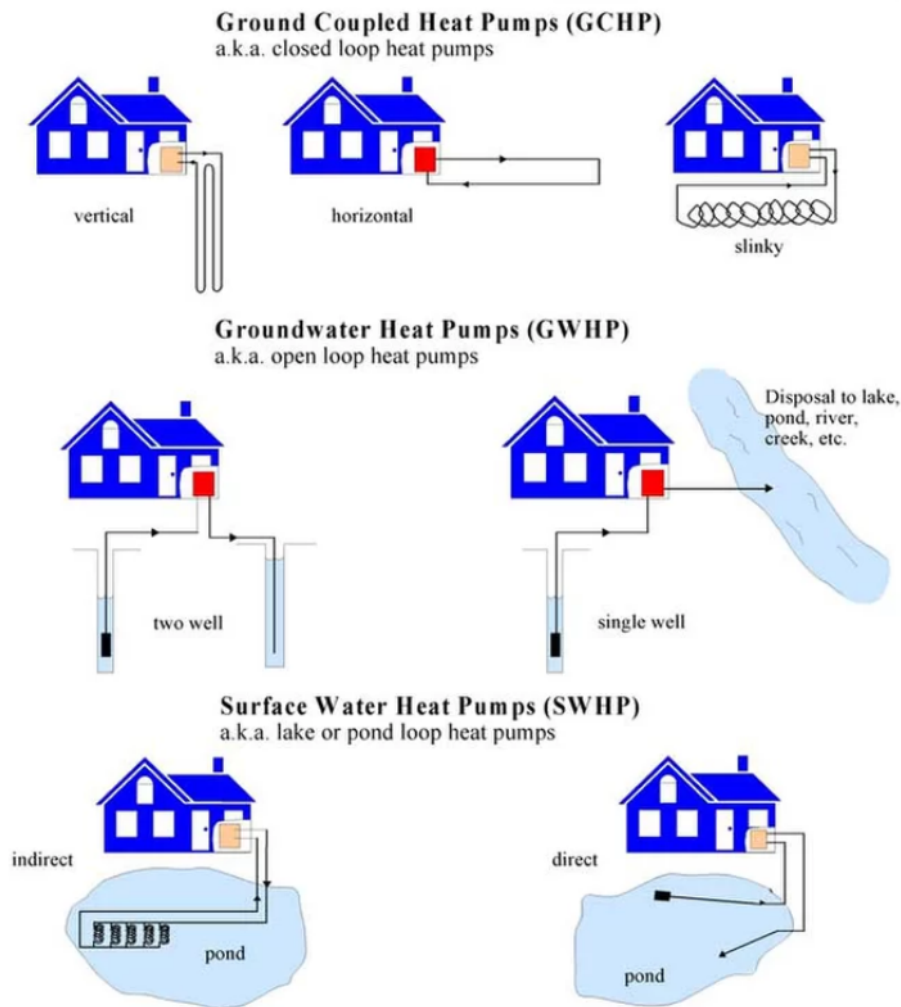


Figure 1.11: Different configurations of ground-source heat pumps.

As already mentioned, at depths below about 10 m, the ground temperature is constant throughout the year; hence, borehole heat exchangers (BHE) show better performance and energy efficiency than horizontal ones [8]. Moreover, they require a limited usage of pipes and pumping energy as well as a reduced ground area; in addition, the pipes are in direct contact with the soil, which has very little temperature and thermal properties variations thanks to the high depth. Therefore, GSHP systems with BHEs are widely used, despite their higher costs for the boreholes drilling with respect to other technologies. In particular, in Sweden, about 20% of the buildings is equipped with GSHP systems with vertical loops: in the last five years around 25 000 units in sizes ranging from 3 kW to 25 kW, and around 1500 units in higher sizes, have been installed every year [9].

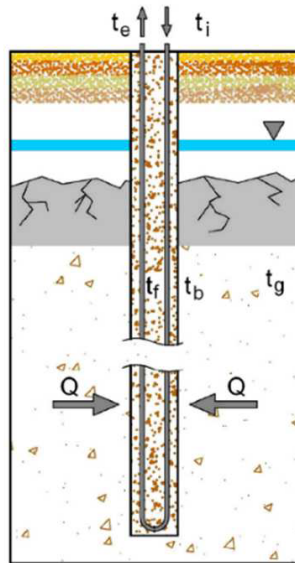


Figure 1.12: Sketch of a U-tube borehole heat exchanger.

1.2.4 Building heating demand and heat pump sizing

The building heating demand strongly depends on the external air temperature and on the type of building; in addition, any variation of solar radiation, wind speed and internal gains affect its value. Hence, large fluctuations of the building heating demand are possible for the same outdoor temperature, as shown in Fig. 1.13.

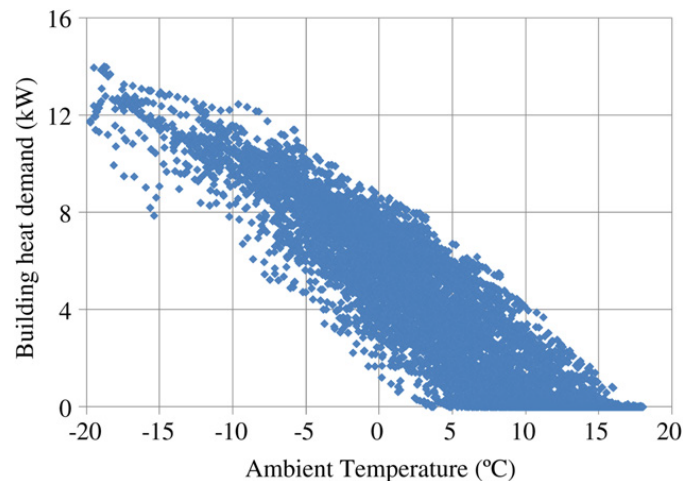


Figure 1.13: Building heating demand at different ambient temperatures. Source: [10].

The coupling between a building and a heat pump system is based, therefore, on the heating demand of the building itself and on the heating system capacity. As shown in Fig. 1.14 on the next page, the building request decreases with increasing ambient temperature, while the heat pump capacity (an air-to-water heat pump is considered) has the opposite trend. The intersection between the two curves occurs in the so called “balance point”, to which corresponds the “bivalent temperature”, which is the outdoor temperature value at which the thermal capacity of the heat

pump matches completely the building thermal load. For temperatures lower than the bivalent temperature, the heating system is not able to satisfy the building heating demand; therefore, an auxiliary heater is required. On the other hand, for temperatures higher than – or equal to – the bivalent temperature, the heat pump operates either modulating or in on/off, as its nominal capacity overrates the load [11].

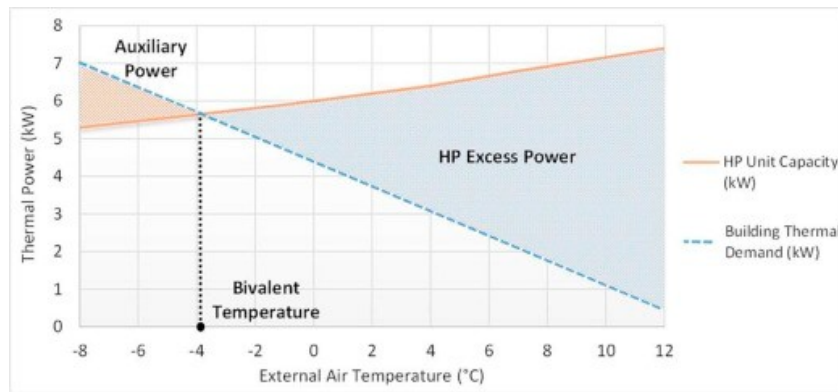


Figure 1.14: Bivalent temperature position. Source: [11].

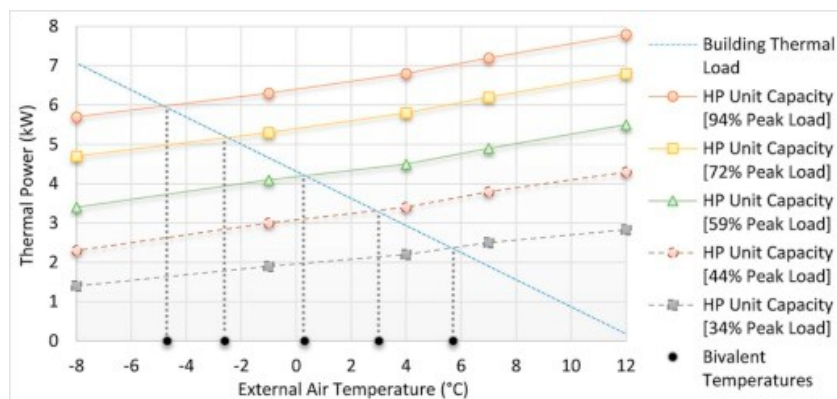


Figure 1.15: Bivalent temperature depending on the heating capacity of the heat pump. Source: [11].

The dimensioning of a HP should be such that the building heating demand is always covered for temperatures higher than the bivalent one. According to heat pump manufacturers, in Sweden, this value should be between -6°C and -3°C . Moreover, as reported by Madani et al. [10], Swedish heat pump units with single-speed compressors are usually dimensioned to cover about 55–70% of the peak heating demand – i.e. the building heating demand at Design Outdoor Temperature (DOT). In addition, they are able to typically cover 85–98% of the annual heating energy demand. Finally, as shown in Fig. 1.15, the higher the heating capacity, the higher the fraction of the peak load covered by the heat pump, and the lower the bivalent temperature, and thus the lower the auxiliary heating demand.

The relation between the ambient temperature and the “required” heat pump supply – or return – temperature, in order to fulfil the building heating demand

1.3. State of the art of heat pump control systems

and to reach the desired indoor temperature, is expressed by the “heating curve” [12]. The required supply temperature depends on the building physical properties and thus on its thermal inertia. Therefore, according to these external conditions, the heating curve slope and intercept can be changed during the heating seasons, in order to satisfy the room comfort condition. In Fig. 1.16, two examples of heating curves are shown, with both supply and return temperatures.

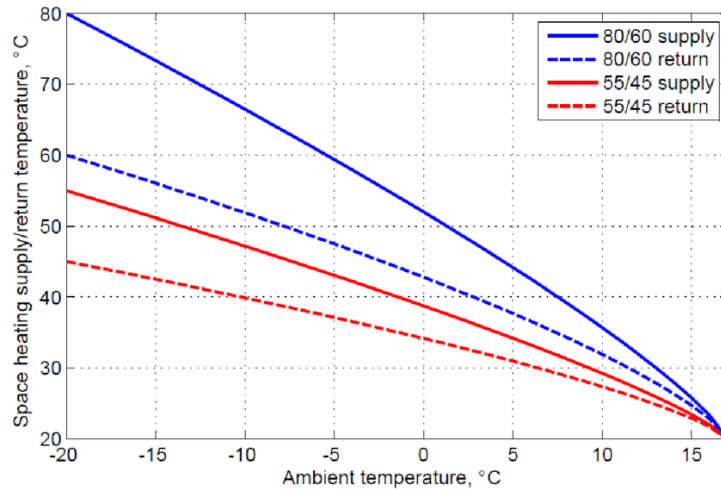


Figure 1.16: Examples of heating curves.

1.3 State of the art of heat pump control systems

In order to meet the building heating demand while maximising the energy efficiency of the heating system, an accurate control strategy should be adopted. As reported in [10], the available heat pump technology consists of two main categories: on/off and variable-speed heat pumps.

The first typology is equipped with a single-speed compressor, whose power changes only according to the operating conditions – mainly the primary and secondary fluid temperatures. Hence, when the heat pump capacity exceeds the heating load, there is the need to run the compressor intermittently in order to meet the heating demand. For instance, looking at Fig. 1.17a on the following page, where the heating capacity of four different heat pump units is shown, together with the building heating demand at different ambient temperatures, it can be seen that the higher the heat pump capacity, the more extended the compressor cycling region.

On the other hand, in the variable-speed heat pumps, the motor that drives the compressor is connected to the grid through a frequency inverter, which allows to modulate the compressor speed and consequently the heat pump capacity. As shown in Fig. 1.17b on the next page, it is possible to select the HP operating condition, varying the compressor speed between a minimum and a maximum value, in order to meet the exact heating demand. A compressor cycling region is still present, however it is shifted to the right-hand side and it is smaller with respect to that of the smallest on/off controlled HP unit [10].

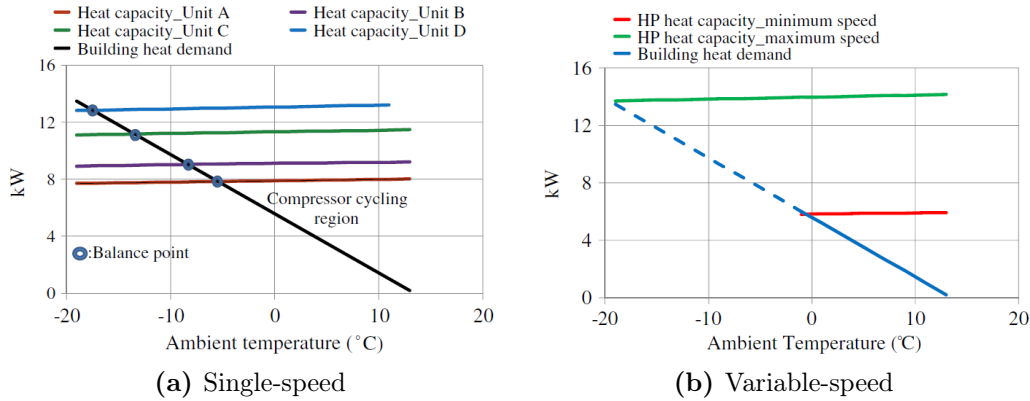


Figure 1.17: Building heating demand at different ambient temperatures for on/off controlled and modulating heat pumps. Source: [10].

Several studies comparing on/off and modulating control strategies can be found in literature. For instance, in the work of Karlsson and Fahlén [13], the comparison was carried out considering the SPF and the COP. In the on/off controlled HP unit, during the on period, the supply temperature is higher than the required one, therefore a higher condensation temperature leads to a lower efficiency. Whereas, in the variable-speed operation, the heat pump provides the exact required heating demand, with a consequent lower condensation temperature and higher efficiency. Moreover, the possibility to modulate the heating capacity allows to reduce the on/off cycles of the compressor, improving the life of the HP unit. However, the authors showed that the potential improvement of about 10–25%, with respect to the intermittent operation, is achievable only with specific design of compressor and inverter. Otherwise, the efficiency losses – mainly related to inverter and liquid pumps – are such that the annual energy efficiency of the variable-speed HP is still lower than the one of the on/off controlled HP.

A more suitable comparison, performed by Madani et al. [10], considered a complete model of the whole GSHP system, including the ground heat source, a typical Swedish building, the heating distribution system, the liquid pumps and the electrical auxiliary heater. In particular, they noticed that the sizing of the on/off controlled HP based on the building peak demand played a significant role in the comparison. In fact, they concluded that the variable capacity system led to a better performance only when the on/off controlled one was dimensioned to cover less than 65% of the peak load (i.e. less than 95% of the annual energy demand), due to the important fraction of the demand covered by the auxiliary heater, which decreases the SPF of the system. On the other hand, for higher fractions of the peak heating demand, covered by the HP, there was no significant difference between the SPFs of the two systems, because the benefits deriving from the modulation of the HP capacity were completely compensated by the efficiency losses related to the inverter and to the liquid pumps: for instance, the energy consumption of the latter can be 5–30% higher in the variable-speed system than in the single-speed one, due to the longer operation time over the year. As a final remark, the authors suggested that, in order to obtain a higher efficiency in the on/off controlled systems, their sizing should be such that the auxiliary heater covers less than 5% of the annual

heating demand.

A further comparison between the two control strategies was carried out by Bagarella et al. [11], considering an air-to-water heat pump system in a single-family house located in the northern Italy. Besides the size of the HP unit, they also took into account the influence of the thermal storage volume and of the cycling losses³ on the system performance: they represent important variables to be considered when comparing on/off controlled and variable-speed HP systems. In fact, they obtained that, when an on/off system is dimensioned to cover a high fraction of the peak load, cycling losses might be higher than 12% of the whole electric consumption of the system, especially if the volume of the thermal storage is small.

Considering the results found in literature, the on/off controlled HP systems are widely used thanks to the higher simplicity and to the lower cost. Therefore, they can be used to perform a first analysis for the improvement of the control system.

1.3.1 Control techniques for on/off controlled heat pumps

Among the different available methods for the on/off control of a heat pump unit, three common ones are here described [12]:

- *Constant hysteresis method.* The control of the HP cycling is based on the return temperature of the primary fluid, which is allowed to divert from the required temperature only within a prefixed range. For instance, if the return temperature decreases under the lower dead-band value (start limit), the controller starts the heat pump and stops it only when the upper dead-band value (stop limit) is reached. As one can expect, a limitation of this method is represented by the fluctuations of the supply temperature. A combination of this algorithm and a time-based approach can be used to control the AH operation: for instance, if the return temperature has been under the start limit for more than a certain amount of time, then the controller starts the auxiliary heater.
- *Floating hysteresis method.* The difference between this technique and the previous one is that the hysteresis is gradually changed according to the variation of the heat pump status (on/off). As a result, with this technique it is possible to avoid too fast or too slow reactions of the controller when sudden temperature variations occur. Hence, the floating hysteresis method is expected to have a better performance, due to its greater sensitivity. When the AH operation is needed, the hysteresis is locked to its maximum value.
- *Degree-minute method.* The third method is based on the “degree-minute” parameter, defined as the difference between the actual supply temperature ($T_{\text{supply},A}$) and the required supply temperature ($T_{\text{supply},R}$), multiplied by the

³Cycling losses can be defined as those inefficiencies that reduce the performance of the HP unit during the transient period. They may be quantified by comparing the efficiency of a cycling unit and the efficiency of the same unit working continuously. They depend on the type of expansion valve adopted in the unit [14].

time t expressed in minutes:

$$DM = (T_{\text{supply},A} - T_{\text{supply},R}) \cdot t \quad (1.4)$$

The degree-minute is then summed over the time and the control signals for the HP and the AH operation are computed accordingly to its value. This method takes into account both the time and the temperature value, therefore it may lead to a better performance of the control system.

Madani et al. [12] carried out a comparative analysis of these three control techniques in terms of supply temperature, indoor temperature, energy consumption and SPF over a year. The results obtained show that all the three methods yield large oscillations of the supply temperature – which may lead to a lower thermal comfort – when the outdoor temperature is relatively high. However, the average supply temperature of the system controlled with the degree-minute method is always close to the required one. Moreover, the lowest total energy use over a year is reached with the degree-minute method, while the constant hysteresis method shows the highest total annual energy consumption. As a final remark, the authors recommended to avoid using constant parameters in the control logic and suggested that the degree-minute method could lead to a further improvement of the control system if some dynamic parameters, such as ambient temperature and inhabitants' behaviour, are given as inputs.

1.3.2 Improved control techniques

As already mentioned in section 1.2.4, a classical heating system based on a heat pump unit is controlled accordingly to the heating curve, which computes the required supply – or return – temperature, taking into account the outdoor temperature only, without considering all the other disturbances that affect the system – such as solar radiation or internal heat gains from human activity and lighting power. In order to improve the control system, it is then necessary to consider also these multiple inputs and their predictions. For this purpose, two main approaches can be found in literature: the Rule-based Control (RBC) and the Model Predictive Control (MPC).

As reported in [15], the RBC approach is based on a series of rules of the form “if *condition*, then *action*” and represents the current practice for the control of complex heating systems. The performance of this method is then strongly dependent on the choice of the adopted set of rules; moreover, it does not consider any predictions related to the future evolution of the system.

On the other hand, the MPC approach uses a system model to predict its future evolution and generates a control vector by means of an optimisation algorithm, taking into account disturbances and constraints. As shown in Fig. 1.18 on the facing page, the dynamics of the building, the predicted disturbances inputs, a proper cost function and the current state of the system are combined together for the statement of the optimisation problem, at each time interval; subsequently, the cost function is minimised by imposing specific constraints and, finally, the output

1.4. Weather information

error is computed and a feedback loop is set to track the desired set-point [16]. As a final remark, a distinction can be made between Deterministic MPC (DMPC) and Stochastic MPC (SMPC). The former is the standard approach that adopts the assumption of perfect prediction of weather forecast, while the latter accounts for the uncertainties in the weather forecast and it allows to enforce constraints to be fulfilled with a predefined probability [15].

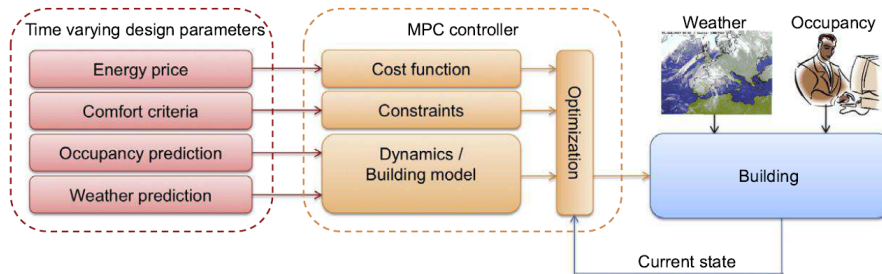


Figure 1.18: Basic principle of MPC for buildings. Source: [16].

According to [15] and [16], MPC shows a high potential to manage all the different disturbances, with a consequent significant energy saving potential with respect to RBC, however it is characterised by a much higher complexity of the system modelling and of the optimisation problem solution. Moreover, the mathematical description of the building is case-sensitive, hence the same system model cannot be adopted for a wide range of different situations; in addition, the minimisation of the cost function is computationally expensive due to non-linearities in the system model.

Contrarily, since it does not involve a complex mathematical problem, RBC is characterised by a higher simplicity of the controller design and it can be easily adapted to many different situations, by adjusting and retuning the set of rules. Even though this approach is not able to account for the disturbances prediction, it can be used as a starting point for a further improvement of the control logic. The control strategies developed in [1] and revisited in the present work have been defined in order to obtain a preliminary “predictive” RBC.

1.4 Weather information

According to the source of the meteorological data, which can be either measured on-site or in a particular horizontal range of validity, three main different methods for weather predictions can be found in literature: Persistence Method (PM), Numerical Weather Prediction (NWP) and Artificial Neural Network (ANN).

- *Persistence Method.* It is the simplest method for solar radiation and temperature prediction with a short-term horizon. Basically, it assumes that the conditions at the time of the forecast will not change. For example, if it is sunny at the time of the prediction, it will be sunny 24 hours later too, with an accuracy of 100%.

- *Numerical Weather Prediction.* The weather forecast is accomplished in a national meteorological station. The main drawback of this method is its limited horizontal resolution, with a maximum accuracy in the order of few kilometres. Nonetheless, meteorological measurements at the building site can be exploited to improve the predictions by means of statistical post-processing.
- *Artificial Neural Network.* This model is inspired by biological neural networks and it is used to compute functions depending on a large number of inputs. In particular, it is a machine learning method where the predictions are achieved by considering correlations and dependencies in the data set, collected during a training period, where the model is taught to emulate the dynamics of the system.

According to the comparisons of these different methods available in literature [17], the most common and efficient weather prediction method is the one that collects the data from a meteorological weather station, which are eventually post-processed.

1.5 Human behaviour information

In order to achieve an improvement in the energy performance of the heating system and an enhancement of the thermal comfort, some information about the inhabitants' behaviour, such as occupancy level and DHW consumption, should be taken into account in the control logic. For instance, by knowing the metabolic rate and the activities of the occupants and the appliances usage, it is possible to estimate the related internal heat gains. Several studies available in literature have investigated the good potential of such control improvements.

Regarding the occupancy level measurements, many solutions are provided, such as Passive InfraRed (PIR), CO₂ sensors and image processing systems. The first solution adopts a Markov Chain algorithm [18] for the prediction of the future occupancy level, while the second one is based on the correlation between the CO₂ indoor concentration and a specific occupancy pattern. The third solution, however, has the highest accuracy level, thanks to infrared cameras that collect data about the different transitions occurring in the room where they are placed; then, a prediction model can be obtained by using these data in a Markov Chain algorithm.

As concerns the DHW consumption, the model developed by Lomet et al. [19] is based on historical consumption data: for instance, the algorithm considers the hot water request data of the previous day and of the same day of the previous week, and it accounts for the consumption variations due to the holidays as well. An interesting approach was followed by Widén et al. [18], who developed a model starting from a dataset collected by a previous Statistics Sweden study, in which the trained participants reported on a diary the time and the description of the activities they performed during the test period. The authors then related the collected data to the energy-load profile, obtaining a model for the generation of electricity and DHW consumption profiles.

1.6. Thermal comfort assessment

An example of integration of the DHW consumption profile in the control logic of a heat pump system is given by the work of Sundbrandt [20], who designed an optimal control strategy based on a MPC controller, which includes the DHW consumption profile in the energy balance equation of the water storage tank. As a result, the controller is able to predict the evolution of the water temperature in the tank, applying optimised control signals over the prediction horizon, with a consequent energy saving of about 1–3% with respect to a basic controller.

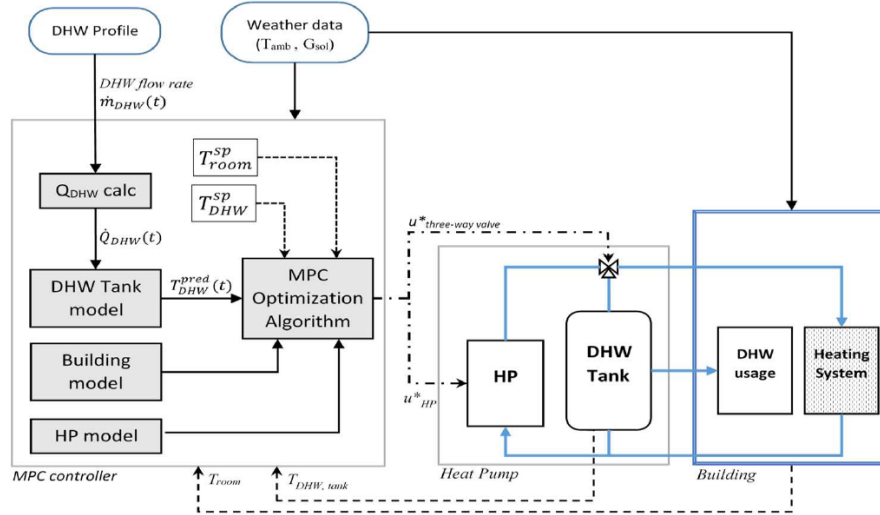


Figure 1.19: Diagram of the DHW consumption profile integration in the MPC controller. Source: [20].

1.6 Thermal comfort assessment

The thermal comfort parameter can be measured according to two major methods, based on the Fanger’s Predicted Mean Vote (PMV) and on the indoor temperature value.

As explained in [21], the PMV indicator varies in a range between -3 and $+3$, according to ambient temperature, radiant temperature, humidity, air velocity and occupants’ clothing. For instance, the comfort condition is represented by a PMV value between -0.5 and $+0.5$, whereas a PMV value greater than $+2$ or lower than -2 indicates, respectively, a hot and a cold comfort situation.

On the other hand, the second method is only dependent on the room temperature: this simple approach is based on the assumption that the thermal comfort is achieved when the ambient temperature is kept in between a lower and an upper threshold, around the set-point temperature value. Thanks to its simplicity, this method is widely adopted in the scientific literature.

Chapter 2

System modelling

The aim of this work is to develop and test some improved control techniques for a ground-source on/off controlled heat pump in a single-family house, after having carried out a comparison between two different layouts of the heating system. As already mentioned in the literature review, nowadays, heat pump systems are controlled according to the current outdoor temperature. However, taking into account different system disturbances, such as inhabitants' occupancy, DHW consumption and solar radiation, could lead to a significant energy saving and thermal comfort enhancement. The starting point of the present work is the system model implemented in [1], which has been used to test different control strategies, based on perfect prediction of weather conditions and human behaviour. In particular, each improved control logic has been implemented in a separate and independent system model, with a system configuration described further below and referred to as "Layout A". A different configuration, referred to as "Layout B", has been here adopted: after performing a comparison between the former and the latter, in terms of SPF, average COP, energy saving and thermal comfort, three different improved control logics are at first tested separately and eventually their combination is implemented within Layout B.

In this chapter, a general⁴ description of the main features of the system model built up in [1] – and of its sub-models – is provided. Particular attention is paid to the differences between Layout A and Layout B, outlining the functions of the new components introduced in the latter configuration. As concerns the control system, the model of a basic degree-minute on/off controller is here illustrated, whereas the description of the improved control system is provided in the next chapter.

2.1 Methodology

The study carried out in [1] and in the present work considers a typical Swedish single-family house located in Stockholm, inhabited by four people – two adults and two children – in order to account for Swedish typical internal heat release and DHW consumption. The heating system is composed by a single-speed GSHP unit, coupled with an electrical auxiliary heater and connected to a U-tube BHE,

⁴For a more detailed description of the system model, please refer to the work of Braida and Tomasetig [1].

providing hot water to a stratified storage tank and to the heating distribution system.

The adopted methodology is based on numerical simulations performed in the TRNSYS[®] software environment, where all the system elements have been modelled. A suitable time resolution has been adopted according to the purpose of the analyses and to the behaviour of the numerical model: in particular, a time step of three minutes has been set for the simulations related to the heating season, whereas, for the summer period, in which the control logic for the DHW heating has been analysed, the simulations have been performed with a time step of one minute, for an enhanced behaviour of the numerical model. Subsequently, the parameters of the modelled system have been tuned through trials and tests, until a behaviour representative of a real system has been obtained [1]. Afterwards, the improved control logics have been implemented, using a trial-and-error procedure for the tuning of their parameters, and the comparison with the base model has been performed.

2.2 Model elements

2.2.1 Building

According to the TABULA (Typology Approach for BUilding stock energy Assessment) database [22], the building properties have been selected in order to create a model representative of a typical Swedish single-family house built in the period 1995–2005. In particular, by means of the embedded TRNBUILD software package, the TRNSYS[®] Type56 component has been used to define all the building properties, such as orientation and size of walls and windows, layers thickness and materials. For the sake of simplicity, the house is represented by a single zone with a flat roof and the glazing surfaces are located only on the walls facing North and South. Furthermore, the building heating process is composed by radiative and convective heat transfer contributions, but also air infiltrations⁵ and internal heat gains are taken into account in the model. The energy and peak power demand for the building heating have been calculated thanks to the “energy mode” option of Type56, which allows to compute the thermal power required to keep the indoor temperature at a desired set-point. More specifically, the building properties – layers thickness and windows dimensions – have been tuned in order to obtain an energy demand close to the values available on the TABULA database: the resulting heating energy demand and the peak power demand are respectively 153 kWh/m² and 6.83 kW. All the aforementioned properties and parameters are reported in Tab. 2.1 on the next page.

⁵According to ASHRAE, the air change per hour parameter (ACH) has been set to 0.8.

2.2. Model elements

Table 2.1: Building properties and parameters.

Element	Materials	Surface [m ²]	Thickness [m]	Thermal transmittance [W/(m ² K)]
External walls	Gypsum plaster Aerated concrete	27x4	0.3	0.314
Floor	Stone wool Cinder base Concrete Yellow pine	125	0.383	0.193
Roof	Shingle roof Sheathing ply- wood Stone wool Polyethylene film Gypsum plaster with sand	125	0.221	0.175
Triple windows	Glass Air	6 (North) 9 (South)	0.036	1.4

2.2.2 System disturbances: weather and human behaviour

The system behaviour is strongly affected by the weather conditions and by the inhabitants' activities, therefore it is of primary importance to account for these disturbances in the system model.

Weather

The building heat and mass transfer with the external environment is dependent on the meteorological conditions, hence different weather parameters have been considered: outdoor temperature, solar radiation, humidity fraction, wind speed and cloudiness. Among the different available methods for collecting these data, the “typical meteorological year” described by the Meteonorm[®] software has been employed [23]. In particular, it represents the typical climate conditions of a specific location – in this instance, the humid continental climate, characteristic of the Stockholm area – and it is computed through statistic combinations of the weather data available for the last decades. The Meteonorm[®] data are implemented in TRNSYS[®] by means of the Type15–6 component, which reads the meteorological conditions recorded by the weather station of Arlanda, Stockholm. This component provides to the building model the solar radiation data, accounting for the walls inclination and cardinal orientation: in particular, it computes the radiation on a tilted surface starting from the horizontal one and accounting for different parameters, such as the time of the year, the solar angle, the latitude and the longitude. Another input required by the building model is the sky temperature,

which is computed by a suited component that considers the dew temperature and the outdoor temperature.

Human behaviour

The human behaviour is modelled considering the heat release from people's activity and domestic lighting, and accounting for the DHW consumption over the time.

In order to account for the internal loads, the stochastic model introduced in the literature review [18] has been used to create a weekly occupancy profile (see Fig. 2.1), to which the metabolic rate and the lighting power have been associated. More specifically, the metabolic rate depends on the type of activity performed by the body, therefore it has been computed considering an activity schedule over the week, with three different types of activities – sleeping, light and medium – during the day, to which a specific metabolic rate is related [24], as reported in Tab. 2.2 and in Fig. 2.2 on the facing page. For the sake of simplicity, the same type of activity, and hence the same metabolic rate, is assumed for all the inhabitants.

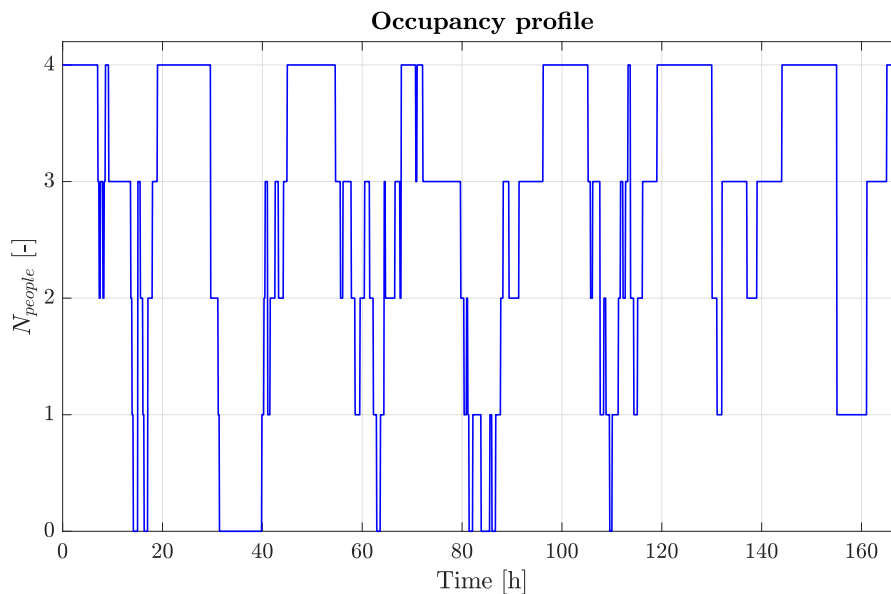


Figure 2.1: Weekly occupancy profile (time resolution: 5 minutes). Source: [18].

Table 2.2: Metabolic rate values according to the type of activity.

Activity	Signal [-]	Metabolic rate [W/person]
Sleeping	0	83
Light	1	167
Medium	2	208

2.2. Model elements

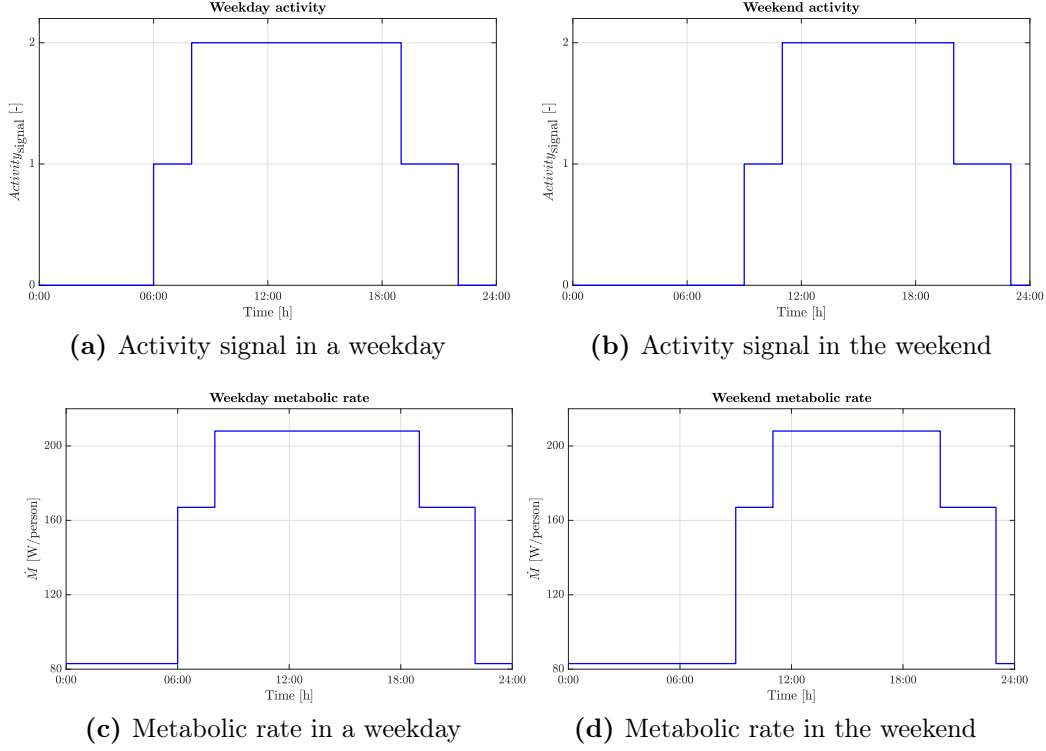


Figure 2.2: Activity signal and metabolic rate during the weekdays and the weekend.

The contribution of the occupants’ activities to the internal loads has been computed by simply multiplying the number of people by the metabolic rate value:

$$\dot{Q}_{\text{people}} = N_{\text{people}} \cdot \dot{M} \quad (2.1)$$

where \dot{Q}_{people} is the thermal power released by the occupants, N_{people} is the number of occupants and \dot{M} is the metabolic rate of a single person.

On the other hand, as reported in the following equations, the contribution of the lighting power to the internal heat release has been computed by considering the actual presence of the inhabitants in the house ($N_{\text{people}} > 0 \Rightarrow \text{Occupancy}_{\text{signal}} = 1$), the type of activity and the solar radiation. More specifically, the lighting system is operating ($\text{Light}_{\text{signal}} \neq 0$) only if the activity is light or medium ($\text{Activity}_{\text{signal}} \neq 0$); moreover, the amount of lighting power emitted is dependent on the external and natural light, and hence on the solar radiation, through the “daylight coefficient”:

$$\text{Daylight}_{\text{coeff}} = G_H / G_{H_0} \quad (2.2)$$

$$\text{Light}_{\text{signal}} = \text{Occupancy}_{\text{signal}} \cdot \text{Activity}_{\text{signal}} \quad (2.3)$$

$$\dot{Q}_{\text{light}} = P_{\text{light},0} \cdot \max(0, 1 - \text{Daylight}_{\text{coeff}}) \cdot \text{Light}_{\text{signal}} \quad (2.4)$$

According to Eq. (2.2), the daylight coefficient is defined as the ratio between the actual value of the total (beam and diffuse) horizontal radiation G_H and its reference value G_{H_0} , which has been set to 1 kW/m^2 . Similarly to the values found in literature [18], the reference lighting power $P_{\text{light},0}$ has been set to 280 W .

As concerns the DHW consumption, the profile of the water draw-offs has been created in order to match a total annual energy demand of about 3932 kWh , which

corresponds to an average consumption of 50 litres of hot water per person per day. Differently from the work of Braida and Tomasetig [1], who adopted a stochastic profile for the DHW consumption with an underestimated total annual energy demand (less than half of the value adopted in the present work), a fixed – or deterministic – weekly profile has been here employed for the water draw-offs. In particular, by means of a Macro in the Excel[®] environment, the thermal energy related to the draw-offs has been set for each day of the week with different values at different times of the day, in order to simulate the various hot water needs – either for shower needs or other purposes – and, due to a better response of the model, a maximum value of 20 kW per each time step has been set for the draw-off power (\dot{Q}_{DHW}). The obtained profile is reported in Fig. 2.3, where, analogously to the activity signal profile, a different trend can be noticed between the weekdays and the weekend. As a remark, the DHW consumption is here computed in terms of thermal power of the draw-offs: in fact, the same profile is then sent to a component described further below, which computes the actual DHW mass flow rate related to each draw-off.

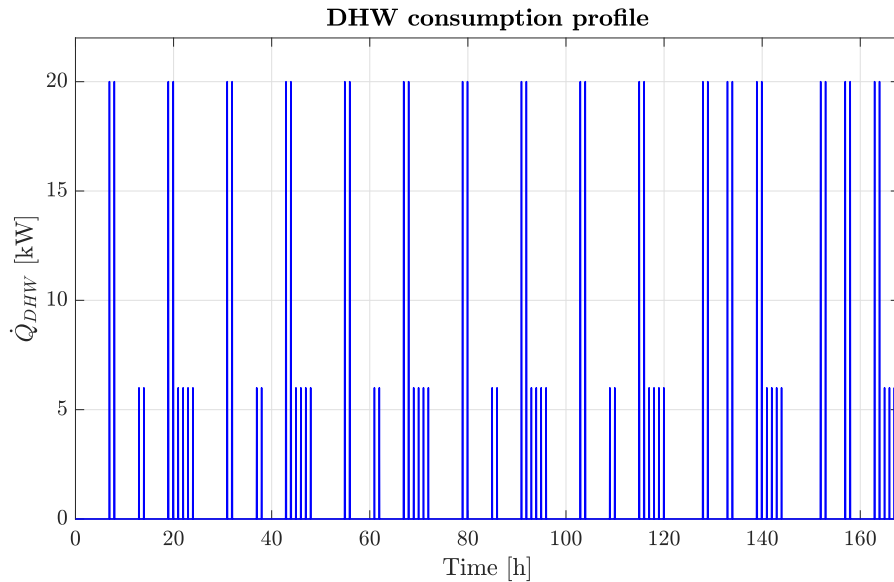


Figure 2.3: Weekly DHW consumption profile (time resolution: 3 minutes).

Subsequently, the occupancy and DHW consumption profiles are provided as inputs to the model by means of two “data reader” components in TRNSYS[®] (Type9), while the activity signal is computed through a simple schedule component and it is then used to calculate the metabolic rate. Finally, as depicted in Fig. 2.4 on the facing page, by providing as input also the solar radiation values for the lighting power estimation, an “equation block” component computes the two contributions to the internal loads, which are then sent as inputs to the building model: in particular, the heat release from people’s activity is considered as a convective contribution, while the heat release from the lighting power is accounted for as a radiative one.

2.2. Model elements

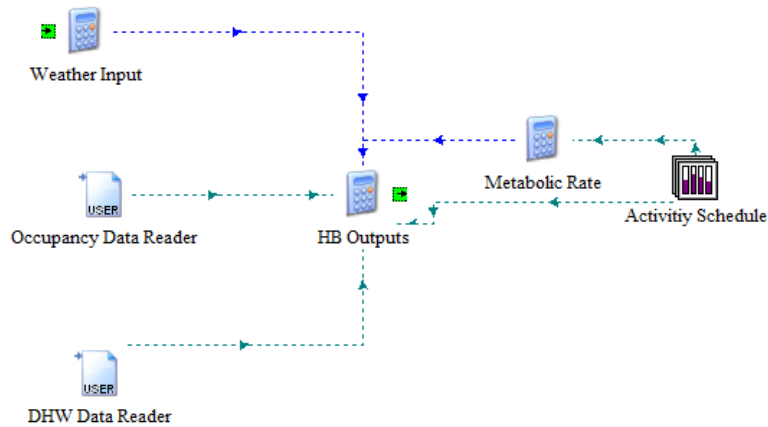


Figure 2.4: TRNSYS[®] components for the human behaviour modelling.

2.2.3 Heating generation loop

In the considered system, the major part of the building energy demand is satisfied by a single-speed ground-source heat pump. When the required energy exceeds the HP capacity, an electrical auxiliary heater is employed – both for SH and DHW purposes. The heating generation loop is then characterised by the heat pump unit, by the borehole heat exchanger on the source side (or brine loop), which also includes the brine pump, by the load side (or load loop) with its load pump, and by the auxiliary heater. Moreover, the inertia of the system is taken into account by modelling the connecting pipes and the tank component described further below.

As already mentioned at the beginning of this chapter, a description of the model components is here provided considering the differences between Layout A and Layout B. Regarding the heating generation loop, as can be observed by Fig. 2.5 and Fig. 2.6 on the next page, the main difference between the two configurations lies in the employment, in Layout B, of the storage tank for DHW purposes only. As a consequence, there is the need to introduce, in the latter configuration, the “load diverter” and “load mixer” components and to remove the AH for SH from the tank and place it after the load diverter. The function of this latter component is to simulate a three-way valve in order to direct the hot water mass flow rate, coming from the HP condenser, either to the tank or to the SH loop, according to the actual needs, but always giving priority to the DHW ones. Analogously, the load mixer component collects the return water, either from the SH loop or from the tank, and sends it to the HP evaporator.

In the following paragraphs, a brief description with the main figures will be provided for the sub-models created in [1], regarding the heat pump, the BHE, the liquid pumps and pipes, and the auxiliary heater.

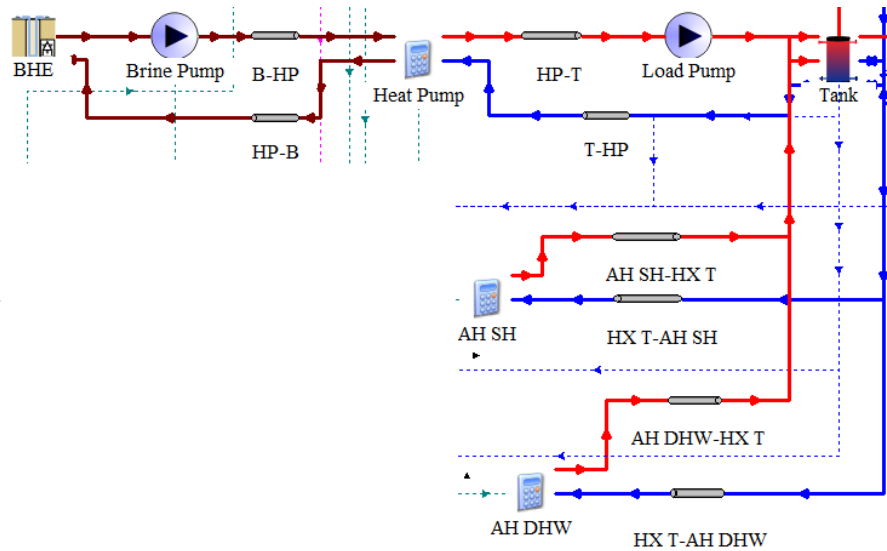


Figure 2.5: TRNSYS[®] heating generation loop: Layout A.

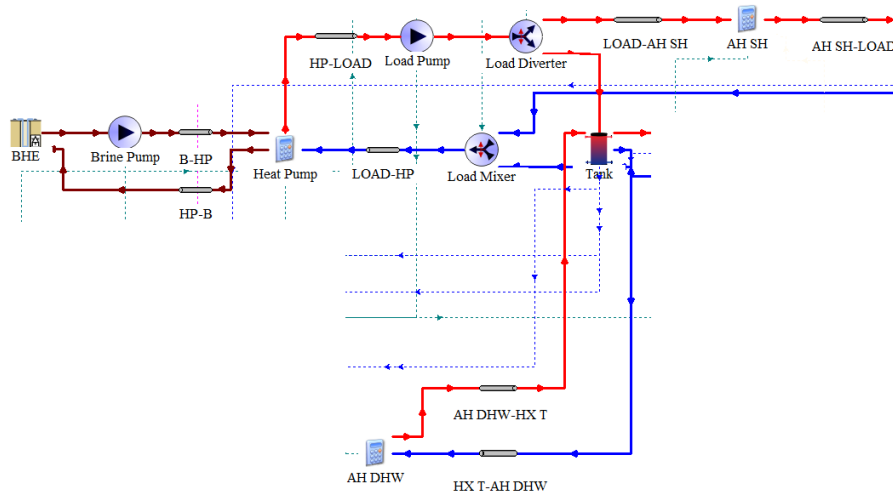


Figure 2.6: TRNSYS[®] heating generation loop: Layout B.

Heat pump modelling and sizing

The heat pump has been modelled by making use of a performance map provided by a project partner, where the compressor power and the condenser and evaporator heat rates are provided for different operating conditions, which depend on the water temperature at the condenser inlet (T_{load} or T_L), on the brine temperature at the evaporator inlet (T_{source} or T_S) and on the compressor frequency (f), as depicted in Fig. 2.7 on the facing page. Indeed, the performance map is referred to a variable-speed HP, however, for the present study, the frequency has been fixed to 50 Hz. The model of the HP is based on the following polynomial functions, which correlate the compressor electrical power and the condenser heat rate with the load

2.2. Model elements

and source temperatures and with the frequency:

$$\begin{aligned}
 P_{\text{compr}} = & p_0 + p_1 T_L + p_2 T_S + p_3 f + p_4 T_L T_S + p_5 T_L f + p_6 T_S f + p_7 T_L^2 \\
 & + p_8 T_S^2 + p_9 f^2 + p_{10} T_L^2 T_S + p_{11} T_L T_S^2 + p_{12} T_L^2 f + p_{13} T_S^2 T_f \\
 & + p_{14} T_L f^2 + p_{15} T_S f^2 + p_{16} T_L T_S f + p_{17} T_L^3 + p_{18} T_S^3 + p_{19} f^3
 \end{aligned} \tag{2.5}$$

$$\begin{aligned}
 \dot{Q}_{\text{cond}} = & c_0 + c_1 T_L + c_2 T_S + c_3 f + c_4 T_L T_S + c_5 T_L f + c_6 T_S f + c_7 T_L^2 \\
 & + c_8 T_S^2 + c_9 f^2 + c_{10} T_L^2 T_S + c_{11} T_L T_S^2 + c_{12} T_L^2 f + c_{13} T_S^2 T_f \\
 & + c_{14} T_L f^2 + c_{15} T_S f^2 + c_{16} T_L T_S f + c_{17} T_L^3 + c_{18} T_S^3 + c_{19} f^3
 \end{aligned} \tag{2.6}$$

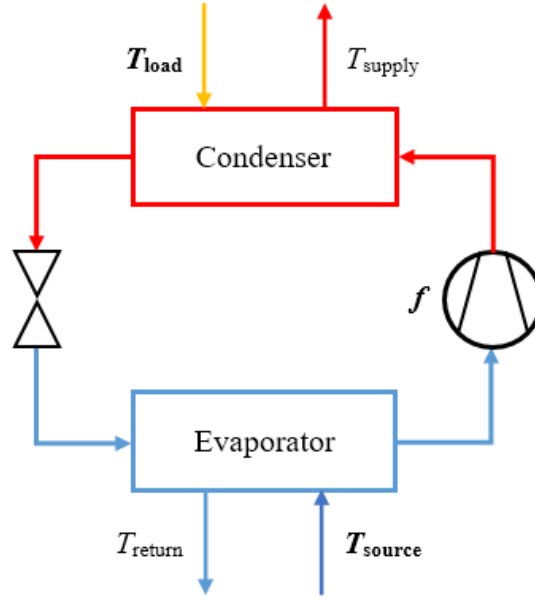


Figure 2.7: Heat pump block diagram.

The polynomial coefficients p_i and c_i , with $i = 1, \dots, 19$, have been found for each operating point of the HP by assuming initial values and changing them in order to minimise the Mean Square Error (MSE), defined as follows, through the solver tool available in the Excel[®] environment:

$$MSE_{\dot{Q}_{\text{cond}}} = \sqrt{\sum_{i=1}^{N_{\text{points}}} \left(\dot{Q}_{\text{cond}}^{\text{map}} - \dot{Q}_{\text{cond}}^{\text{poly}} \right)_i^2} \tag{2.7}$$

$$MSE_{P_{\text{compr}}} = \sqrt{\sum_{i=1}^{N_{\text{points}}} \left(P_{\text{compr}}^{\text{map}} - P_{\text{compr}}^{\text{poly}} \right)_i^2} \tag{2.8}$$

where the superscripts “map” and “poly”, used for the compressor power and the condenser heat rate, respectively refer to the values provided by the manufacturer and to those computed through the polynomial functions. Subsequently, by simply applying the energy balance to the HP, it is possible to obtain the evaporator heat rate, assuming that a fraction of 5% of the compressor electrical power is dissipated in the form of heat to the environment. Moreover, applying again the first law of

thermodynamics to the condenser and to the evaporator in two separate control volumes, it is possible to compute the water temperature at the condenser outlet (T_{supply}) and the brine temperature at the evaporator outlet (T_{return}), being the mass flow rates of the primary (\dot{m}_w) and secondary (\dot{m}_b) fluids fixed, and neglecting the thermal losses:

$$\dot{Q}_{\text{eva}} = \dot{Q}_{\text{cond}} - 0.95 \cdot P_{\text{compr}} \quad (2.9)$$

$$T_{\text{supply}} = T_{\text{load}} + \frac{\dot{Q}_{\text{cond}}}{\dot{m}_w \cdot c_{p,w}} \quad (2.10)$$

$$T_{\text{return}} = T_{\text{source}} - \frac{\dot{Q}_{\text{eva}}}{\dot{m}_b \cdot c_{p,b}} \quad (2.11)$$

where $c_{p,w}$ and $c_{p,b}$ are respectively the specific heat of water and brine. The validation of the model has been performed by computing the COP variation with respect to the load temperature at a fixed source temperature – and vice versa – and verifying that for a temperature change of about 1 K, the corresponding COP variation in absolute terms is in the range of 1–3%.

As a remark, according to the data provided in the performance map, the HP resulted to be oversized (37 kW) for the needs of a single-family house; therefore, it was necessary to resize the HP capacity, by means of a normalisation of the polynomial functions, assuming an arbitrary reference point from the performance map.

Subsequently, the HP sizing has been obtained by means of a trial-and-error procedure, in order to obtain, as mentioned in the literature review [10], a bivalent temperature included in between -6°C and -3°C and a fraction of the building peak load and of the total annual energy demand, covered by the HP, of respectively 75% and 95%. Therefore, the selected nominal HP capacity is of about 6.5 kW, to which corresponds a compressor electrical consumption of about 1.26 kW in nominal conditions – i.e. with a COP of about 5.14, when the inlet and outlet temperatures of the primary fluid are respectively equal to 22°C and 25°C , and those of the secondary fluid are respectively equal to 9.7°C and 6.7°C . In the TRNSYS[®] environment, the HP model has been implemented by means of a simple equation block, where the polynomial functions are provided, and where the intermittent operation of the HP is obtained by multiplying the condenser heat rate and the compressor power by a control signal (CS_{HP}).

Borehole heat exchanger

The borehole heat exchanger is modelled by means of the TRNSYS[®] Type243, which simulates a vertical BHE with a single U-tube configuration, where a water-ethanol mixture flows (the antifreeze concentration is 30%). The heat transfer between the ground and the brine is evaluated by dividing the borehole into successive layers and by applying the “thermal resistance and capacity model”. The main features of the BHE component are reported in Tab. 2.3 on the next page.

2.2. Model elements

Table 2.3: Main parameters and settings of the BHE component.

Parameter	Value	Unit
U-tube length	250	m
BHE buried depth	1	m
BHE radius	0.075	m
Outer radius of U-tube pipe	0.016	m
Inner radius of U-tube pipe	0.013	m
Geothermal gradient	0.025	°C/m
Average ambient temperature	5.5	°C
Fluid specific heat	3.4	kJ/(kg K)
Fluid thermal conductivity	0.597	W/(m K)
Fluid density	974	kg/m ³

Brine and load pumps and pipes

The mass flow rates of the fluids circulating in the source and load loops are controlled respectively by the brine and load pumps. The former operates intermittently as the HP compressor, while the latter operates continuously in order to always recirculate the primary fluid in the condenser. The mass flow rate values of 0.55 kg/s (2000 kg/h), for the source loop, and of 0.21 kg/s (750 kg/h), for the load loop, have been chosen after a trial-and-error procedure, in order to obtain a reasonable temperature difference in the heat exchangers of about 3 °C to 6 °C, according to the thermal power. Moreover, for the load loop mass flow rate, it has also been verified that its value is higher than the minimum required mass flow rate in the radiator loop, estimated by considering the building peak heating demand, therefore at DOT conditions (for the location of Stockholm, the DOT value is -18 °C), and assuming, for the water in the radiator loop, a temperature drop of 10 °C: the resulting minimum mass flow rate value is of about 587 kg/h.

In order to account for the thermal inertia of the hydronic system, the pipes connecting the different components are modelled by defining their length and internal diameters (see Tab. 2.4); moreover, they are assumed as perfectly insulated from the environment.

Table 2.4: Geometrical parameters for the pipes modelling.

Parameter	Unit	Source loop	Load loop	AH loop
Length	m	60	10	10
Inner diameter	mm	26	37.5	37.5

Auxiliary heater

In order to completely satisfy the peak heating demand, an electrical auxiliary heater, with an efficiency of 90%, is employed. In particular, in Layout A, this component is connected to two coiled heat exchangers (HX), immersed in the top and in the middle of the storage tank, in order to supply additional thermal power, respectively for DHW and SH needs. Whereas, in Layout B, since the tank is used for DHW purposes only, the heat exchanger for SH is placed after the load diverter component. More specifically, the AH is able to provide a maximum thermal power of 9 kW ($\dot{Q}_{AH,max}$), through nine different electrical resistances of 1 kW each: when an additional power is required for the DHW, the AH supplies 5 kW, while it delivers up to 9 kW in three different stages of 3 kW each, when the space heating demand exceeds the HP capacity. Considering the control logic, the AH receives as control signal, from the degree-minute controller, an integer number from one to three, according to the additional power required; therefore, the delivered power for SH is computed as follows:

$$\dot{Q}_{AH} = \frac{1}{3} CS_{AH,SH} \cdot \dot{Q}_{AH,max} \quad (2.12)$$

where \dot{Q}_{AH} is the supplied thermal power and $CS_{AH,SH}$ is the control signal computed by the degree-minute controller.

The temperature of the water exiting the AH ($T_{AH,out}$) is computed by simply applying the energy balance to the component, given the temperature of the entering water ($T_{AH,in}$) from the tank or from the load diverter, and being fixed the mass flow rate (\dot{m}_{AH}) circulating inside the AH. In Layout A, its value – obtained once again with a trial-and-error procedure – is of 0.14 kg/s (500 kg/h), while in Layout B, the same mass flow rate leaving the HP condenser flows through the AH:

$$T_{AH,out} = T_{AH,in} + \frac{\dot{Q}_{AH}}{\dot{m}_{AH} \cdot c_{p,w}} \quad (2.13)$$

2.2.4 Stratified storage tank

The hot water tank employed in the system model is the TRNSYS[®] Type534, called “vertical cylindrical storage tank with immersed heat exchangers”. It is characterised by a constant volume of 300 litres and a height of 1.5 m and it presents a vertical temperature stratification (see Fig. 2.8 on the next page), based on the definition of ten layers (or nodes), in order to minimise the temperature difference between the internal water and the entering flow, hence reducing the exergy losses due to the mixing process of two fluids at different temperatures.

According to the two different system layouts compared in the present work, the tank is equipped with either two or three ports dedicated to the HP, SH (only in Layout A) and DHW loops. For each port, the inlet node position depends on the water temperature entering the tank, in order to preserve the thermal stratification, while the outlet node is predefined, as reported in Tab. 2.5 on the facing page. In particular, for the HP loop, the return water to the condenser is drawn from the bottom of the tank (node 10); for the DHW loop, the hot water leaves the tank

2.2. Model elements

from the top (node 1) and it is reintegrated by cold tap water at 10°C from node 10, being the one with lowest temperature; as concerns the SH loop in Layout A, the hot water is delivered to the heating distribution system from the middle of the tank (node 5). Moreover, being the tank volume constant, each outflow must be balanced by the corresponding entering flow. As a remark, according to the mathematical reference of the storage tank library, available in the TRNSYS® documentation, the inlet fluid into a node is completely mixed with the storage tank fluid at every time step, before it moves on to the next node (the fluid flow path is directly from the inlet node to the outlet node).

As it will be shown in the next chapter, thanks to the introduction of the storage tank in the heating system it is possible to uncouple the thermal power production – i.e. the HP unit and the AH – from the energy consumption, represented by the SH and the DHW request. Therefore, in Layout A, the thermal inertia of the system is increased and the oscillations of the supplied water temperature are reduced, differently from Layout B, where a lower stability of the room conditions is expected.

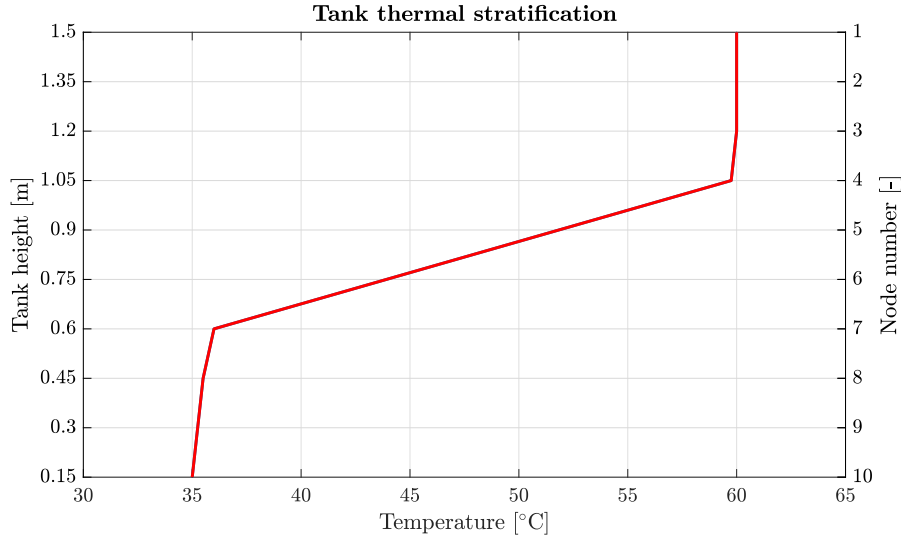


Figure 2.8: Temperature stratification of the storage tank.

Table 2.5: Ports configuration of the tank in Layout A and Layout B.

Layout	Port	Inlet node	Outlet node
A, B	1 (HP)	Closest to flow temperature	10
A	2 (SH)	Closest to flow temperature	5
A, B	3 (DHW)	Closest to flow temperature	1

Finally, as previously mentioned, the HP is coupled with an AH which is connected to a coiled heat exchanger for DHW, placed at top of the tank, and, only in Layout A, to another one for SH, placed at the middle of the tank. Their main parameters are reported in Tab. 2.6 on the next page. As regards the tank thermal losses, a simplification has been made assuming the lateral surface as adiabatic,

while a loss coefficient of $2.8 \text{ W}/(\text{m}^2 \text{ K})$ has been adopted for the top and bottom surfaces of the tank, with a constant temperature of the surrounding environment equal to 20°C .

Table 2.6: Main parameters of the coiled heat exchanger.

Parameter	Value	Unit
Tube inner diameter	20	mm
Tube outer diameter	22	mm
Tube length	20	m
Coil diameter	500	mm
Coil pitch	20	mm
Wall conductivity	20	$\text{W}/(\text{m K})$

DHW consumption

As explained in section 2.2.2, the data related to the DHW consumption are provided in terms of thermal power of the draw-offs. In particular, as illustrated in Fig. 2.9, the mass flow rate of the DHW consumed by the occupants, during each draw-off, is computed in an external and ideal heat exchanger, modelled in TRNSYS[®] by means of a simple equation block. The input values provided to the HX are the thermal power related to the draw-off (\dot{Q}_{DHW}), the water temperature at the top node of the tank (T_{N1}), where the draw-off occurs, and the water temperature at the bottom node of the tank (T_{N10}), where cold tap water at 10°C is introduced. Therefore, the mass flow rate of DHW is computed as follows:

$$\dot{m}_{DHW} = \min \left(\frac{\dot{Q}_{DHW}}{c_{p,w} \cdot (T_{N1} - T_{N10})}, \dot{m}_{DHW,max} \right) \quad (2.14)$$

where $\dot{m}_{DHW,max}$ is a limit value for the DHW mass flow rate from the tank, in order to avoid its abnormal increase in the event of a small temperature difference between the top and bottom nodes of the tank. In particular, the value has been set to 0.57 kg/s , considering the pipes diameter (see Tab. 2.4 on page 35) and assuming a maximum flow velocity of 0.5 m/s .

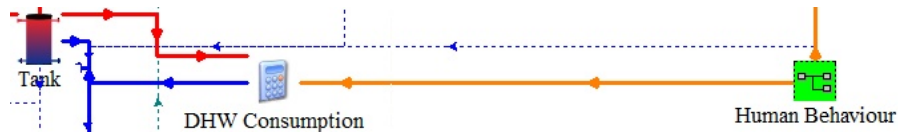


Figure 2.9: DHW consumption in the TRNSYS[®] model.

2.2.5 Heating distribution loop

As already mentioned, the main difference between Layout A and Layout B lies in the heating distribution loop. In the former, the required thermal power is

2.2. Model elements

released from the storage tank, while in the latter the space heating loop is fed directly from the condenser of the heat pump.

Thanks to the uncoupling from the heating generation loop, through the storage tank, it is possible to obtain an increased thermal inertia of the system in Layout A; in addition, the indoor temperature stability is enhanced also by using a PI (Proportional-Integral) controller, as depicted in Fig. 2.10. More specifically, the value of the required supply temperature, provided from the heating curve component (described in the next section), is chosen as set-point for the PI controller, while the monitored variable is the actual temperature value of the water entering the radiator. Therefore, the computation of the output control signal is made in order to reduce as much as possible the difference between these two temperature values, by mixing the incoming flow of hot water from the tank with the exhaust water flow leaving the radiator. The control signal is sent to a diverter, which accordingly divides the mass flow rate coming from the radiator into two separate flows, which are then merged together in the mixer component, respecting the mass balance of the radiator loop. As regards the PI controller settings, its control signal can float between a minimum and a maximum value, respectively set to 0 and 1, its gain constant is 0.55 and its integral time is set to 1 h. The computed control signal is also sent to the radiator model and to a variable-speed pump, whose delivered mass flow rate to the radiator is obtained by multiplying its prefixed maximum value (the same value adopted for the load pump) by the control signal itself.

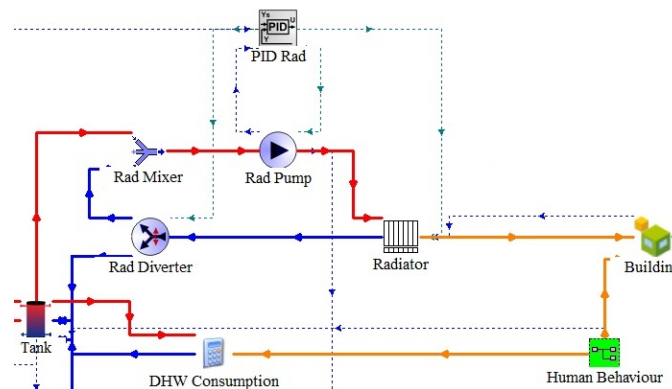


Figure 2.10: TRNSYS[®] heating distribution loop: Layout A.

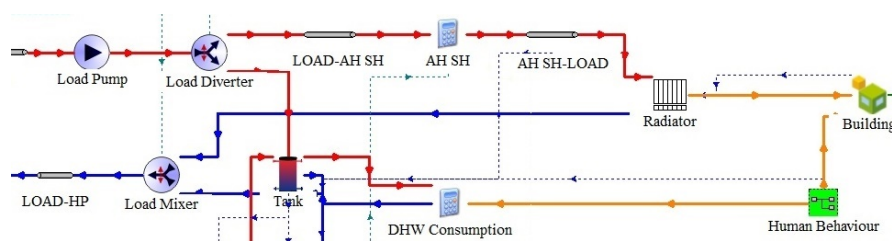


Figure 2.11: TRNSYS[®] heating distribution loop: Layout B.

The employment of a PI controller in Layout B is complicated by the direct connection between the heating generation loop and the radiator loop; since the

mass flow rate at the inlet and outlet of the HP condenser must be the same, it cannot be divided in two separate flows in a diverter, when returning from the radiator loop. Therefore, as can be seen in Fig. 2.11 on the previous page, the hot water leaving the HP condenser is sent to a mass flow diverter which, accordingly to the type of energy request (DHW or SH), directs the flow either to the tank or to the space heating loop; if the building heating demand exceeds the HP capacity, the supplemental power required is delivered by the electrical AH placed before the radiator loop. As one can expect, such a configuration leads to frequent oscillations of the supply water temperature and, consequently, of the indoor temperature.

As concerns the radiator model, the TRNSYS[®] Type362 – called “Dynamic radiator model with pipes” – has been adopted. Its heating capacity is computed by considering the room temperature and the energy delivered by the supply water flow. According to the available documentation of Type362 [25], the coupling with the building model (Type56) is made by switching off its heating equipment and providing to it as input, instead, the emitted power from the radiator, composed by a convective and a radiative fraction of 80% and 20% respectively. The main features of the radiator component are reported in Tab. 2.7, where it can be observed that the thermal inertia of the radiator loop is already accounted for by the presence of the pipes inside the model.

Table 2.7: Adopted parameters for the radiator model.

Parameter	Value	Unit
Length of supply pipes	30	m
Length of exhaust pipes	30	m
Pipes diameter	37.5	mm
Nominal power of radiator	10	kW
Radiator exponent	1.3	–
Emissivity	1	–

2.2.6 Control system

The performance evaluation of the improved control logics, described in the next chapter, has been carried out by means of a comparison with a basic control logic system, composed by different elements, which are necessary to achieve the correct operation of the whole heating system: the heating curve, the on/off hysteresis controller, the so called “HUB” component, and the degree-minute controller along with the auxiliary heater controller for DHW. Fig. 2.12 and Fig. 2.13 on the next page illustrate, respectively, a block diagram of the basic control logic system and its model in the TRNSYS[®] environment.

2.2. Model elements

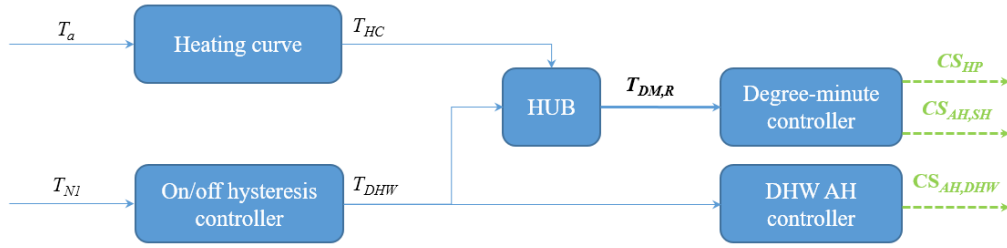


Figure 2.12: Block diagram of the basic control logic.

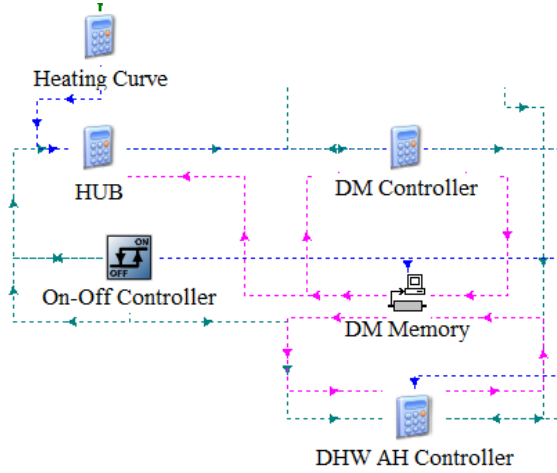


Figure 2.13: TRNSYS[®] model for the basic control logic system.

Heating curve

As described in the literature review, the function of the heating curve (HC) is to compute the required supply temperature for the space heating (T_{HC}), according to the outdoor temperature. Different models for the heating curve are available in literature, however, for a simpler implementation, a linear model has been used in [1] and in the present work. In particular, the adopted heating curve has been defined by means of a piecewise linear function, divided in two intervals, for a better tracking of the room temperature with respect to the ambient one, as shown in Fig. 2.14 on the following page and according to the following equation:

$$T_{HC} = \begin{cases} m_1 \cdot T_a + q_1, & \text{if } T_a \leq T_{a,\text{limit}} \\ m_2 \cdot T_a + q_2, & \text{if } T_a > T_{a,\text{limit}} \end{cases} \quad (2.15)$$

where T_a is the ambient temperature, $T_{a,\text{limit}}$ is the outdoor temperature value at which the heating curve changes behaviour, and m_i and q_i are, respectively, the slope and the intercept of the linear function in the i -th interval, with $i = 1, 2$.

The parameters m_i and q_i of the heating curve have been tuned by means of a trial-and-error procedure, in order to obtain, over a fixed simulated period, a uniform distribution of the observed room temperature around the set-point value of 21 °C. In the TRNSYS[®] model, the heating curve and its parameters are implemented in an equation block. Moreover, given the different climate conditions

with respect to the different periods of the heating season, both in terms of outdoor temperature and solar radiation, the employment of a heating curve with varying parameters accordingly to the period of the year leads to a better performance in terms of indoor conditions, with respect to the employment of a unique formulation of the HC for the whole heating season. Hence, for each of the analysed periods of the heating season, specific parameters have been tuned through the aforementioned procedure.

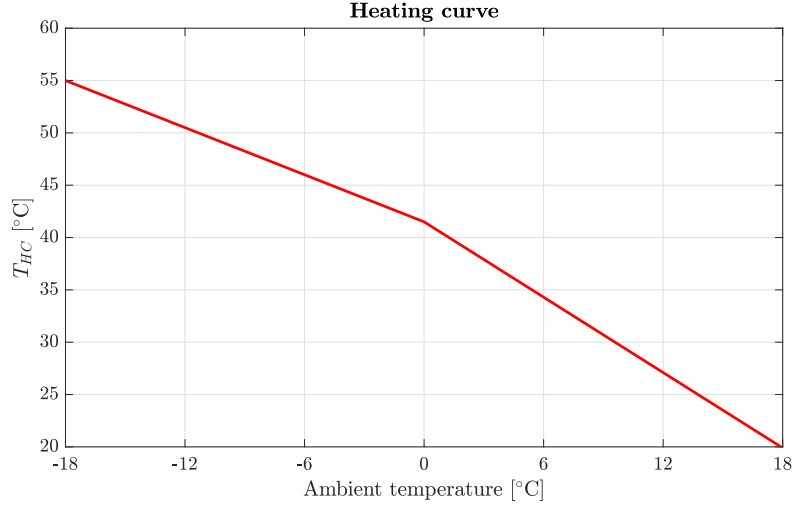


Figure 2.14: Example of heating curve adopted in the simulations.

On/off hysteresis controller and HUB component

Since priority is always given to the DHW demand rather than to the SH request, considering also the greater thermal inertia of the latter, the on/off hysteresis controller is used to compute a control signal (CS_{mode}), which can be one or zero, depending on the two possible operating modes of the heating system: “DHW mode” or “SH mode”. The computed signal is based on the tank top node temperature, which cannot be lower than an imposed threshold value of 44.5 °C, for safety – i.e. to avoid the spreading of Legionella – and comfort reasons. Moreover, the constant hysteresis value has been set to ± 1.5 °C, around the adopted set-point temperature for DHW, which is 60 °C in the present work, differently from the set-point of 45 °C, with a hysteresis of ± 2.5 °C, used in [1].

The signal provided by the on/off hysteresis controller is then sent to the HUB component – modelled by means of an equation block – which has the function to compute the temperature value tracked by the degree-minute controller, according to the operating mode of the system. Therefore, as explained by Eq. (2.16), when there is a space heating request, the signal computed by the on/off hysteresis controller is zero and the required temperature value, provided by the HUB component to the DM controller ($T_{DM,R}$), is the one computed by the heating curve component (T_{HC}). On the other hand, when there is a DHW demand, the control signal is one and the temperature value is the set-point temperature for DHW (T_{DHW}).

$$T_{DM,R} = \begin{cases} T_{HC}, & \text{if } CS_{mode} = 0 \\ T_{DHW}, & \text{if } CS_{mode} = 1 \end{cases} \quad (2.16)$$

2.2. Model elements

Degree-minute controller

The key element of the control logic system is the degree-minute controller, since it provides the control signals for the HP, the brine pump and the AH operation. The aim of this control method is to keep the actual supply temperature, monitored in a specific point of the heating system, as close as possible to the required one, which is provided by the HUB component. As already mentioned in the literature review and as explained by Madani et al. [12], this method is particularly suited for the on/off controlled single-speed HP units. With reference to Eq. (1.4), the provided output is the current DM value (DM_{current}), computed as the summation over the simulated period of the difference between the actual supply temperature and the required one, multiplied by the adopted time step t , expressed in minutes:

$$DM_{\text{current}} = (T_{\text{supply},A} - T_{\text{supply},R}) \cdot t + DM_{\text{old}} \quad (2.17)$$

where DM_{old} is the the degree-minute value at the previous iteration.

Subsequently, the computed DM value is used in the control logic for turning on or off the HP, the source loop pump – whereas the load loop pump is continuously operating – and the different stages of the AH for the space heating demand. The threshold values, employed for the start and stop of the operation of these components, are based on the study of Madani et al. [12] and they are outlined in Tab. 2.8 on the next page.

In particular, the HP is turned on when the current DM value reaches -60°C min and it is turned off when it goes back to zero. Whereas the first, second and third stage of the electrical AH for the space heating request are turned on when the DM value reaches -600°C min , -680°C min and -760°C min respectively, and they are turned off, in reverse order, when the difference between the actual supply temperature and the required one (ΔT_{supply}) is higher or equal to 1°C , 2°C and 3°C respectively. Moreover, the DM parameter is reset to zero when ΔT_{supply} is greater or equal to 10°C or when the DM value is greater or equal to 300°C min . The former constraint is adopted to avoid any undesired increase of the supplied water temperature with respect to the required value, while the latter is used to accelerate the response of the controller. Finally, the DM parameter is reset to zero also when the operating mode of the heating system switches from SH to DHW, or vice versa.

It is worth outlining that the HP control approach is always the same during the SH mode and the DHW mode. The main difference is in the adopted set-point temperature for the two operating modes, provided by the HUB component, as previously explained. Moreover, as a final remark, during the DHW mode, the electrical AH for the DHW demand is controlled by a specific component (the “DHW AH controller” in Fig. 2.12 and Fig. 2.13 on page 41), according to the tank top node temperature. In particular, if the latter remains below the limit of 44.5°C for more than twenty minutes after the starting of the DHW mode, then the auxiliary heater is turned on by the corresponding control signal ($CS_{AH,DHW}$), delivering a power of 5 kW, until the temperature goes back to the imposed limit.

Table 2.8: Threshold values for turning on or off the HP and the AH for the SH demand.

	Component	Turn on	Unit	Turn off	Unit
	HP	$DM_{\text{current}} \leq -60$	$^{\circ}\text{C min}$	$DM_{\text{current}} = 0$	$^{\circ}\text{C min}$
AH	1 st stage (3 kW)	$DM_{\text{current}} \leq -600$	$^{\circ}\text{C min}$	$\Delta T_{\text{supply}} \geq 3$	$^{\circ}\text{C}$
for	2 nd stage (6 kW)	$DM_{\text{current}} \leq -680$	$^{\circ}\text{C min}$	$\Delta T_{\text{supply}} \geq 2$	$^{\circ}\text{C}$
SH	3 rd stage (9 kW)	$DM_{\text{current}} \leq -760$	$^{\circ}\text{C min}$	$\Delta T_{\text{supply}} \geq 1$	$^{\circ}\text{C}$

The described algorithms for the computation of the DM value and of the control signal for the HP activation are reported below:

$$\begin{aligned}
 & \text{if } AND(\Delta T_{\text{supply}} < 10^{\circ}\text{C}, DM_{\text{old}} < 300^{\circ}\text{C min}, CS_{\text{mode}} = CS_{\text{mode,old}}) \\
 & \quad \text{then } DM_{\text{current}} = (T_{\text{supply,A}} - T_{\text{supply,R}}) \cdot t + DM_{\text{old}} \\
 & \quad \text{else } DM_{\text{current}} = 0
 \end{aligned} \tag{2.18}$$

$$\begin{aligned}
 & \text{if } DM_{\text{current}} \leq -60^{\circ}\text{C min} \\
 & \quad \text{then } CS_{HP} = 1 \\
 & \quad \text{else if } -60^{\circ}\text{C min} < DM_{\text{current}} < 0^{\circ}\text{C min} \\
 & \quad \quad \text{then } CS_{HP} = CS_{HP,\text{old}} \\
 & \quad \quad \text{else } CS_{HP} = 0
 \end{aligned} \tag{2.19}$$

where $CS_{\text{mode,old}}$ and $CS_{HP,\text{old}}$ are the control signals of the previous iteration, referring, respectively, to the operating mode of the system and to the activation of the HP. In fact, according to the third condition inside the Boolean AND operator of the former algorithm, when the switching from one operating mode to the other occurs, the DM value is reset to zero, as already explained. Moreover, as stated by the latter algorithm, when the DM value is in between -60°C min and 0°C min , the HP status is kept unchanged, until either the turning on or the turning off threshold value is reached.

Chapter 3

Layout comparison and improved control strategies

3.1 Overview

The present chapter is focused on the comparison of the two system layouts, previously introduced, and on the description of three improved control strategies, which take into account the internal and the external system disturbances. The former are represented by the human behaviour, whose components are the DHW consumption and the internal heat gains from people's activity and domestic lighting. The latter are represented by the weather conditions, in particular by the solar radiation. Accordingly, the developed control strategies are based on the perfect prediction of the DHW consumption and on the heating curve correction method, which considers the internal heat gains profile, adopting both a predictive and non-predictive approach, and the external heat gains, based on the solar radiation data. Hence, this kind of strategy can be implemented within the whole control system, without significant alterations of the heating system design, being therefore applicable to a pre-existing installation. Moreover, considering Layout B, an existing fossil fuel-based heating system, for instance, directly connected to a heating distribution loop and to a thermal storage tank for DHW, can be replaced by a heat pump system, without considerable modifications to the heating distribution loop and to the storage tank.

In the following sections, the details of the control strategy for the DHW consumption are outlined, at first, since it is employed in both system layouts for their subsequent comparison. Afterwards, the improved control logics based on the internal gains profile and on the solar radiation data, applied to Layout B, are described. Eventually, the complete system model, characterized by the combination of all the aforementioned control techniques, is presented.

3.1.1 Heating curve modulation and performance evaluation

The system model described in the previous chapter, adopting the configuration represented by Layout B, has been employed for the testing and evaluation of the developed control strategies, through a learning process based on several TRNSYS®

numerical simulations. As already mentioned, all the different parameters of the described control logics have been tuned by means of a trial-and-error procedure, with the aim of evaluating their maximum potential in terms of energy saving and thermal comfort. Before proceeding with their description and with the layout comparison, it is worth introducing the adopted heating curve correction method and the performance indicators, employed indeed for the evaluation of the developed control strategies and for the comparison of the two system layouts.

As explained in section 2.2.6, the heating curve provides the required supply temperature for the space heating, according to the outdoor temperature, allowing to maintain the room temperature close to the desired set-point. Therefore, if a positive heat gain deriving from a specific disturbance – either internal or external – is expected, the corresponding indoor temperature increase can be compensated by reducing the supply water temperature: this can be performed by acting on the slope and/or on the intercept of the heating curve, reported in Eq. (2.15). The implementation of the control logics based on the heating curve modulation, and described in the present chapter, has been carried out according to the results achieved by the study of Braida and Tomasetig [1].

For the layout comparison and for the performance evaluation of the developed control logics – by means of a comparison with the basic controller –, different parameters or indicators, reported in Tab. 3.1, have been adopted. In particular, they are referred either to the consumed and delivered energy of a specific component, or to the efficiency of the system, or to the comfort conditions.

Table 3.1: Adopted parameters/indicators for the layout comparison and the performance evaluation of the developed control logics.

Energy indicators	Unit
Compressor electrical energy consumption – E_{compr}	
Condenser supplied thermal energy – Q_{cond}	
AH electrical energy consumption – E_{AH}	kWh
AH supplied thermal energy – Q_{AH}	
Total electrical energy consumption – E_{tot}	
Total supplied thermal energy – Q_{tot}	
Efficiency indicators	Unit
COP_{avg}	–
SPF	–
Comfort indicators	Unit
DBD_{DHW}	°C min
DBD_{SH}	°C min
SH comfort time	%

3.2. Improved control logic for the DHW heating

While the energy and efficiency related indicators have already been introduced, a definition of the comfort parameters has not been provided yet. With reference to the ‘‘SH comfort time’’, it is defined as the percentage of the total hours of the simulated period in which the indoor temperature is kept in between 20 °C and 22 °C. Whereas, the dead-band deviation parameter is related to the imposed comfort condition for either the DHW mode (DBD_{DHW}) or the SH mode (DBD_{SH}) of the heating system. In particular, it considers both the duration and the importance of the deviation from the set-point temperature selected as comfort condition.

The DBD parameter for the DHW comfort is computed considering only the time intervals in which the hot water draw-offs for shower needs occur, from the top node of the tank, and it is defined as follows:

$$DBD_{DHW} = \sum_{i=1}^n (T_{\text{limit},i}^{DHW} - T_{N1,i}) \cdot (t_i - t_{i-1}), \quad \text{if } T_{N1,i} < T_{\text{limit},i}^{DHW} \quad (3.1)$$

where n is the number of time steps in the considered period and T_{limit}^{DHW} is the threshold temperature for the supplied DHW, set to 55 °C.

On the other hand, the DBD parameter for the SH comfort is computed as follows:

$$DBD_{SH} = \begin{cases} \sum_{i=1}^n (T_{\text{low},i}^{SH} - T_{\text{room},i}) \cdot (t_i - t_{i-1}), & \text{if } T_{\text{room},i}^{SH} < T_{\text{low},i}^{SH} \\ \sum_{i=1}^n (T_{\text{room},i} - T_{\text{high},i}^{SH}) \cdot (t_i - t_{i-1}), & \text{if } T_{\text{room},i} > T_{\text{high},i}^{SH} \end{cases} \quad (3.2)$$

where T_{room} is the actual indoor temperature, while T_{low}^{SH} and T_{high}^{SH} represent, respectively, the lower and upper limit of the adopted dead-band of ± 0.5 °C around the indoor set-point temperature of 21 °C; therefore, their values are 20.5 °C and 21.5 °C respectively.

3.2 Improved control logic for the DHW heating

The internal disturbance represented by the DHW consumption is here analysed, investigating the potential improvement of the control system, with the aim of minimising the electrical energy consumption, while satisfying the comfort condition for the DHW request. As described in the previous chapter, to each draw-off of hot water from the top of the storage tank corresponds an introduction of cold water from its bottom, resulting in a direct reduction of the water temperature in the tank and in a disturbance to its thermal stratification. Therefore, assuming a perfect prediction of the time in which the water draw-offs will occur, and of their duration, it is possible to overcome the described issues. Moreover, for a preliminary investigation of the control improvement, the influence of the SH request on the tuning of the control logic parameters has been avoided by performing the analysis during the summer season, when only the DHW demand is present. The adopted configuration of the system model is Layout B, however there is no significant difference between the two layouts when only the DHW demand is present.

3.2.1 DHW schedule and “three set-points” configuration

In order to simulate the DHW consumption from the occupants, a fixed weekly schedule has been created, according to the profile of the draw-offs, reported in Fig. 2.3 on page 30. In particular, the schedule profile is provided to the TRNSYS[®] model, by means of a data reader component, in the form of a control signal (CS_{schedule}), which can assume the values reported in Tab. 3.2, according to a configuration based on three set-points. When the schedule value is zero, there is no need for DHW so the system switches to the SH mode, and the temperature value computed by the HUB component is the one provided by the heating curve. Whereas, when the schedule value is one or two, the DHW set-point temperature is 45 °C or 60 °C, respectively: in the first case, called “Normal mode”, DHW at lower temperature is needed for general purposes, while in the second case, called “Shower mode”, the DHW demand is for shower purposes, with a corresponding higher set-point temperature.

Table 3.2: DHW set-point temperature according to the schedule value.

CS_{schedule}	Configuration	Set-point temperature
0	No action \Rightarrow SH mode	T_{HC}
1	Normal mode	45 °C
2	Shower mode	60 °C

Similarly to the draw-offs profile, the DHW schedule profile has a different trend in the weekend if compared to that of the weekdays, as depicted in Fig. 3.1. The obtained weekly profile of the DHW schedule is shown in Fig. 3.2 on the next page, with a time resolution of five minutes, together with the so-called “slide schedule” profile, which basically corresponds to the normal schedule shifted backwards in time (by three hours, in this instance), and it is used in the control logic for the anticipation of the activation of the HP for the DHW demand, as explained further below.

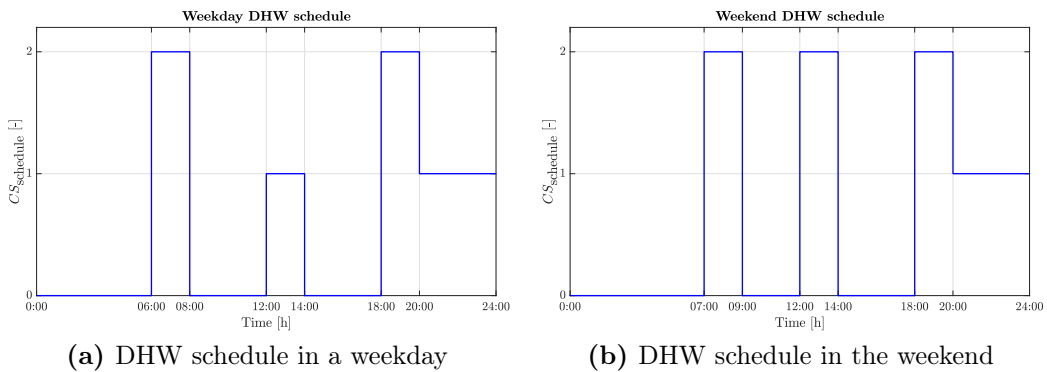


Figure 3.1: DHW schedule profile during the weekdays and the weekend.

3.2. Improved control logic for the DHW heating

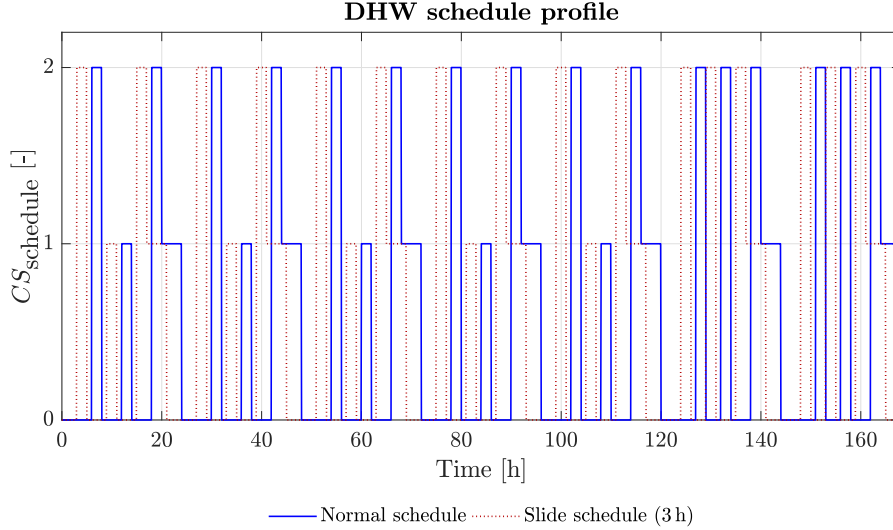


Figure 3.2: Weekly profile of the DHW schedule (time resolution: 5 minutes).

3.2.2 TRNSYS[®] implementation

The implementation of the improved control logic in the TRNSYS[®] model takes place in the HUB element, which is now represented by a “macro” made up of different components, differently from the case of the basic controller, as illustrated in Fig. 3.3 on the following page.

As already mentioned, the DHW schedule profile is provided as input to the “DHW Schedule Reader” component⁶. Subsequently, the control signal CS_{schedule} is provided, together with the value of the tank top node temperature (T_{N1}), to the “Shower Mode” component. Here, the control signal CS_{shower} is computed by means of the following Boolean OR and AND operators:

$$\begin{aligned}
 & \text{if } OR(AND(T_{N1} < 58.5^\circ\text{C}, CS_{\text{schedule}} = 2), \dots \\
 & \quad AND(T_{N1} < 61.5^\circ\text{C}, CS_{\text{schedule}} = 2, CS_{\text{shower,old}} = 1)) \\
 & \quad \text{then } CS_{\text{shower}} = 1 \\
 & \quad \text{else } CS_{\text{shower}} = 0
 \end{aligned} \tag{3.3}$$

where $CS_{\text{shower,old}}$ is the control signal for the Shower mode of the previous iteration. It can be noticed that the same hysteresis value of $\pm 1.5^\circ\text{C}$ around the set-point temperature of 60°C , adopted for the basic controller, has been employed also in the improved control logic, in view of their performance comparison. Therefore, according to this algorithm, the control signal for the Shower mode is equal to one only if, when the schedule value is two, the top node temperature of the tank is in between the lower and upper threshold of the hysteresis. Moreover, for a better fulfilment of the comfort condition, the actual supply temperature of the DHW is read from the middle of the tank (node 5), rather than from the actual supply node: in such a way, the whole upper half-volume of the tank is kept as close as possible to the required supply temperature.

⁶For a correct elaboration of the input data, it is important that their time resolution is an integer multiple of the adopted simulation time step.

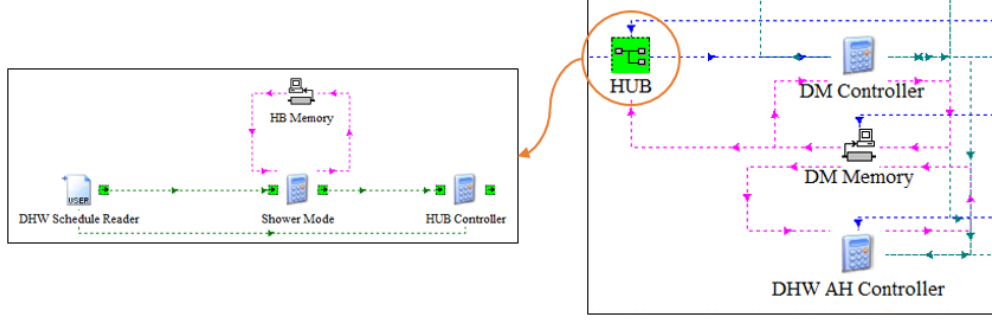


Figure 3.3: TRNSYS[®] model of the HUB component in the improved control logic.

Once the control signal for the Shower mode has been computed, it is sent to the HUB controller component, which has the function to provide, as in the basic control logic, the required supply temperature to the DM controller, according to the operating mode of the system. However, in order to reduce the response time of the DM controller during the DHW mode, when the Shower mode is activated, only for the first iteration, the value assumed by CS_{shower} is two, while it is set to one for the following iterations, as long as the conditions of the above algorithm are verified. In particular, when the Shower mode is activated, the required supply temperature is set to a higher value than the set-point one, by considering the current DM value and the actual supply temperature, in order to reach in a single iteration the threshold value for the activation of the HP. In fact, providing a higher value of the required supply temperature, there is a rapid decrease of the DM parameter, with a consequent quite immediate activation of the HP for the shower needs.

The required supply temperature tracked by the DM controller, reported in Eq. (2.16), in the improved control logic assumes the following definition:

$$T_{DM,R} = \begin{cases} T_{HC}, & \text{if } AND(CS_{\text{schedule}} = 0, CS_{\text{shower}} = 0) \\ T_{\text{supply},A} + \frac{61 + DM_{\text{old}}}{t}, & \text{if } CS_{\text{shower}} = 2 \\ 60^{\circ}\text{C}, & \text{if } CS_{\text{shower}} = 1 \\ 45^{\circ}\text{C}, & \text{if } AND(CS_{\text{schedule}} = 1, T_{N1} < 44.5, ^{\circ}\text{C}) \end{cases} \quad (3.4)$$

where the second identity derives from Eq. (2.17), having set the current DM value below the threshold for turning on the HP ($DM_{\text{current}} = -61^{\circ}\text{C min}$). It is worth outlining that, since there is no SH request during the summer season, the value of T_{HC} is set to zero.

The aim of the described control logic, based on different set-points of the DHW temperature, is also to observe the trend of the tank temperatures, in order to verify whether the magnitude of its thermal inertia is such that, for instance, a single DHW heating in Shower mode might be sufficient enough for several draw-offs during the day. This behaviour might represent an advantage when considering Layout B during the heating season, when also the SH request is present but it has no influence on the storage tank, as it happens instead in Layout A.

For the perfect prediction of the DHW consumption, different prediction horizons, varying from 2 to 3.5 hours, have been tested. They represent the anticipation time

3.3. Comparison between Layout A and Layout B

for the activation of the HP when a DHW demand is expected. The procedure consists in providing to the schedule reader component different profiles of the slide schedule (see Fig. 3.2 on page 49), characterized by different anticipation times, with respect to the normal schedule, which is based on the actual profile of the hot water draw-offs.

In conclusion, a block diagram of the improved control logic for the DHW heating is shown in Fig. 3.4, where also the memory parameters of the HUB component and of the DM controller are reported.

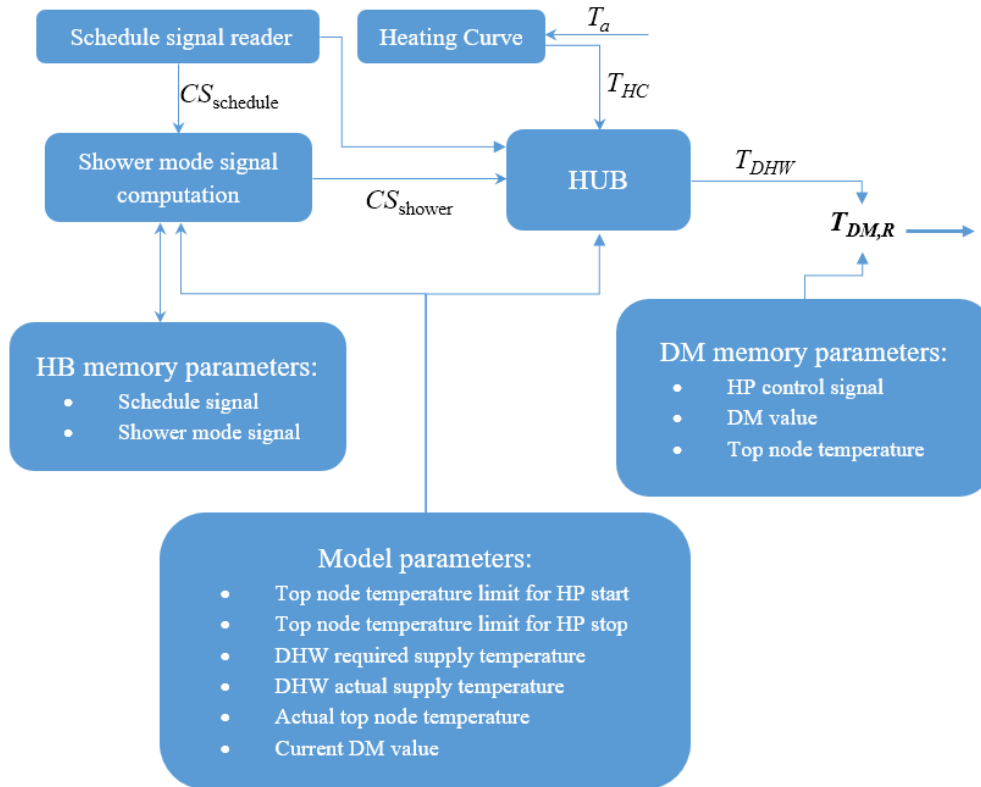


Figure 3.4: Block diagram of the improved control logic for the DHW heating.

3.3 Comparison between Layout A and Layout B

As explained in the previous chapter, the main difference between the two configurations of the system model lies in the employment of the storage tank for both DHW and SH purposes, in Layout A, or for DHW purposes only, in Layout B, where there is a direct connection between the heating generation and the heating distribution loops. Without the thermal inertia provided by the storage tank, frequent oscillations of the indoor temperature are expected, in Layout B, during the SH mode. On the other hand, the influence of the SH request on the tank temperatures, in Layout A, has to be investigated, analysing the consequent impact on the energy consumption, from the HP and the AH, and on the fulfilment of the DHW comfort condition. The TRNSYS[®] models of Layout A and Layout B are illustrated, respectively, in Fig. 3.5 and Fig. 3.6 on the next page.

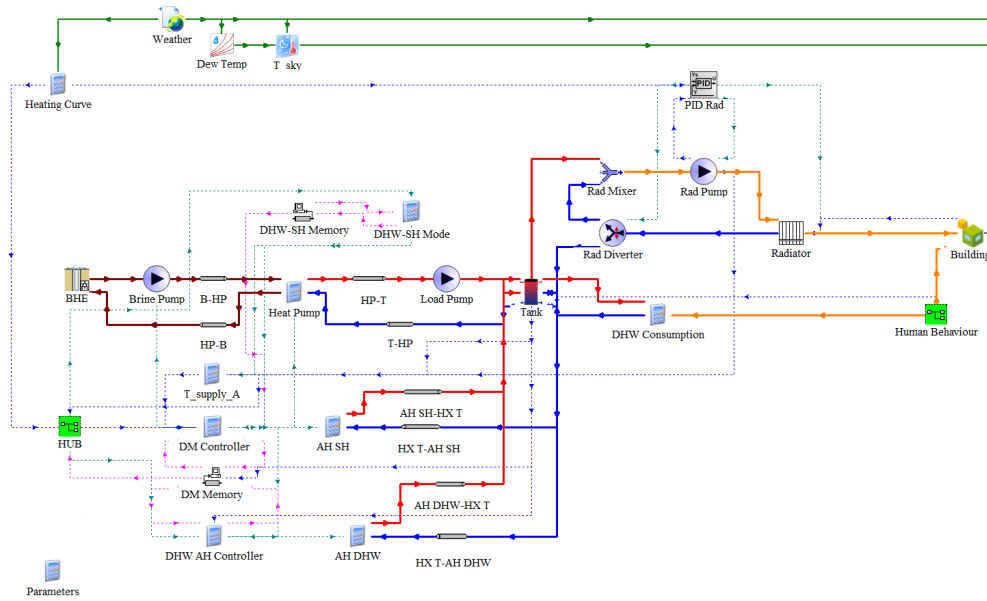


Figure 3.5: TRNSYS[®] model of Layout A.

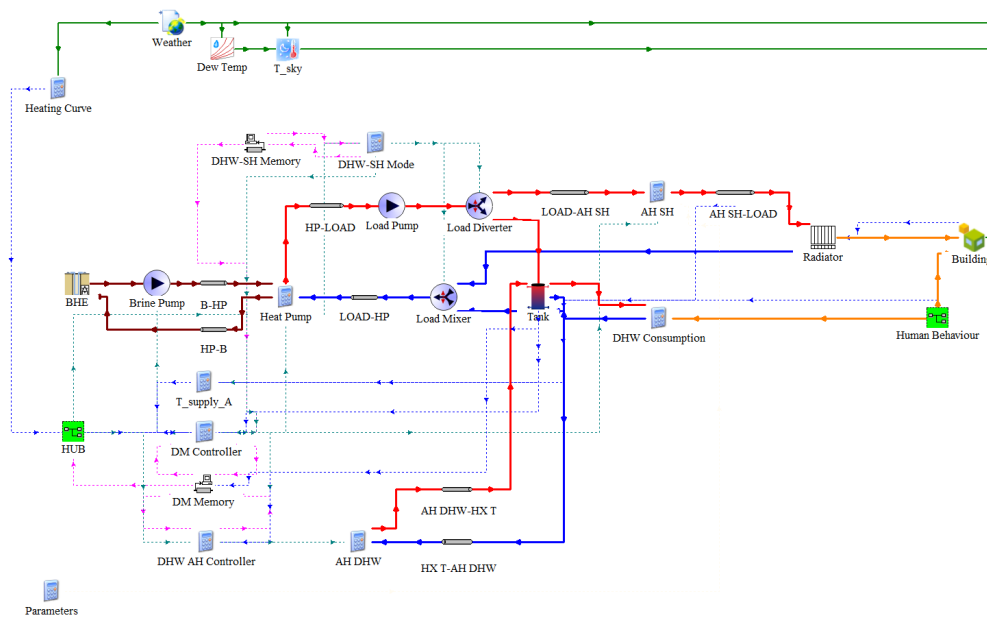


Figure 3.6: TRNSYS[®] model of Layout B.

3.3.1 Combined operating modes during the heating season

The comparison has been performed considering the heating season period, where both operating modes of the heating system are experienced. At this purpose, it is worth to point out the function of the components “DHW-SH Mode” and “T_supply_A”, not yet introduced and both implemented by means of an equation block.

The “DHW-SH Mode” element is particularly suited for Layout B, since it controls the load diverter and load mixer components, according to the operating

3.3. Comparison between Layout A and Layout B

mode of the heating system, and therefore to the value of CS_{mode} . In fact, the load mass flow rate is entirely sent to the tank or to the radiator loop, when the system is operating, respectively, in DHW mode or in SH mode. This is possible thanks to the thermal inertia of the building and of the storage tank (employed for DHW purposes only), but also thanks to the limited duration of the time intervals in which the draw-offs occur. Moreover, given the different values of the required supply temperature during the DHW mode and the SH mode, a partial load mass flow rate sent to the tank and to radiator loop would lead to a discomfort situation in both operating modes. However, if the duration of an operating mode is needed to be longer, thanks to the related memory component (“DHW-SH Memory”), it is possible to set a time delay for the operating mode switching; nevertheless, in the performed simulations, this option has not been considered. Analogously, by means of the “DM Memory” component, a time delay of twenty minutes has been set for the HP control signal, in Layout B, to reduce the already expected and frequent signal switching during the SH mode. Furthermore, a time delay of ten minutes has been set for the control signal of the electrical AH for the space heating, in both layouts.

As concerns the “T_supply_A” element, it provides to the DM controller the actual supply temperature value, which is read from a specific component of the system, depending on its operating mode. In particular, in Layout B, the actual supply temperature during the SH mode is read from the outlet of the electrical AH for the space heating, while it is read from the middle node of the tank during the DHW mode, as previously mentioned. On the other hand, in Layout A, given the presence, in the middle of the tank, of the port dedicated to the SH loop, the actual supply temperature during the DHW mode is read from the top node, so there is no more the possibility to keep the whole upper half-volume of the tank close to the DHW set-point temperature; during the SH mode, instead, the actual supply temperature is read from the outlet of the radiator loop pump.

As a final remark, the same control logic for the DHW heating, previously described, has been adopted in both system layouts, but without any prediction horizons – i.e. the normal DHW schedule profile has been used.

3.3.2 Methodology and adopted parameters

The indicators reported in Tab. 3.1 on page 46 have been adopted for the evaluation of the system performance, in the two different configurations. In particular, the layout comparison has been performed considering the SH comfort time, the SPF, the average COP, computed as the average of the COP values in the considered period, and the energy saving, defined as the percentage relative difference between the total electrical energy consumption in Layout B and the one in Layout A. Moreover, the percentage relative variations of the DBD_{DHW} and DBD_{SH} parameters have been considered as well, for the thermal comfort assessment during the two operating modes of the system.

A preliminary comparison has been carried out by assuming constant values of the solar radiation, in order to avoid its disturbance and to simplify the analyses: in particular, as depicted in Fig. 3.7 on the next page, by means of an equation

block, the building inputs related to the beam radiation, to the total radiation on a tilted surface and to the incidence angle, have been substituted, for all the different surfaces of the building, by fixed daily average values of the solar radiation and by a fixed incidence angle of 45° . Subsequently, this assumption has been removed and the influence of the actual solar radiation on the system performance has been analysed, for both system layouts.

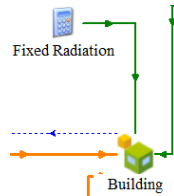


Figure 3.7: TRNSYS[®] equation block for constant solar radiation values.

For the comparative analysis, three different test months of the Swedish heating season have been considered: October, January and April. They are characterised, of course, by very different values of the outdoor temperature and of the solar radiation. As already mentioned in the previous chapter, the HC parameters have been tuned by means of a trial-and-error procedure, for each of the three test months. The adopted parameters for the analysis with the constant solar radiation values are reported in Tab. 3.3, together with the start and stop time of the simulation, expressed as hour of the year. As concerns the analysis with the real solar radiation values, only the months of January and April have been considered, since they feature significantly different magnitudes of the solar radiation – while there is no substantial difference between the months of October and April. Therefore, different parameters of the HC have been tuned, given the different external disturbance of the building, and they are reported in Tab. 3.4, once again together with the start and stop time of the simulation.

Table 3.3: HC parameters for three test months of the heating season (constant solar radiation).

Month	$T_{a,limit}$ [°C]	m_1 [-]	q_1 [°C]	m_2 [-]	q_2 [°C]	Start time [h]	Stop time [h]
October	0	-0.2	39	-1.2	40.5	6552	7296
January	0	-0.85	42	-1.2	41.5	168	912
April	0	-0.2	36	-1.2	36	2160	2880

Table 3.4: HC parameters for two test months of the heating season (real solar radiation).

Month	$T_{a,limit}$ [°C]	m_1 [-]	q_1 [°C]	m_2 [-]	q_2 [°C]	Start time [h]	Stop time [h]
January	0	-0.95	41.5	-1.2	41.5	168	912
April	0	-0.2	36	-1.1	37.5	2160	2880

3.4 HC modulation based on the internal gains

The internal disturbance represented by the heat release from people’s activity and domestic lighting has a direct influence on the indoor temperature variation. In particular, being a positive contribution, it causes the increase of the room temperature, with a consequent reduction of the comfort condition. Therefore, in order to overcome the described issues related to the internal loads, a suited control logic has been applied to the HC component, by means of the equation block depicted in Fig. 3.8, with the aim of adjusting the required supply temperature for the space heating and, thus, reducing the thermal energy provided by the heating system.

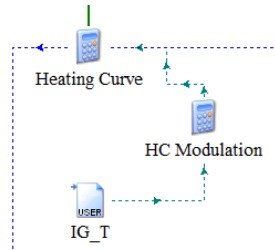


Figure 3.8: TRNSYS[®] equation block for the internal gains-based HC modulation.

3.4.1 Creation of the internal gains profile

The information about the internal heat release is provided to the system model by means of the data reader “IG_T”, featuring in Fig. 3.8. In particular, the contributions to the internal loads from people and lighting, computed according to Eq. (2.1) and Eq. (2.4), have been summed together obtaining a “raw” profile of the total internal heat gains (\dot{Q}_{IG}):

$$\dot{Q}_{IG} = \dot{Q}_{\text{people}} + \dot{Q}_{\text{light}} \quad (3.5)$$

In order to improve the response of the control logic, the same procedure carried out in [1] has been adopted, with a modification of the time resolution of the occupancy profile, from five to fifteen minutes, since it needs to be an integer multiple of the adopted simulation time-step of three minutes, for a correct elaboration of the input data. In particular, in the Matlab[®] software environment, starting from the raw profile, a linear interpolation has been applied to an hourly averaged profile and, eventually, the Matlab[®] built-in “smooth” function has been used for the profile filtering, with a “span” parameter equal to fifty. Subsequently, a comparison between the obtained smooth profile and the original raw profile has been performed, considering the total annual energy amount of the internal gains, which is 4514.74 kWh, with an observed maximum thermal power of 1.11 kW. The energy difference between the two profiles is of 0.085 kWh, which is negligible with respect to the annual energy release, therefore the smooth profile can be properly employed in the improved control logic. The two described profiles are shown in Fig. 3.9 on the following page.

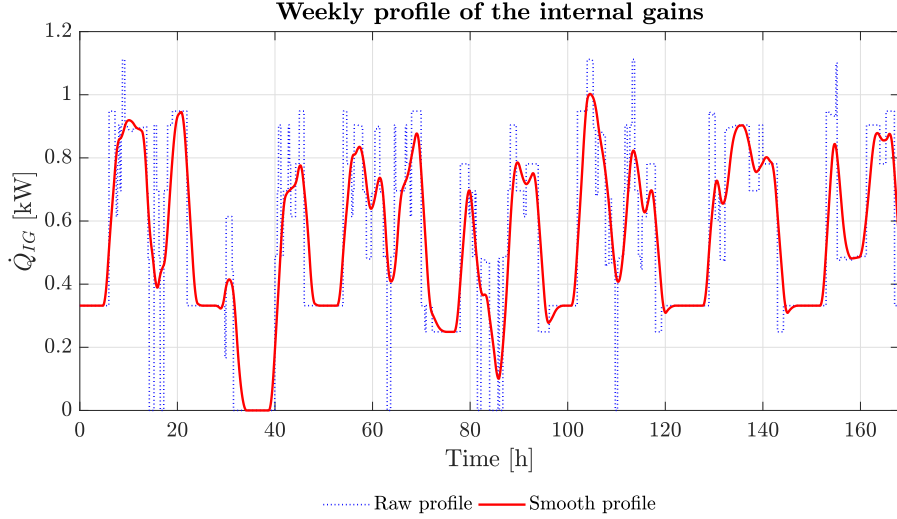


Figure 3.9: Original and filtered weekly profile of the internal heat gains.

3.4.2 TRNSYS[®] implementation

The heating curve modulation consists in the correction of the required supply temperature, provided to the DM controller, according to the amount of the expected internal gains. In particular, the assumption of a linear correlation between the heat release and the magnitude of the correction ($IG_{\text{correction}}$) has been assumed, as reported in the following equations:

$$IG_{\text{correction}} = a \cdot \dot{Q}_{IG} + b \quad (3.6)$$

$$T_{DM,R} = T_{HC} + IG_{\text{correction}} \quad (3.7)$$

where a and b are the corrective coefficients, representing the slope and the intercept, respectively, of the correction applied to the required supply temperature.

The improved control logic has been tested considering the months of January and April, with the heating system operating in both DHW mode and SH mode, and assuming constant values of the solar radiation for a simplified analysis. For each of the selected months, six different tests have been performed, characterised by different corrective coefficients, which have been tuned, as already explained, by means of a trial-and-error procedure. In particular, two different performance criteria have been considered, according to the aim of the control logic: the so-called “Energy mode”, whose purpose is the reduction of the energy consumption of the heating system, and the so-called “Comfort mode”, whose purpose, instead, is the enhancement of the indoor thermal comfort conditions.

The adopted corrective coefficients for the six performed tests are reported in Tab. 3.5 on the next page and the corresponding linear correlations with the magnitude of the internal heat gains are shown in Fig. 3.10 and Fig. 3.11 on the facing page, for the month of January and April, respectively.

3.4. HC modulation based on the internal gains

Table 3.5: Adopted corrective coefficients in the performed tests for the months of January and April.

Test	January		April	
	a [°C/kW]	b [°C]	a [°C/kW]	b [°C]
1	-1	0	-0.75	0
2	-2	0.25	-1.75	0.5
3	-2.75	0.5	-2	0.25
4	-3.5	0.75	-3	0.75
5	-4	1.25	-4.25	1.25
6	-3.75	1	-5	1.75

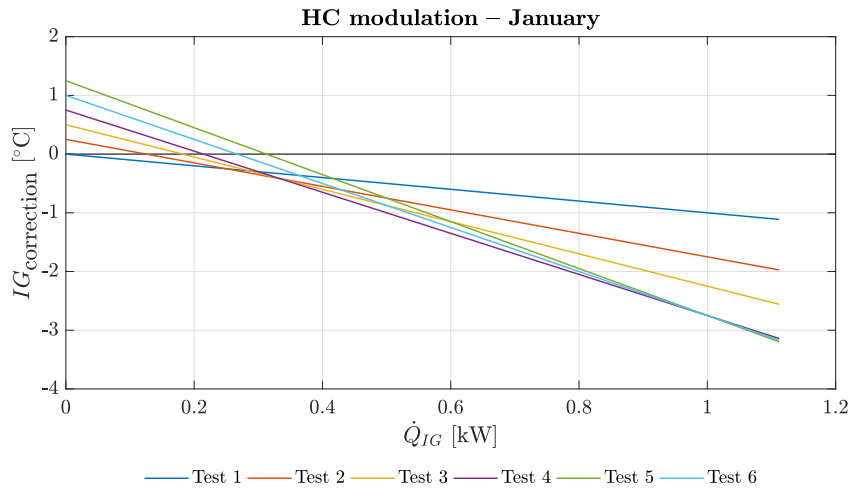


Figure 3.10: HC correction according to the internal heat release, in the performed tests for the month of January.

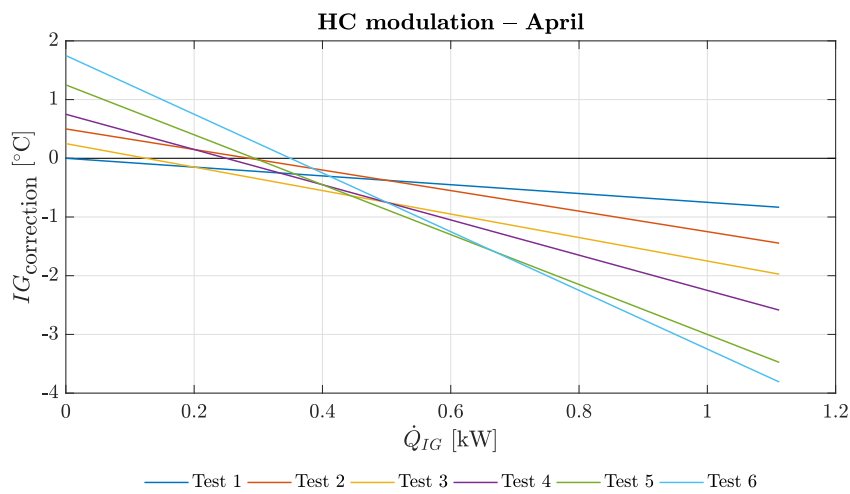


Figure 3.11: HC correction according to the internal heat release, in the performed tests for the month of April.

Once the parameters of the control logic have been set, three different prediction horizons have been tested for the considered months. At first, a non-predictive approach has been adopted, by providing to the model the current value of the internal gains and, therefore, using a “zero hours” prediction horizon. Subsequently, similarly to the procedure adopted in the improved control logic for the DHW heating, assuming a perfect prediction, the profile of the forecast internal gains has been provided with an anticipation time of one hour and two hours.

The same corrective coefficients reported in Tab. 3.5 on the previous page have been employed for the three cases and, thereafter, a comparison has been carried out, considering both the purposes of the energy saving and of the thermal comfort enhancement. Eventually, for each of the two criteria and for each of the considered months, the best performing test has been selected, according to a good compromise between the Energy mode and the Comfort mode performances. As one can expect, all the accomplished tests yield an overall energy saving in the considered period, given the lower amount of supplied thermal energy from the heating system. However, some of the performed tests reveal a thermal comfort reduction, due to either an excessive or insufficient correction of the required supply temperature. Therefore, they have been excluded a priori from the selection and only the tests showing a positive performance for both criteria have been considered.

3.5 HC modulation based on the solar radiation

The external disturbance represented by the solar radiation strongly affects the thermal behaviour of the building, leading to important deviations of the indoor temperature from the desired set-point. Moreover, it represents an important energy gain which can be exploited in order to reduce the supplied thermal energy by the heating system. For this purpose, the control strategy developed in [1] takes into account the energy contribution provided by the solar radiation, with a resulting increase of both the energy saving and the indoor comfort conditions. In the present section, a general description is provided, at first, for the above-mentioned control logic, which has been implemented in a simplified system model where the influence of the DHW consumption and of the internal heat release has not been considered. Subsequently, a further improvement of the same control strategy, carried out in the present work, is described. In particular, it takes into account the overheating of the indoor environment, observed after the sunset, when the thermal energy stored by the building during the day is released into the indoor ambient. Eventually, the complete system model, characterised by the combination of all the described control logics, is illustrated, together with the details of its comparison with the basic controller.

3.5.1 Working principle of the control strategy

As already mentioned, the adopted method for the improved control logic is the heating curve modulation, which makes use of different corrective coefficients for the adjustment of the required supply temperature value, according to the expected amount of thermal energy, deriving from the solar radiation contribution, which

3.5. HC modulation based on the solar radiation

gradually changes during the day. In particular, the solar energy gain is monitored during the day, setting a first threshold in the morning in order to delay the activation of the control strategy, since the energy received by the building is stored before being released into the indoor ambient; a further energy limit is set in the last hours of the daylight, in order to delay the deactivation, instead, of the control logic, according to the rate of reduction of the solar energy contribution, with the aim of exploiting the building thermal inertia. Moreover, a further correction of the required supply temperature is applied also after the sunset, in order to compensate the observed ambient overheating, due to the thermal energy stored by the building during the day.

3.5.2 TRNSYS[®] implementation

Since the amount of the incident solar radiation is dependent on the cardinal orientation and on the inclination of a given surface (S), the total irradiance (G_{tot}) received by the building⁷ has been computed as a weighted average on its five surfaces (see Tab. 2.1 on page 27), by using the Meteonorm[®] data on the total horizontal radiation (G_H), for the roof, and those about the total radiation on a tilted surface (G_T), for the lateral walls:

$$G_{\text{tot}} = \frac{G_H \cdot S_{\text{roof}} + G_{T,N} \cdot S_N + G_{T,S} \cdot S_S + G_{T,E} \cdot S_E + G_{T,W} \cdot S_W}{S_{\text{tot}}} \quad (3.8)$$

where $S_{\text{tot}} = S_{\text{roof}} + S_N + S_S + S_E + S_W$ is the total area of the building surfaces. Furthermore, the solar contribution to the building energy balance (E_s) is computed as the integral, over a specified period of time $\Delta t = t_2 - t_1$, of the total irradiance multiplied by the total area of the building surfaces:

$$E_s = \int_{t_1}^{t_2} G_{\text{tot}} \cdot S_{\text{tot}} dt \quad (3.9)$$

As previously explained, the control strategy is activated in the morning only when the corresponding energy threshold ($E_{s,\text{limit}}$) is exceeded. Afterwards, as depicted in Fig. 3.12 on the next page, at a predetermined time instant (t_-) before the sunset time (t_s), computed as $t_s - \Delta t_-$, the corresponding value of the irradiance is saved and set as a fixed input variable ($G_{\text{tot},k}$) for the following time-steps, where it is used for the computation of a “complementary” integral (CI), defined as follows:

$$CI = \int_{t_-}^{t_s} (G_{\text{tot},k} - G_{\text{tot}}) dt \quad (3.10)$$

which corresponds to the green area in Fig. 3.12 on the following page.

Subsequently, the correction of the required supply temperature is performed according to the value of $G_{\text{tot},k}$ and CI , and only if the latter exceeds the corresponding threshold (CI_{limit}). Finally, in order to compensate the ambient overheating experienced at the end of the day, the same procedure for the HC modulation

⁷The building model is characterised by a single zone, therefore all the received solar energy is released in the same room.

is adopted also in the time interval Δt_+ , whose value has been chosen after a trial-and-error procedure, according to the control logic performance in terms of both energy saving and indoor thermal comfort.

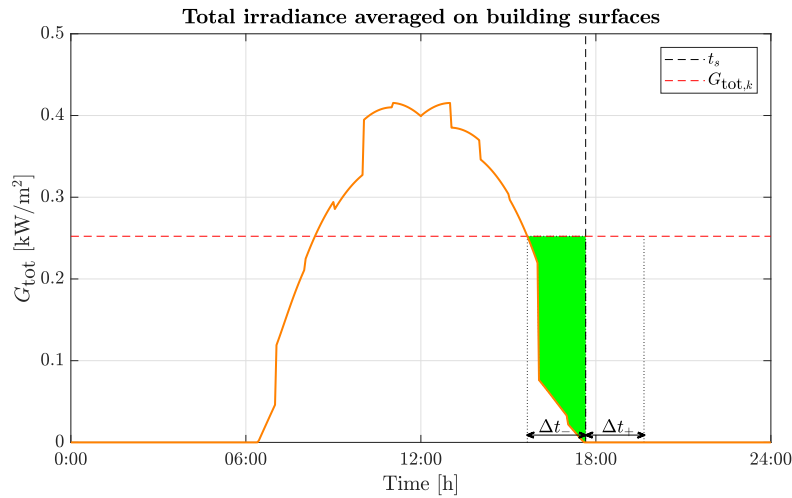


Figure 3.12: Total solar radiation averaged on the building surfaces, over a day period in March, with the green area representing the complementary integral CI in the time interval Δt_- .

The hourly average values of the solar radiation, obtained in a Matlab[®] script which elaborates the Meteonorm[®] weather data, are provided to the control logic model, by means of the data reader component “Radiation Data”, illustrated in Fig. 3.13, with a “zero hours” prediction horizon. Subsequently, the HC modulation takes place in the corresponding equation block, where all the parameters of the control logic are set.

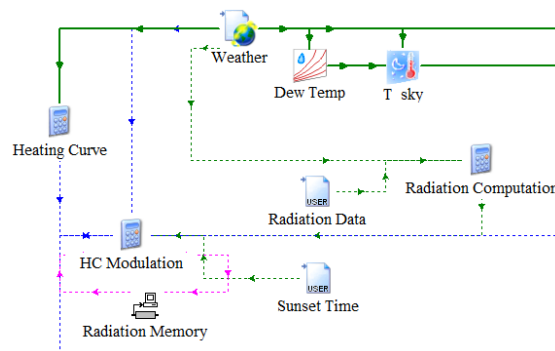


Figure 3.13: TRNSYS[®] model for the solar radiation-based HC modulation.

The adopted procedure consists in identifying, at first, the current outdoor temperature, in order to select the proper interval where to apply the HC correction. In particular, the correction is applied to both the slope and the intercept of the HC, according to the magnitude of the solar radiation. In fact, all the corrective coefficients are multiplied by the provided hourly value of the total irradiance. Moreover, the actual outdoor temperature is multiplied by the corresponding

3.6. Complete system model

coefficient in order to act on the slope of the HC. Finally, the resulting four corrective coefficients are used in the control strategy, after having been evaluated, together with the other parameters, by means of a trial-and-error procedure. The algorithms for the implementation of the described control logic are reported below:

$$\begin{aligned}
 & \text{if } AND(E_s > E_{s,\text{limit}}, T_a \leq T_{a,\text{limit}}) \\
 & \quad \text{then } SR_1 = \alpha_1 \cdot G_{\text{tot}} \cdot T_a - \beta_1 \cdot G_{\text{tot}} \\
 & \text{else if } AND(E_s > E_{s,\text{limit}}, T_a > T_{a,\text{limit}}) \\
 & \quad \text{then } SR_2 = \alpha_2 \cdot G_{\text{tot}} \cdot T_a - \beta_2 \cdot G_{\text{tot}} \\
 & SR = SR_1 + SR_2
 \end{aligned} \tag{3.11}$$

$$\begin{aligned}
 & \text{if } AND(t_s - \Delta t_- < t \leq t_s + \Delta t_+, CI > CI_{\text{limit}}) \\
 & \quad \text{then } SR_{\text{correction}} = SR_{\text{old}} \\
 & \text{else if } OR(t \leq t_s - \Delta t_-, t > t_s + \Delta t_+) \\
 & \quad \text{then } SR_{\text{correction}} = SR
 \end{aligned} \tag{3.12}$$

where α and β are the corrective coefficients applied, respectively, to the slope and to the intercept of the HC, and the subscripts 1 and 2 refer to the outdoor temperature interval where the correction occurs; the resulting adjustment of the required supplied temperature is expressed by the coefficient $SR_{\text{correction}}$, which corresponds to the current value SR or to SR_{old} – the latter is based on the fixed input variable $G_{\text{tot},k}$ –, according to the time of the day. In conclusion, taking into account the solar radiation contribution, the required supply temperature provided to the DM controller, during the SH mode, is computed as follows:

$$T_{DM,R} = T_{HC} + SR_{\text{correction}} \tag{3.13}$$

3.6 Complete system model

The complete system model, illustrated in Fig. 3.14 on the following page, is characterised by the combination of all the three control strategies described in the present chapter, implemented within Layout B. As regards the HC modulation based on the internal gains and on the solar radiation, the correction of the required supply temperature provided to the DM controller, during the SH mode, is computed as follows:

$$T_{DM,R} = T_{HC} + IG_{\text{correction}} + SR_{\text{correction}} \tag{3.14}$$

For the system performance evaluation during the heating season, the test month of March has been considered. To this end, the parameters of the heating curve have been re-tuned, once again with a trial-and-error procedure: they are reported in Tab. 3.6, together with the start and stop time of the simulation.

Table 3.6: HC parameters for the test month of March.

Month	$T_{a,\text{limit}}$ [°C]	m_1 [-]	q_1 [°C]	m_2 [-]	q_2 [°C]	Start time [h]	Stop time [h]
March	5	-0.7	42	-1.1	42	1416	2160

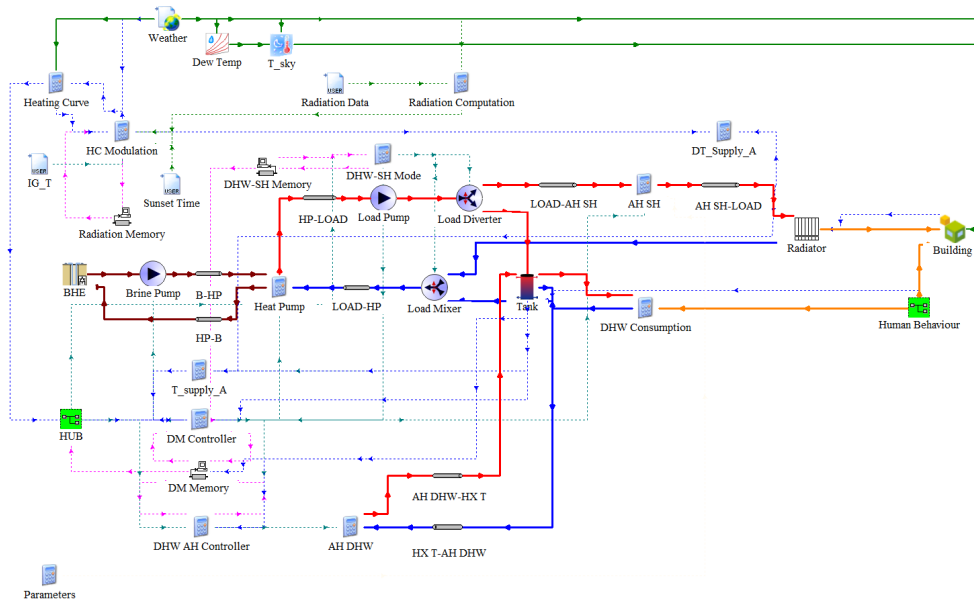


Figure 3.14: Complete TRNSYS[®] system model of Layout B: combination of all the developed control strategies.

In the comparison with the basic on/off controller, a cycling period of thirty minutes has been adopted for the switching of the operating mode. In particular, from 6 a.m. to 8 p.m., the heating system with the basic control logic is alternately operating between DHW mode and SH mode, whereas, from 8 p.m. to 6 a.m., it is working in SH mode only.

In conclusion, the adopted parameters of the improved control logics and all the described corrective coefficients, employed in the complete system model, are reported in Tab. 3.7.

Table 3.7: Adopted parameters and corrective coefficients, for the combined control strategies, in the complete system model.

Parameter	Value	Unit
a	-3	°C/kW
b	0.75	°C
α_1	-1	m ² h/MJ
β_1	12	°C m ² h/MJ
α_2	-3	m ² h/MJ
β_2	12	°C m ² h/MJ
$E_{s,limit}$	3	MJ
CI_{limit}	3	MJ
Δt_-	2	h
Δt_+	2	h

Chapter 4

Results

The present chapter reports the results obtained from the comparison between Layout A and Layout B and from the application, in the latter configuration, of the improved control logics previously described. The performance evaluation of the developed control strategies is carried out by comparing the results of the TRNSYS[®] numerical simulations, achieved by the system model based on the improved controller, with those obtained from the one which employs the basic controller. For this purpose, as already mentioned, the energy and comfort related indicators in Tab. 3.1 on page 46 have been adopted, together with some graphical representations showing the observed behaviour of the heating system. A similar procedure has been followed for the layout comparison as well. In conclusion, the results are presented according to the same order adopted in the previous chapter.

4.1 DHW heating over the summer season

As explained in section 3.2, the improved control logic for the DHW heating has been tested over the summer season, in order to avoid the influence of the SH request on the heating system behaviour. A first analysis has been performed taking into account the simulation results over the test month of June: this choice is completely arbitrary since the outdoor temperature is not considered in the control logic, having set to zero the value of T_{HC} , for the above-mentioned reason. Furthermore, the system behaviour has the same trend over weekly periods, given the shape of the fixed weekly profile of the hot water draw-offs (see Fig. 2.3 on page 30) and of the DHW schedule (see Fig. 3.2 on page 49). Eventually, the simulation has been carried out over the whole summer season.

Considering the results obtained in the month of June, thanks to the improved control logic, it is possible to achieve an increase of the seasonal performance factor and a corresponding energy saving, with respect to the basic controller, as depicted in Fig. 4.1 on the following page and Fig. 4.2 on page 65. In particular, the former shows the comparison between the *SPF* value obtained with the basic control logic and the values achieved by providing to the model the DHW schedule, with different prediction horizons, from 0 h to 3.5 h. The latter, instead, illustrates the HP performance variation achieved with the considered prediction horizons, with respect to the base case, accounting for the thermal energy delivered in the

condenser, the electrical energy consumed by the compressor and the corresponding average COP in the considered period. In the case where the normal schedule is adopted, it is possible to achieve an increase of the SPF from 2.16 to 2.23, and a corresponding energy saving of about 4%. Whereas, when the slide schedule is employed, an increment of the SPF up to 2.39 and an energy saving up to about 11% can be obtained.

It is worth outlining that in the performed simulations, due to the adopted control settings described in section 2.2.6, the electrical auxiliary heater is never switched on. Therefore, the overall observed values of the SPF are very close to the average values of the COP . In particular, the latter are lower than the expected value in nominal conditions, described in section 2.2.3, given the relatively higher load temperature (T_{load}) – which corresponds, during the DHW mode, to the bottom node temperature of the tank (T_{N10}) – deriving from the adopted DHW set-point temperature for shower needs, equal to 60 °C.

As shown in Fig. 4.3 on the facing page, if compared to the base case, the heat pump is characterised by a shorter operating time – and a consequent energy saving –, when the slide schedule is adopted, with a prediction horizon higher than two hours. On the other hand, an overall increase of the DBD_{DHW} parameter is observed, even though quite restrained, with rising values of the prediction horizon. In fact, the on/off hysteresis controller, in the base case, is always able to keep the top node temperature above the corresponding threshold for the draw-offs in Shower mode (T_{limit}^{DHW}), with a resulting null DBD_{DHW} parameter. However, the basic controller has no information about the time when the draw-offs will occur, therefore the improved control logic allows the HP to operate only if a positive value of the $CS_{schedule}$ is expected and if the top node temperature of the tank is below the desired set-point, obtaining the observed energy consumption reduction.

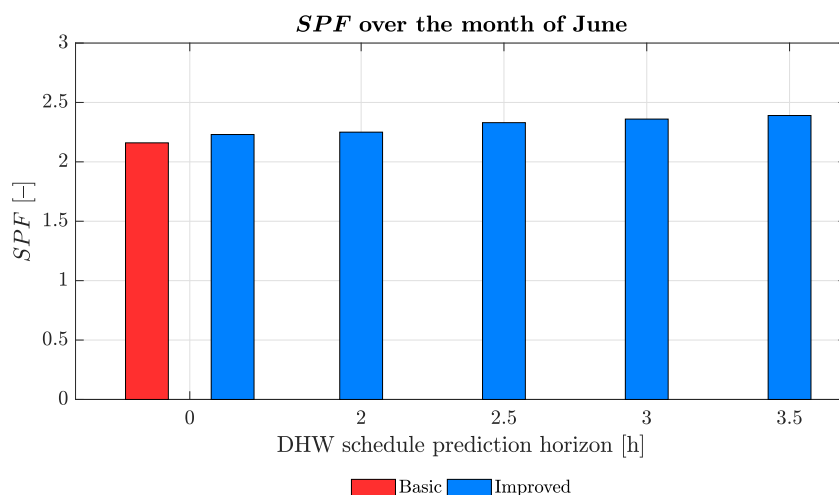


Figure 4.1: SPF values obtained with the basic controller and with the improved control logic, adopting different prediction horizons of the DHW schedule, over the test month of June.

4.1. DHW heating over the summer season

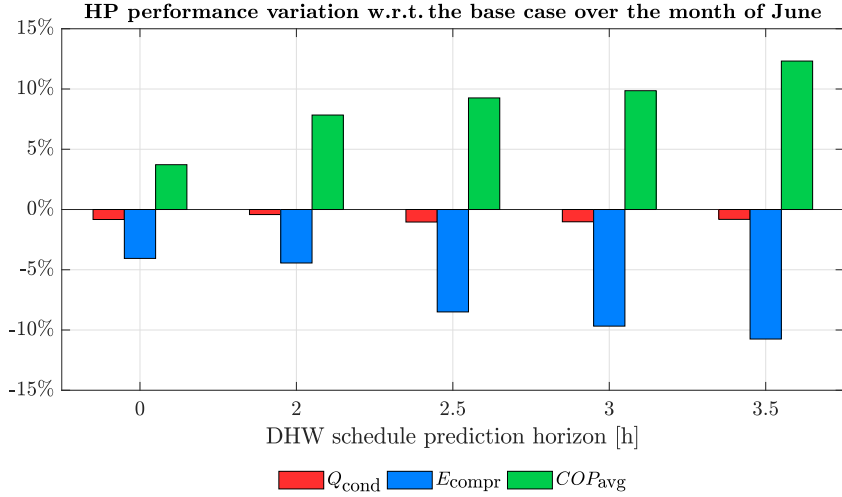


Figure 4.2: Condenser thermal energy, compressor electrical energy and corresponding average COP variations with respect to the base case, obtained adopting different prediction horizons of the DHW schedule, over the test month of June.

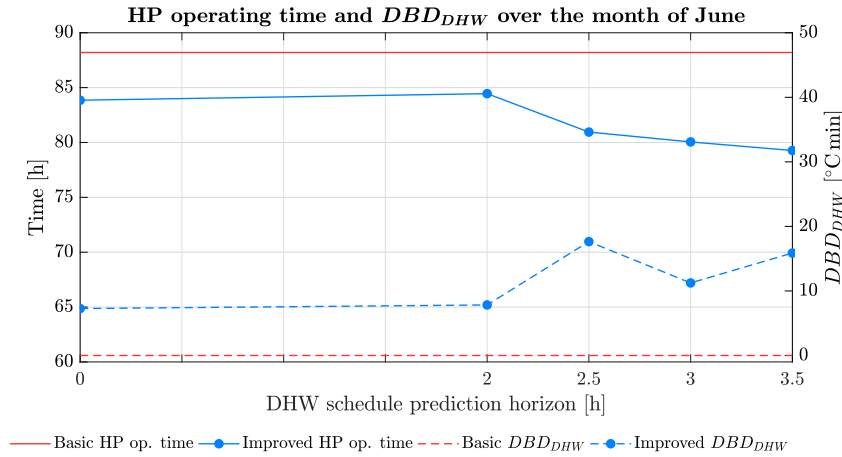


Figure 4.3: Operating time of the HP, on the left-hand side of the y -axis, and DBD_{DHW} parameter, on the right-hand side of the y -axis, in the base case and with the improved control logic, adopting different prediction horizons of the DHW schedule, over the test month of June.

The obtained increasing performance of the heat pump, with rising values of the DHW schedule prediction horizon, can be explained observing the plots reported in Fig. 4.4 and Fig. 4.5 on the next page, where a day period of the weekend has been considered. In particular, they show the tank temperatures on the left-hand side of the y -axis and the control signals of the heat pump and of the DHW schedule, together with the COP and the draw-offs power, on the right-hand side of the y -axis. When the normal schedule is used (see Fig. 4.4), the HP is activated during the time interval in which the draw-offs are expected. Whereas, when the slide schedule is adopted (see Fig. 4.5), the HP is turned on with a certain anticipation time – of three hours in this instance – until the required temperature is reached and as long as the control signal CS_{shower} is different from zero.

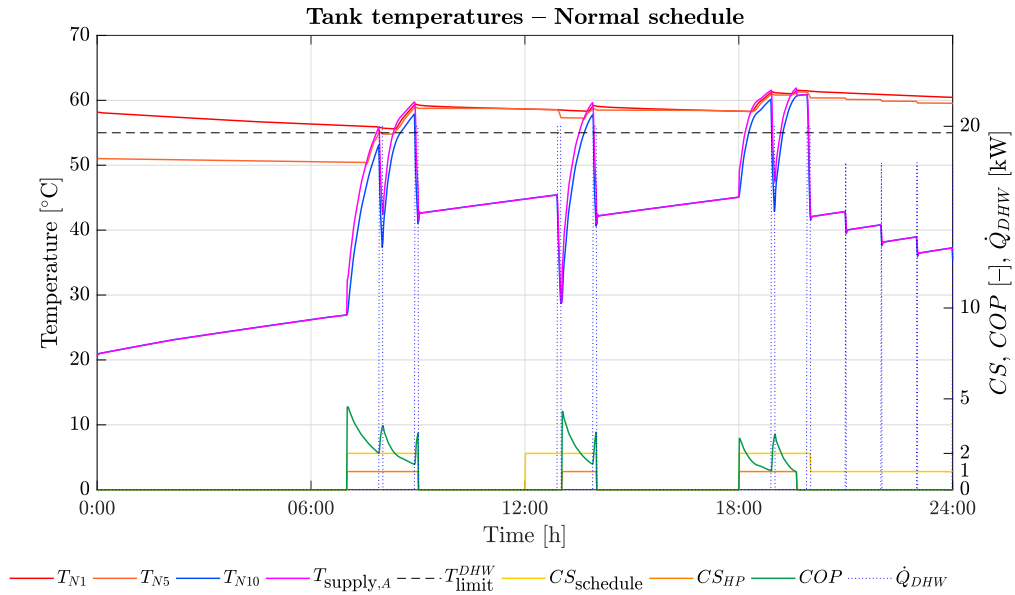


Figure 4.4: Tank temperatures, on the left-hand side of the y -axis, and control signals of the heat pump and of the normal schedule, together with the COP and the draw-offs power, on the right-hand side of the y -axis, over a day period of the weekend, during the test month of June.

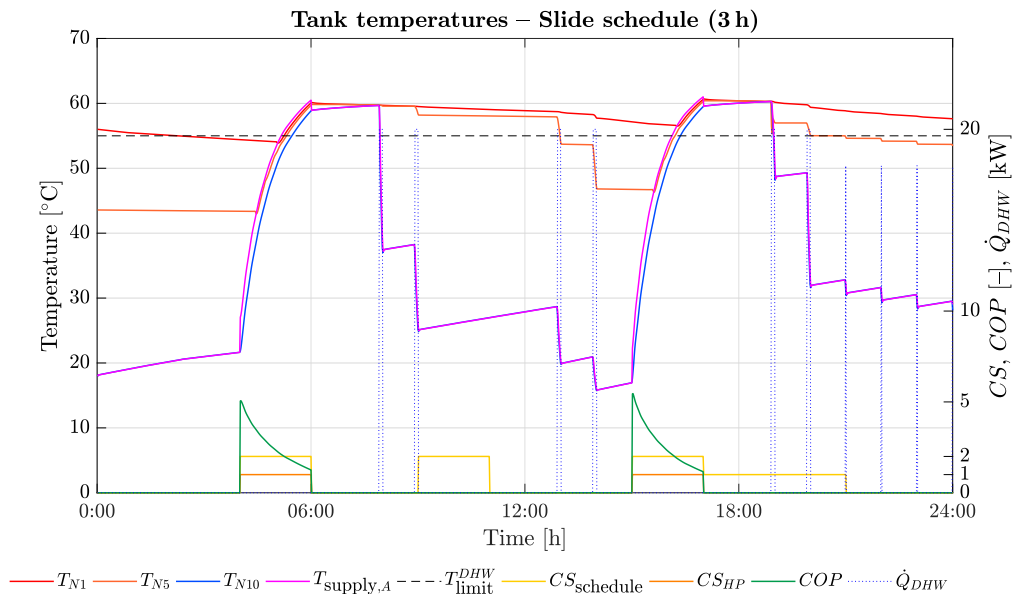


Figure 4.5: Tank temperatures, on the left-hand side of the y -axis, and control signals of the heat pump and of the slide schedule (prediction horizon: 3 h), together with the COP and the draw-offs power, on the right-hand side of the y -axis, over a day period of the weekend, during the test month of June.

Subsequently, the thermal inertia of the storage tank is exploited for the following draw-offs, which affect the tank thermal stratification by reducing to a large extent the bottom node temperature, while the top node is kept closer to the imposed threshold, avoiding therefore a further activation of the HP during the subsequent draw-off. Moreover, when the next HP activation occur, it starts working with a

4.1. DHW heating over the summer season

relatively higher COP , due to the lower temperature reached by the bottom node of the tank, with a resulting lower value of the load temperature.

In conclusion, as a good compromise between the energy saving and the thermal comfort condition for the DHW, the prediction horizon of three hours has been selected for the slide schedule, in order to perform the simulation over the whole summer season. It is worth specifying that with prediction horizons longer than the considered ones, besides a further increase of the DBD_{DHW} , an overlapping might occur between the schedule values of two subsequent periods, with a resulting behaviour similar to the one observed for the normal DHW schedule.

The obtained results from the simulation carried out over the whole summer season are reported in Tab. 4.1. The achieved energy saving is due to the previously described reasons. Indeed, while guaranteeing an average top node temperature above the imposed threshold, the improved control logic, with respect to the basic controller, leads to a lower average temperature of the bottom node of the tank, which corresponds to a lower load temperature, with a consequent higher performance of the heat pump.

Table 4.1: Comparison of the simulation results obtained with the basic controller and with the improved control logic, over the whole summer season.

Parameter	Unit	Basic	Improved
E_{compr}	kWh	436.85	396.37
E_{AH}	kWh	0	0
Energy saving	%		9.27
DBD_{DHW}	°C min	0	30.11
SPF	–	2.14	2.36
SPF variation	%		10.28
$T_{N1,\text{max}}$	°C	61.56	61.56
$T_{N1,\text{avg}}$	°C	60.04	58.23
$T_{N1,\text{min}}$	°C	57.04	52.67
$T_{N10,\text{avg}}$	°C	41.24	34.59

4.2 Layout comparison over the heating season

As mentioned in section 3.3, the performance comparison between Layout A and Layout B has been carried out over the test months of October, January and April, assuming, at first, constant values of the solar radiation. Subsequently, this assumption has been removed and the simulations have been performed only over the test months of January and April.

As can be seen from the comparison of the achieved SPF values in the two layouts, reported in Fig. 4.6, an overall higher SPF is obtained in Layout B with respect to Layout A. Moreover, some other parameters, among those reported in Tab. 3.1 on page 46, such as the energy saving, the average COP and the SH comfort time, have been taken into account. In particular, Fig. 4.7 on the next page shows the percentage relative difference between the considered parameter obtained in Layout B and the same parameter achieved in Layout A. As one can expect, for both system layouts, the SPF is lower in the cold month of January rather than in October or April – where similar values are observed –, due to the greater difference between the load temperature and the source temperature of the heat pump. As a matter of fact, a higher supply temperature is required for the space heating in January, while the ground temperature is approximately constant over the time. Furthermore, while a similar variation of the average COP is observed in October and April, the energy saving and the percentage increase of the SPF are more significant during the cold month of January, due to the electrical energy consumption of the auxiliary heater. Indeed, as reported in Tab. 4.2 on the facing page, the AH is never switched on during the months of October and April, while in January it is possible to obtain, in Layout B, a 62.45% reduction of its energy consumption, with respect to Layout A.

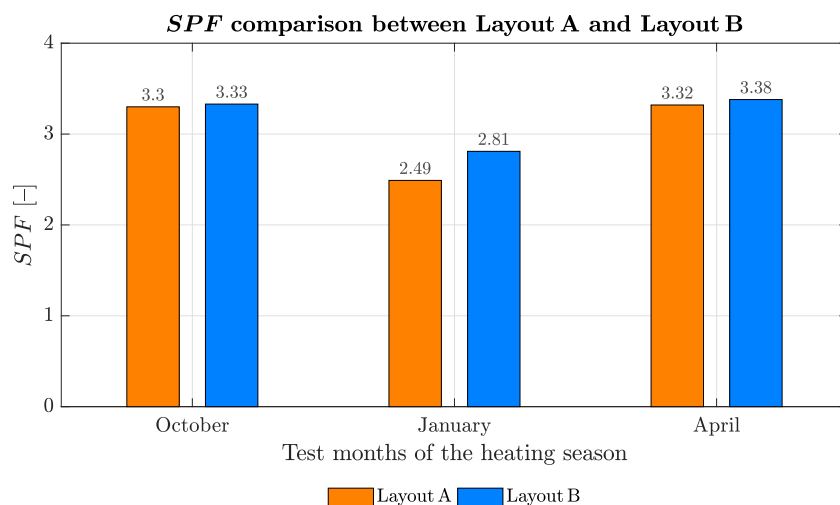


Figure 4.6: SPF comparison between Layout A and Layout B, over the test months of the heating season.

4.2. Layout comparison over the heating season

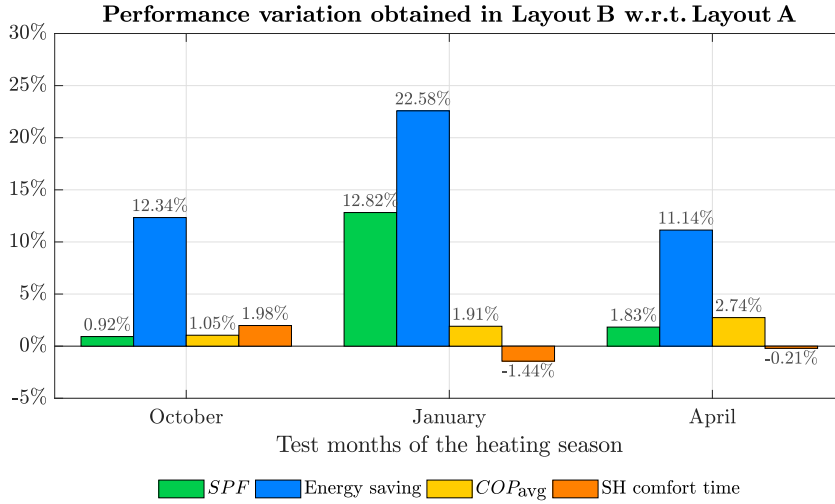


Figure 4.7: Performance variation observed in Layout B with respect to Layout A, over the test months of the heating season.

Table 4.2: Performance comparison between Layout A and Layout B, over the test months of the heating season.

Parameter	Unit	October		January		April	
		A	B	A	B	A	B
E_{compr}	kWh	447.50	392.27	1011.69	913.97	405.72	360.52
E_{AH}	kWh	0	0	328.00	123.17	0	0
SH comfort time	%	86.85	88.58	84.69	83.47	86.00	85.82
DBD_{DHW} variation	%	-96.67		-98.28		-96.51	
DHW mode duration	h	140.95	105.30	124.65	109.30	128.30	92.55
$T_{room,avg}$	°C	20.57	21.16	20.56	21.22	20.53	21.15
$T_{room,STD}$	°C	0.50	0.62	0.57	0.67	0.50	0.67
$T_{N1,avg}$	°C	52.70	58.07	53.94	57.84	53.04	58.10
$T_{N1,min}$	°C	46.33	40.93	45.51	52.25	46.93	41.31
$T_{load,avg}$	°C	39.35	38.64	42.26	41.64	39.15	38.13

According to the obtained results reported in Tab. 4.2, although the average indoor temperature over the considered period ($T_{room,avg}$) is close to the desired set-point of 21 °C and similar values of the SH comfort time are observed in the two layouts, the room temperature standard deviation from its mean value ($T_{room,STD}$) is higher in Layout B. This represents, as expected, the main drawback of the latter configuration. Indeed, as depicted in Fig. 4.8 on the following page, where a day period in April has been considered, higher and frequent oscillations of the indoor temperature are observed in Layout B, due to the absence of the thermal

inertia provided by the storage tank during the SH mode. For the same day of April, also the HP control signal and the required supply temperature are shown, respectively, in Fig. 4.9 and in Fig. 4.10 on the next page, for both system layouts. In particular, as explained in section 3.2.2, the required supply temperature for the DHW is 60 °C, during the Shower mode, except for the first iteration when the latter is activated, when it is set to a higher value in order to improve the response of the DM controller. On the other hand, during the SH mode, the required supply temperature is the one provided by the heating curve, and it is depending on the outdoor temperature only.

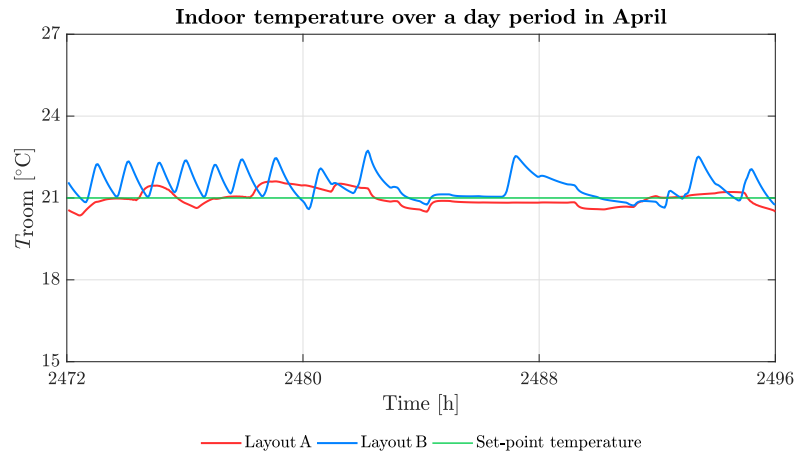


Figure 4.8: Comparison of the indoor temperature observed in Layout A and in Layout B, over a day period in April.

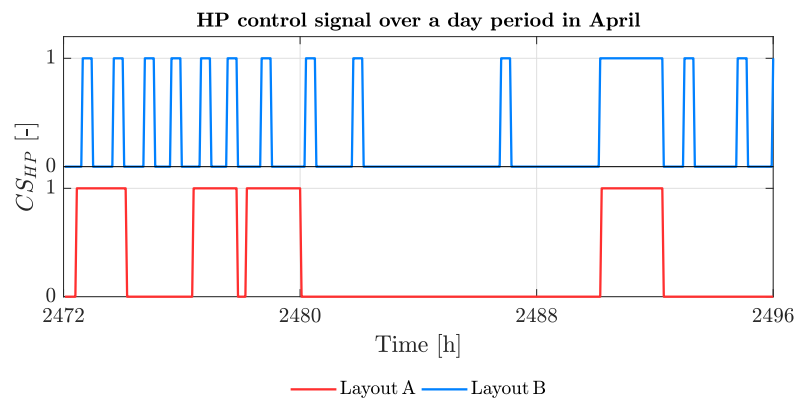


Figure 4.9: Comparison of the HP control signal observed in Layout A and in Layout B, over a day period in April.

In Fig. 4.10 on the facing page, it is already possible to observe the main advantage of Layout B with respect to Layout A, which is the lower duration of the DHW mode (see Tab. 4.2 on the previous page). Indeed, with the improved control logic for the DHW heating and by using the storage tank for DHW purposes only, it is possible to better exploit, in Layout B, the thermal inertia of the storage tank, allowing less frequent and/or shorter activations of the DHW mode, in which the

4.2. Layout comparison over the heating season

HP performance is lower with respect to that observed during the SH mode, given the higher required supply temperature.

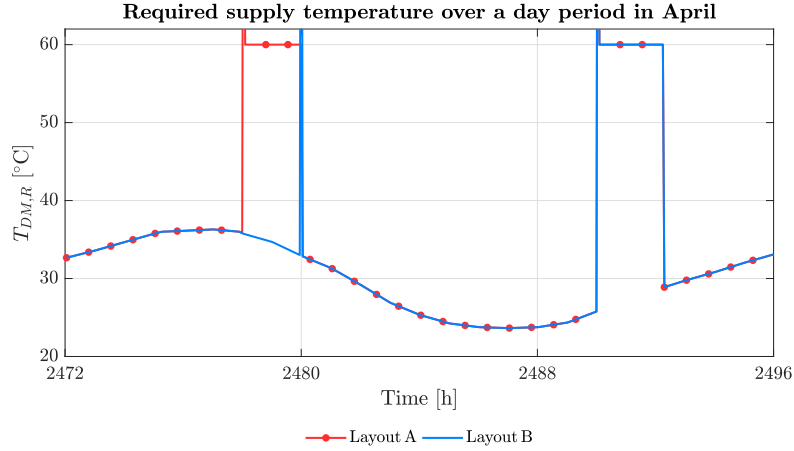


Figure 4.10: Comparison of the required supply temperature observed in Layout A and in Layout B, over a day period in April.

If a longer period of time is observed, it is possible to better understand the above described system behaviour in the two configurations. In particular, a period of three days in April has been considered. As can be observed in Fig. 4.11, the actual supply temperature of the DHW, which corresponds to the top node temperature of the tank (T_{N1}), is overall higher in Layout B rather than in Layout A. In particular, in the latter configuration, the average temperature of the tank top node, is lower than the imposed threshold T_{limit}^{DHW} , as also reported in Tab. 4.2 on page 69. This leads to the significant reduction of the DBD_{DHW} parameter obtained in Layout B.

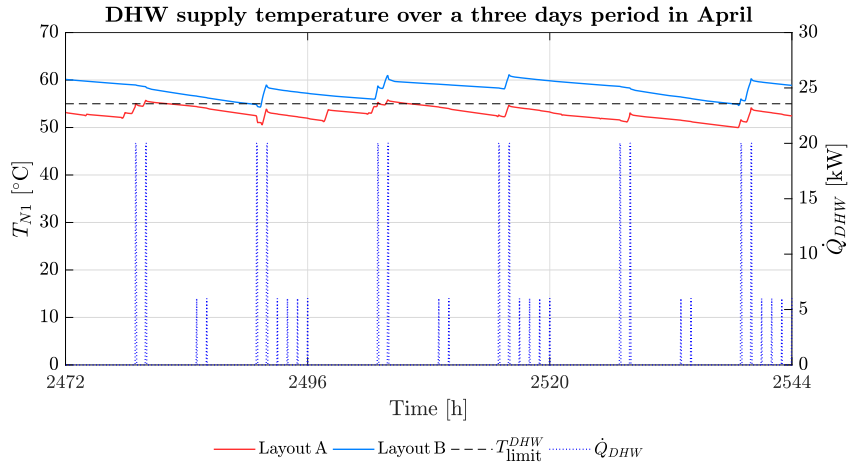


Figure 4.11: Comparison of the DHW supply temperature observed in Layout A and in Layout B, on the left-hand side of the y -axis, and draw-offs power, on the right-hand side of the y -axis, over a three days period in April.

The observed system behaviour can be explained by comparing the tank temperature distribution over the considered nodes (T_{N1} , T_{N5} and T_{N10}), in the two configurations, shown in Fig. 4.12 on the following page, for Layout A, and in

Fig. 4.13, for Layout B. As regards the former configuration, the connection of the space heating loop with the tank, by means of the port located in the middle node, has a strong influence on the top and bottom node temperatures. In fact, with the adopted set-point temperature for the DHW and with the employed geometrical configuration (volume and height) of the tank, during the DHW mode, the mass flow rate circulating in the port for the SH loop is always influencing the thermal stratification of the tank, preventing the top node temperature from reaching the required set-point value, within the time interval established by DHW schedule. However, in Layout B, since the tank is employed for DHW purposes only, the disturbance on the tank thermal stratification is represented only by the draw-offs and by the thermal losses, allowing the top node temperature to remain close to the required set-point for a longer time.

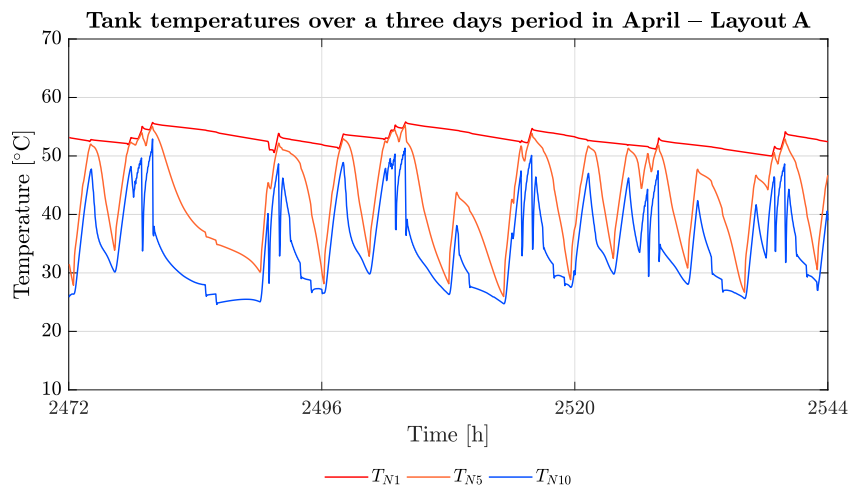


Figure 4.12: Tank temperatures observed in Layout A, over a three days period in April.

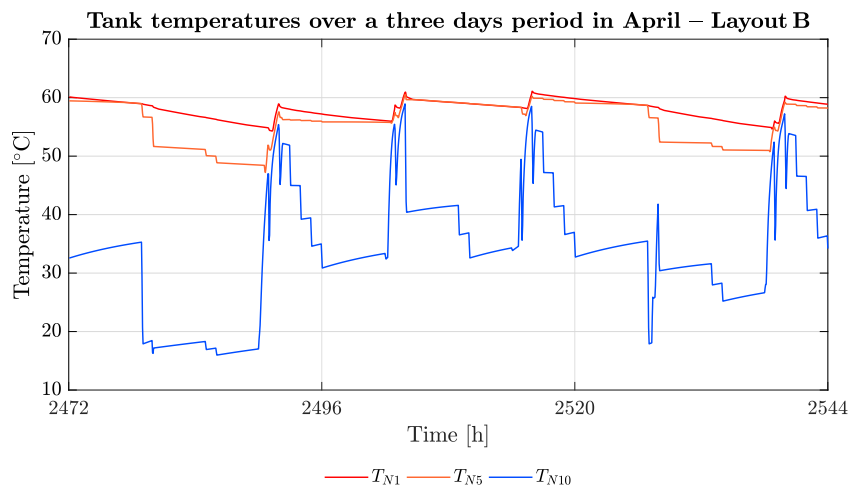


Figure 4.13: Tank temperatures observed in Layout B, over a three days period in April.

In Fig. 4.14 and Fig. 4.15 on the facing page, the required supplied temperature and the load temperature are shown, respectively, for the two layouts, in the considered period of three days in April. From the former, it can be noticed, once

4.2. Layout comparison over the heating season

again, the shorter duration of the DHW mode in Layout B, with respect to that observed in Layout A. Whereas, from the latter, it is possible to distinguish the different behaviour of the heating system during the DHW mode and the SH mode, given the corresponding different temperature levels. To this end, the average COP values of the heat pump have been reported in Tab. 4.3 on the next page, according to the operating mode of the heating system.

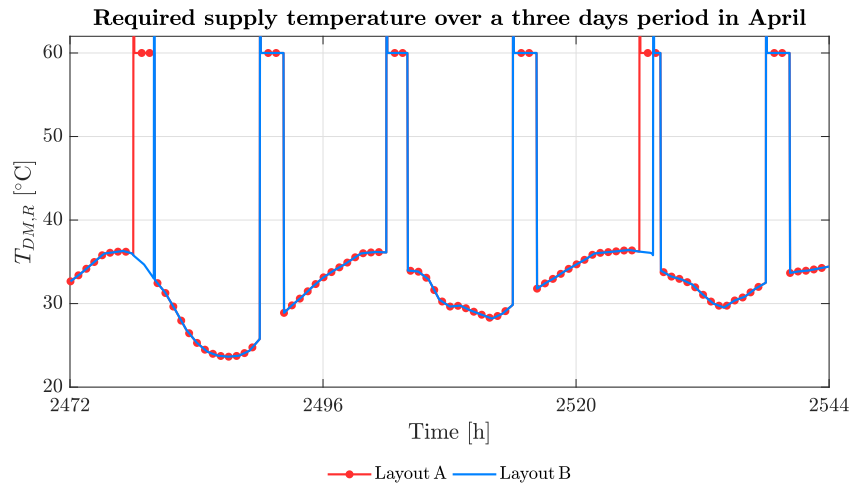


Figure 4.14: Comparison of the required supply temperature observed in Layout A and in Layout B, over a three days period in April.

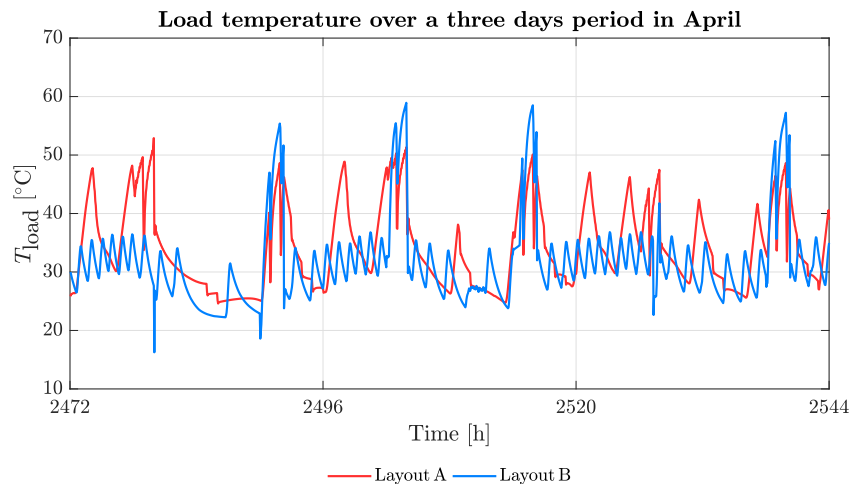


Figure 4.15: Comparison of the load temperature observed in Layout A and in Layout B, over a three days period in April.

More specifically, during the DHW mode, the HP is operating with a lower average COP in Layout B, due to a higher load temperature – for the above-mentioned reasons – with respect to the observed behaviour in Layout A. Conversely, during the SH mode, the HP has a better performance in Layout B rather than in Layout A. However, if no distinction is made between the two operating modes, the overall average COP values are quite similar.

Table 4.3: Average COP comparison between Layout A and Layout B, over the test months of the heating season, according to the operating mode of the heating system.

Parameter	Unit	Operating mode	October		January		April	
			A	B	A	B	A	B
COP_{avg}	-	DHW	3.14	2.34	3.32	2.39	3.17	2.42
		SH	3.50	4.04	2.96	3.22	3.52	4.09
		DHW+SH	3.35	3.38	3.06	3.11	3.33	3.42

As a final remark, the achieved energy saving in Layout B, with respect to Layout A, is mainly due to the lower duration, in the former, of the DHW mode, in which the HP has a lower performance given the higher load temperature. Indeed, if the storage tank is employed for DHW purposes only, it is possible to better exploit its thermal inertia, allowing the HP to work for a longer time in SH mode, with a lower load temperature and, thus, with a higher performance. On the other hand, without the thermal inertia provided by the tank during the SH mode, combined with the supply temperature adjustment through the PI controller – as explained in the second chapter –, frequent oscillations of the room temperature are experienced in Layout B, with a consequent reduction, even though restrained, of the indoor thermal comfort conditions. More importantly, the frequent on/off cycles have a negative impact on the life of the HP components. Therefore, in order to overcome this issue, a possible solution might be the employment of a variable-speed heat pump, whose capacity is modulated by acting on the compressor frequency, as explained in the literature review.

Subsequently, the simulations have been performed considering the real solar radiation values. As shown in Fig. 4.16 and Fig. 4.17 on the facing page, the obtained SPF values and the performance variation, obtained in Layout B with respect to Layout A, are similar to those observed when assuming constant values of the solar radiation. In fact, as one can expect, the solar energy contribution has the same impact on both system layouts. However, as illustrated in Fig. 4.18 on the next page and in Fig. 4.19 on page 76, the solar radiation influence is much more significant on the thermal comfort performance of the two system layouts, rather than on their energy performance. In particular, the percentage variation of the SH comfort time is more important in the month of April rather than in January, as one can expect, given the longer duration of the daylight in the former. This behaviour can be explained by considering that the control logic of the heating system is based on the required supply temperature value provided by the heating curve, which is dependent on the outdoor temperature only. Therefore, the controller has no information about the solar radiation, which can be a significant external gain for the building and have a huge impact on the room temperature stability, with possible overheating of the indoor environment and a consequent reduction of the thermal comfort conditions.

4.2. Layout comparison over the heating season

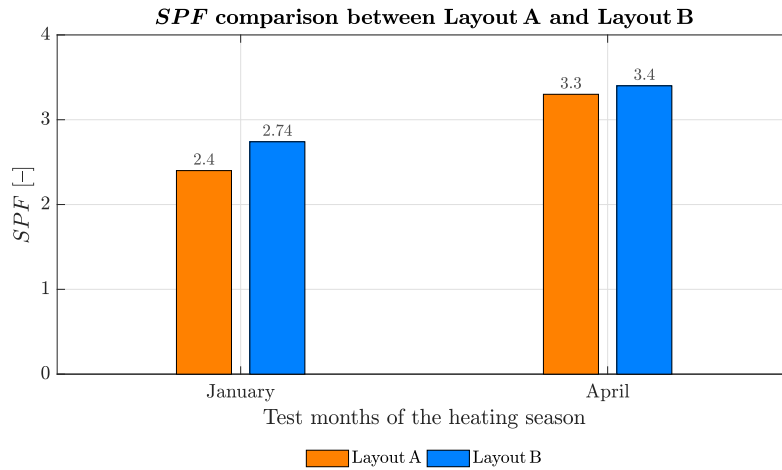


Figure 4.16: *SPF* comparison between Layout A and Layout B, over the test months of the heating season, with real solar radiation values.

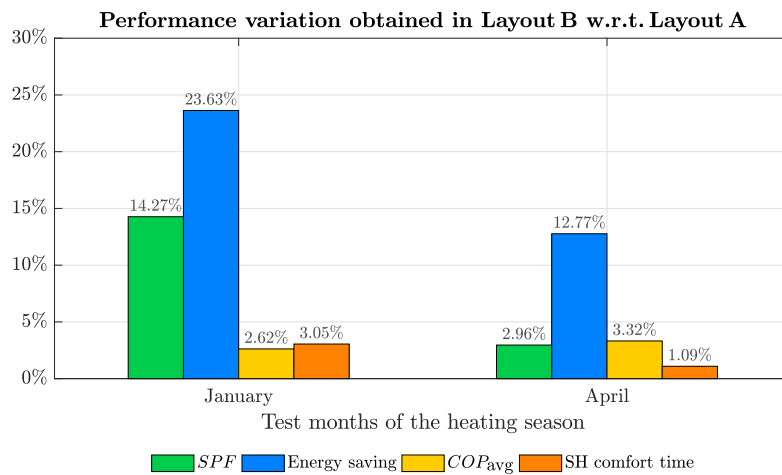


Figure 4.17: Performance variation observed in Layout B with respect to Layout A, over the test months of the heating season, with real solar radiation values.

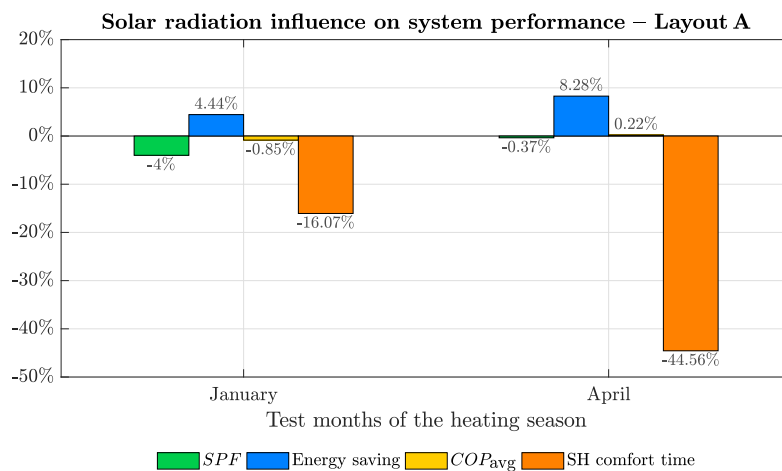


Figure 4.18: Solar radiation influence on the heating system performance, observed in Layout A, over the test months of the heating season.

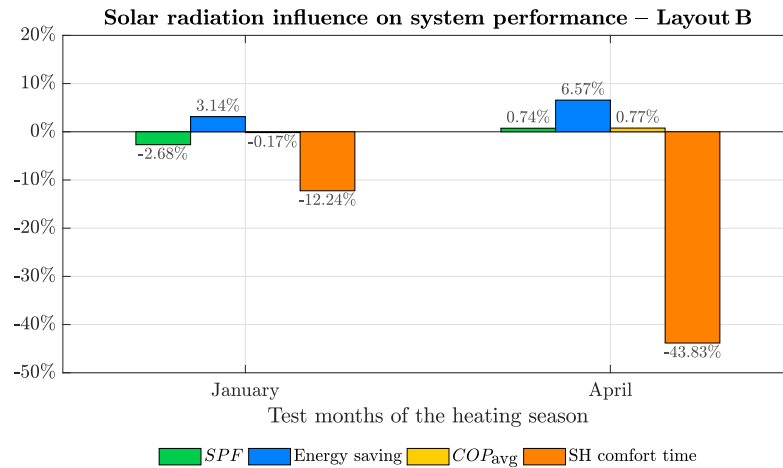


Figure 4.19: Solar radiation influence on the heating system performance, observed in Layout B, over the test months of the heating season.

4.3 Internal gains

The present section reports the results obtained from the application, in Layout B, of the improved control logic based on the internal gains profile. As explained in section 3.4, different tests have been performed, characterized by different corrective coefficients for the heating curve modulation, assuming constant values of the solar radiation. The analyses have been carried out over the test months of January and April, selecting, eventually, the best performing test for each of the two considered criteria – i.e. the Energy mode and the Comfort mode. More specifically, the selection has been made also considering the obtained SPF values, reported in Fig. 4.20, for the month of January, and in Fig. 4.21 on the facing page, for the month of April, where the SPF achieved with the basic control logic is shown as well.

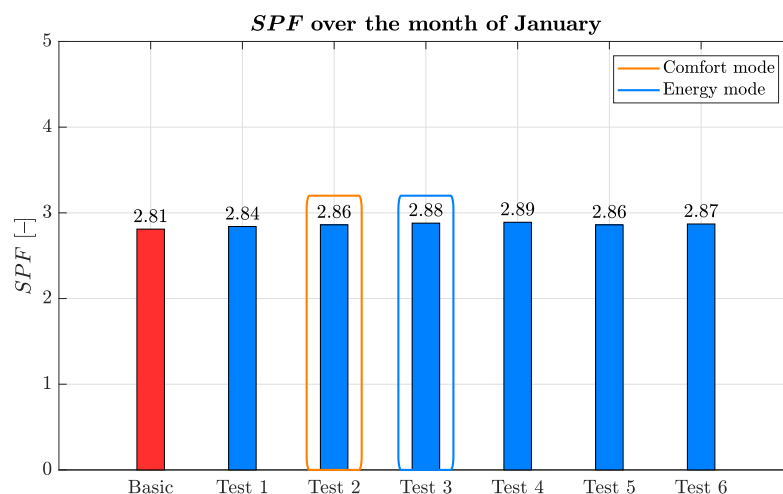


Figure 4.20: Comparison of the SPF values obtained in the base case and in the performed tests, over the month of January. The best performing tests, for the Energy mode and for the Comfort mode, are highlighted.

4.3. Internal gains

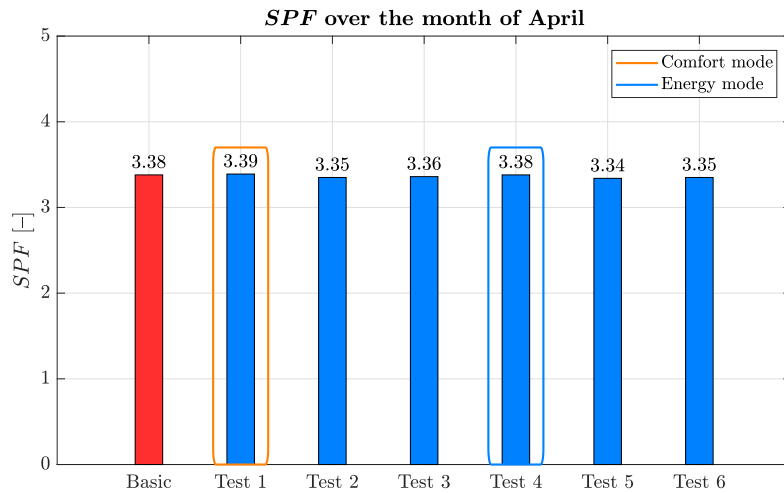


Figure 4.21: Comparison of the SPF values obtained in the base case and in the performed tests, over the month of April. The best performing tests, for the Energy mode and for the Comfort mode, are highlighted.

For each of the performed tests, the corresponding energy saving and indoor thermal comfort variation, with respect to the base case, are reported in Fig. 4.22, for the month of January, and in Fig. 4.23 on the following page, for the month of April. For the selection of the best performing tests, only those yielding an increase of the SPF have been considered. Subsequently, according to a good performance in terms of both energy saving and thermal comfort enhancement, the selected tests for the Energy mode and the Comfort mode, respectively, are Test 2 and Test 3, for the month of January, and Test 1 and Test 4, for the month of April.

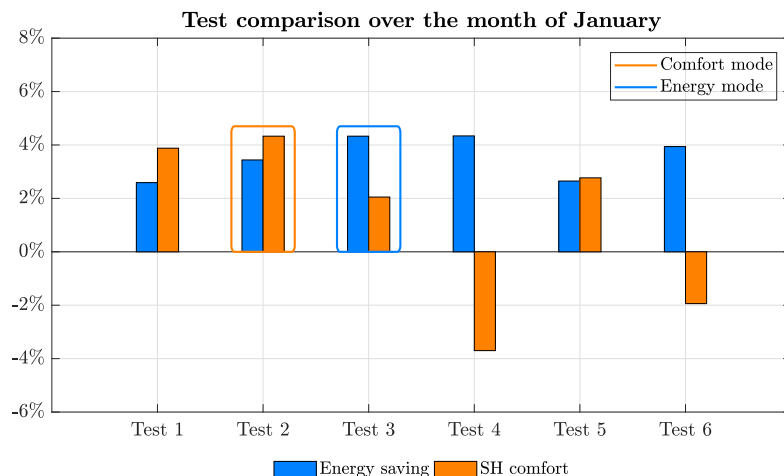


Figure 4.22: Comparison of the performed tests in terms of energy saving and indoor thermal comfort variation, with respect to the base case, over the month of January. The best performing tests, for the Energy mode and for the Comfort mode, are highlighted.

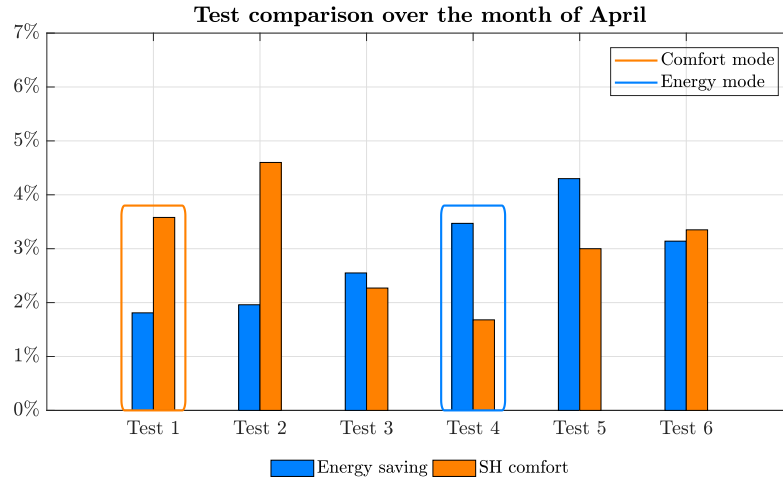


Figure 4.23: Comparison of the performed tests in terms of energy saving and indoor thermal comfort variation, with respect to the base case, over the month of April. The best performing tests, for the Energy mode and for the Comfort mode, are highlighted.

The corrective coefficients of the chosen tests can be found in Tab. 3.5 on page 57, while their corresponding performance variation with respect to the base case is reported, for both the Energy mode and the Comfort mode, in Tab. 4.4, for the month of January, and in Tab. 4.5 on the next page, for the month of April. As a remark, the values of the performance parameters related to the base case, and achieved in Layout B, can be found in Tab. 4.2 on page 69.

The negative variation of the total electrical energy consumption and the positive one of the SH comfort time outline the possibility to obtain a better performance of the heating system. In fact, the control improvement compensates for the overheating of the indoor environment, deriving from the internal heat release, by reducing the required supply temperature for the space heating, and thus reducing the compressor energy consumption and the usage of the electrical auxiliary heater, while enhancing the thermal comfort conditions. It is worth outlining that, for the month of April, the AH is never switched on, both in the base case and in the one with the improved control logic (see also Tab. 4.2 on page 69).

Table 4.4: Obtained performance variation with respect to the base case, with the selected tests for the Energy mode and the Comfort mode, for the month of January.

Parameter	Variation w.r.t. the base case [%]	
	Energy mode	Comfort mode
E_{AH}	-15.43	-10.55
E_{tot}	-4.33	-3.44
SH comfort time	2.05	4.33
SPF	2.21	1.68

4.3. Internal gains

Table 4.5: Obtained performance variation with respect to the base case, with the selected tests for the Energy mode and the Comfort mode, for the month of April.

Parameter	Variation w.r.t. the base case [%]	
	Energy mode	Comfort mode
E_{AH}	0	0
E_{tot}	-3.47	-1.81
SH comfort time	1.68	3.58
SPF	0.15	0.41

As a final remark, and as already shown in the layout comparison, since the heating curve is dependent on the outdoor temperature only, if the real solar radiation were considered for the HC modulation, it would have a very low impact on the energy performance of the system, but it would significantly reduce the indoor thermal comfort.

The above described results have been obtained adopting a non-predictive approach in the improved control logic. Subsequently, the system behaviour has been investigated, considering the Energy mode and the Comfort mode criteria separately, when a prediction horizon of one hour and two hours is employed for the elaboration of the internal gains profile. To this end, the same corrective coefficients in Tab. 3.5 on page 57 have been used for the performed tests, comparing the obtained variations with respect to the base case.

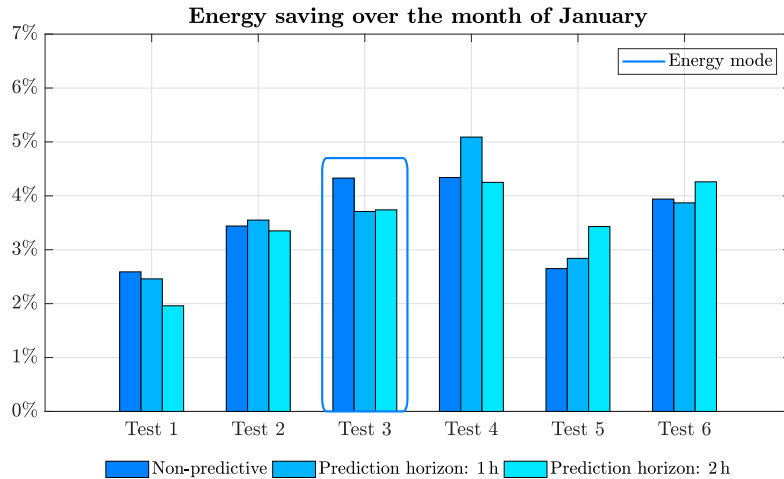


Figure 4.24: Energy saving obtained in the performed tests, with respect to the base case, adopting different prediction horizons of the internal gains profile, over the month of January. The selected test for the Energy mode is highlighted.

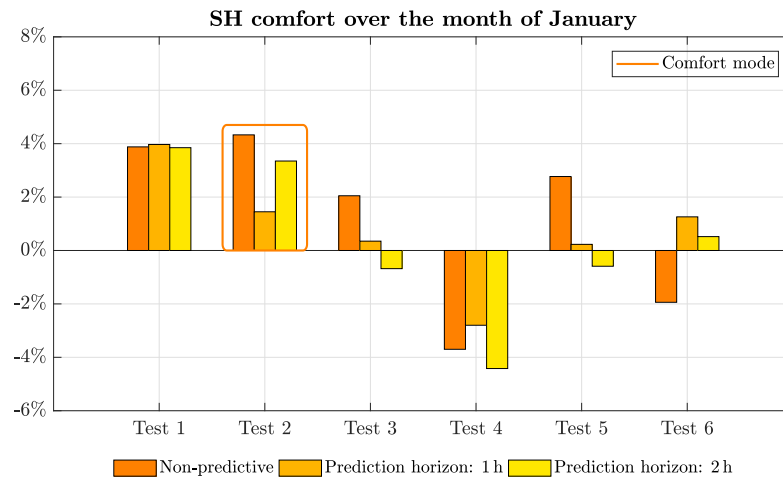


Figure 4.25: Indoor thermal comfort variation obtained in the performed tests, with respect to the base case, adopting different prediction horizons of the internal gains profile, over the month of January. The selected test for the Comfort mode is highlighted.

The obtained results in the month of January are reported, in Fig. 4.24 on the previous page, regarding the energy saving, and in Fig. 4.25, concerning the SH comfort time. While the results achieved in the month of April are shown, in the same order, in Fig. 4.26 and in Fig. 4.27 on the facing page.

According to the obtained values, the overall energy saving is approximately unchanged, still in the range of 1–4%, given the positive gain represented by the internal heat release, and the consequent reduction of the required supply temperature and of the total electrical energy consumption. However, the SH comfort time shows an overall negative variation with respect to the observed behaviour when the non-predictive logic is employed.

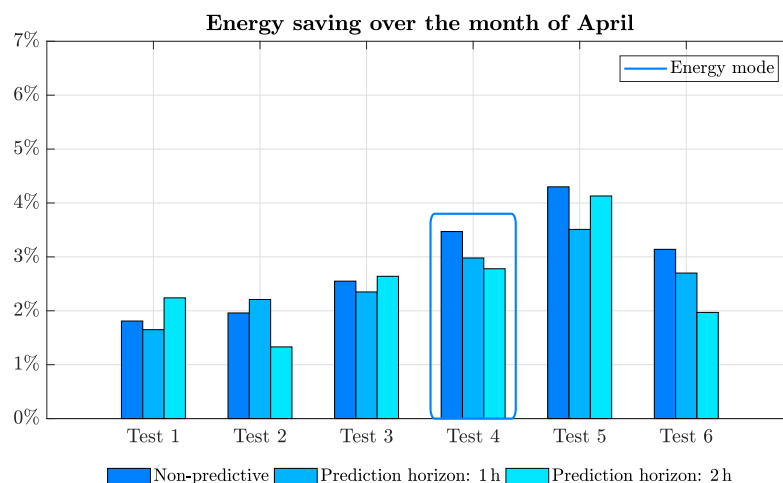


Figure 4.26: Energy saving obtained in the performed tests, with respect to the base case, adopting different prediction horizons of the internal gains profile, over the month of April. The selected test for the Energy mode is highlighted.

4.3. Internal gains

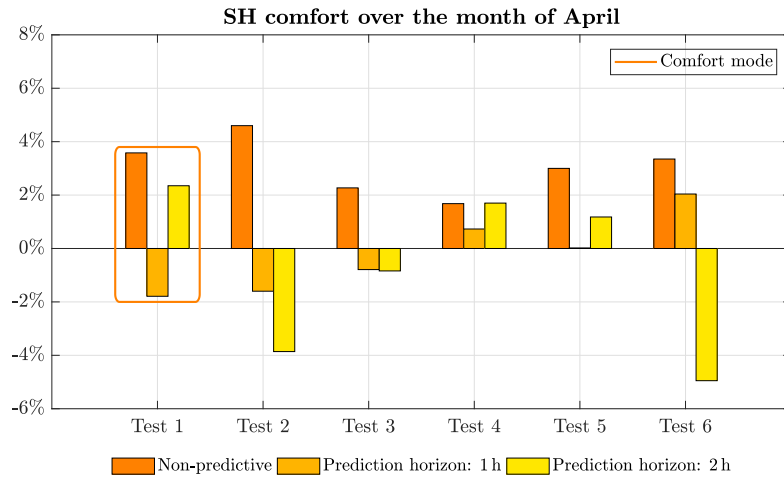


Figure 4.27: Indoor thermal comfort variation obtained in the performed tests, with respect to the base case, adopting different prediction horizons of the internal gains profile, over the month of April. The selected test for the Comfort mode is highlighted.

The observed behaviour can be explained by considering the linear correlation reported in Eq. (3.6), between the magnitude of the internal gains and the correction applied to the heating curve. Due to the negative slope, an energy saving is always present for all the performed tests, either using a non-predictive or a predictive approach. However, as concerns the indoor thermal comfort, when the improved control logic is applied with a prediction horizon of one or two hours, the required supply temperature for the SH is corrected according to the amount of the forecast internal gains, but still considering the actual outdoor temperature. Therefore, the improved control logic based on a non-predictive approach leads to better results in terms of indoor thermal comfort.

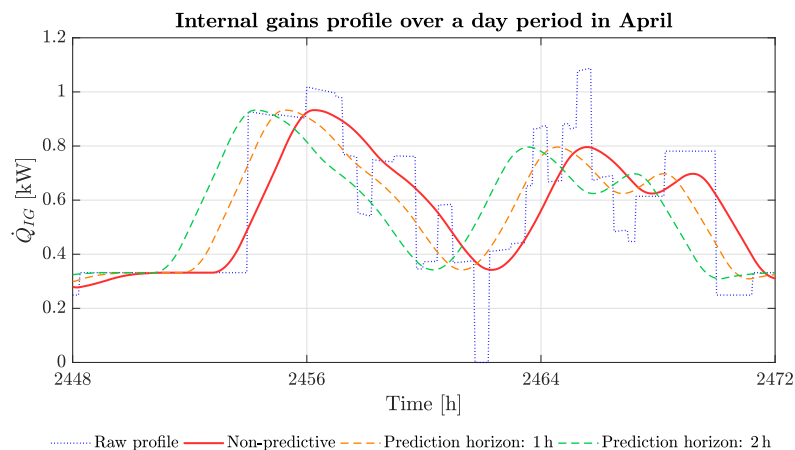


Figure 4.28: Original and filtered profiles of the internal heat gains, adopting different prediction horizons, over a day period in April.

In conclusion, the internal gains profile, over a day period in April, is shown in Fig. 4.28, for the three considered cases, together with the original raw profile. Whereas, Fig. 4.29 on the following page illustrates, for the same day of April, the

indoor temperature reduction obtained when the non-predictive improved control logic is applied, in comparison with the case when the basic controller is used.

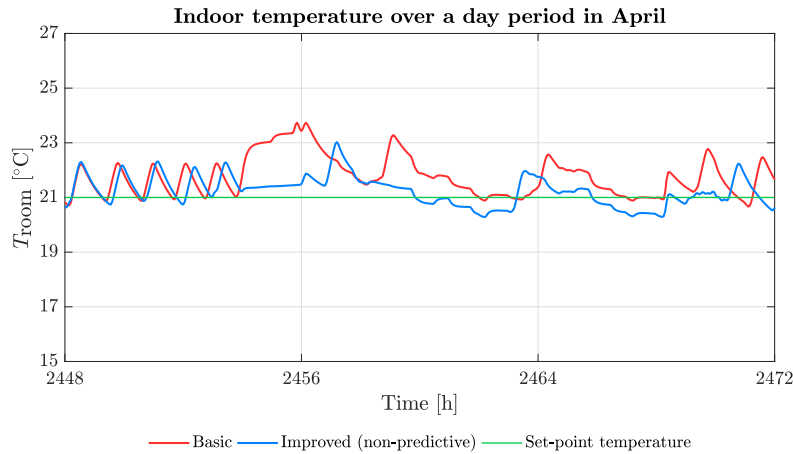


Figure 4.29: Comparison of the indoor temperature observed in the base case and with the improved control logic, adopting a non-predictive approach, over a day period in April.

4.4 Solar radiation and complete system model

The present section shows the results achieved by means of the combined implementation of all the described control strategies, considering also the heating curve modulation based on the solar radiation contribution. The procedure explained in section 3.5 and in section 3.6 has been followed.

The potential energy saving and the thermal comfort enhancement, obtained thanks to the improved control logic based on the solar radiation data, and already shown in [1], can be further increased if the HC correction is applied after sunset as well, when the thermal energy stored by the building, during the day, is released into the indoor environment, causing a reduction of the thermal comfort. To this end, the HC modulation after sunset has been applied considering different time intervals for its duration, over the test month of March, which is characterised by different irradiation magnitudes along with low ambient temperature values.

The obtained results are reported in Fig. 4.30 on the next page, which illustrates the energy saving and the indoor thermal comfort variation, achieved with the HC correction after sunset and adopting different values of Δt_+ , with respect to the observed behaviour when the correction is applied only until the sundown. The best performance, in terms of both energy saving and SH comfort time, is achieved with a time interval of two hours.

Subsequently, the performance of the complete system model, based on the combination of all the improved control logics, has been compared with the one achieved when the basic on/off controller is employed. In particular, the DHW schedule with a prediction horizon of three hours has been adopted within the control logic, together with the parameters reported in Tab 3.7 on page 62.

4.4. Solar radiation and complete system model

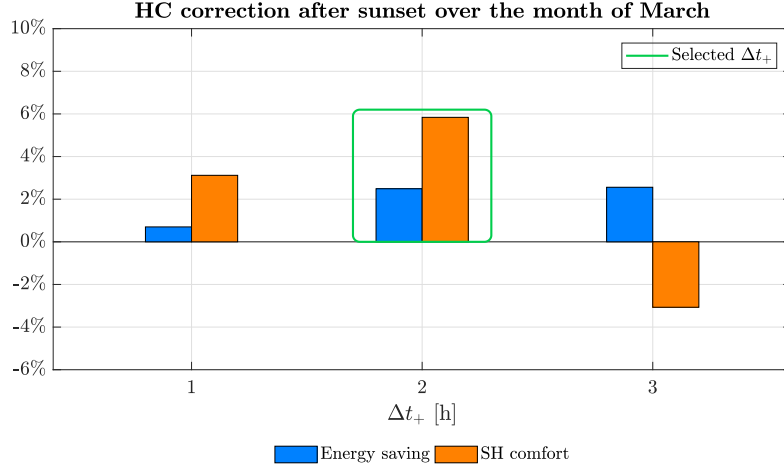


Figure 4.30: Energy saving and indoor thermal comfort variation obtained with the HC correction after sunset, adopting different values of Δt_+ , over the test month of March.

The obtained results, reported in Tab. 4.6, reveal an increase of the SPF and a significant reduction of the DBD_{SH} and DBD_{DHW} parameters, with respect to the base case. Moreover, Tab. 4.7 on the following page shows the increment of the average COP , achieved with the combined control logics, according to the operating mode of the system. The increased DHW comfort is obtained thanks to the employed control logic for the DHW heating and considering that, in the base case, the heating system is operating alternately between DHW mode and SH mode, from 6 a.m. to 8 p.m., with a cycling period of thirty minutes, while it operates only in SH mode for the rest of the time. Regarding the enhanced indoor thermal comfort, as can be seen from the lower average indoor temperature and its corresponding lower standard deviation, the achieved improvement is especially due to the HC modulation based on the solar radiation data.

Table 4.6: Comparison of the simulation results obtained with the basic controller and with the combined improved control logics, over the test month of March.

Parameter	Unit	Basic	Improved
SPF	–	3.10	3.26
SPF variation	%		5.35
DBD_{SH} variation	%		–81.32
DBD_{DHW} variation	%		–40.12
$T_{\text{room,avg}}$	°C	22.86	20.83
$T_{\text{room,STD}}$	°C	1.91	0.87
$T_{N1,avg}$	°C	57.79	57.25
$T_{\text{load,avg}}$	°C	41.58	39.45

Table 4.7: Comparison of the average COP values obtained with the basic controller and with the combined improved control logics, over the test month of March, according to the operating mode of the heating system.

Parameter	Unit	Operating mode	Basic	Improved
COP_{avg}	-	DHW	2.46	2.57
		SH	3.38	3.53
		DHW+SH	3.13	3.30

In Fig. 4.31 and in Fig. 4.32 on the facing page, it is possible to observe, over a day period in March, the obtained reduction of the indoor temperature and of the required supply temperature for the space heating, respectively, with respect to the corresponding trends experienced when the basic controller is employed. In particular, in both plots, a red circle highlights the further reduction of the indoor environment overheating and of the required supply temperature, obtained with the HC correction after sunset.

In conclusion, despite the frequent oscillations of the indoor temperature, by means of the combined application of the three described control strategies, it is possible to achieve an increased SPF of the heating system and a significant enhancement of the thermal comfort conditions.

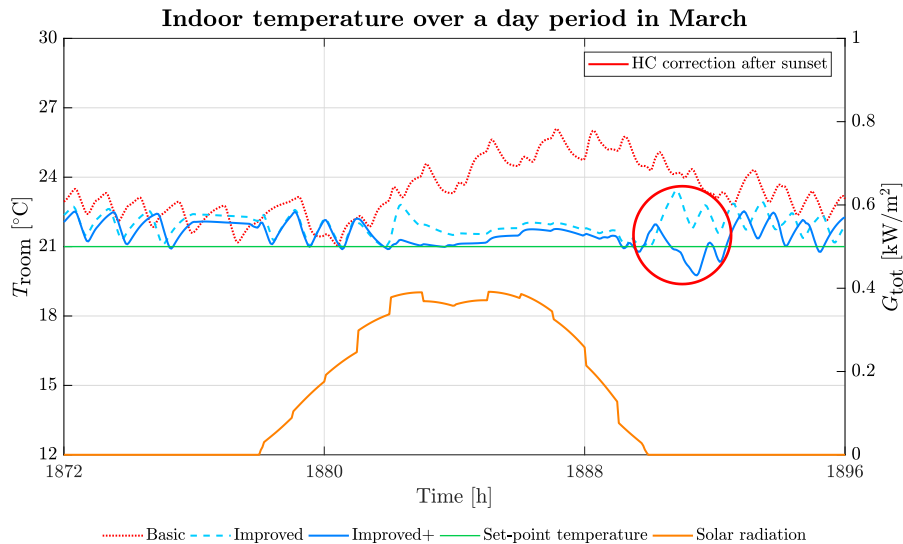


Figure 4.31: On the left-hand side of the y -axis: comparison of the indoor temperature observed in the base case, with the improved control logics and when also the HC correction after sunset is applied. On the right-hand side of the y -axis: total irradiance averaged on the building surfaces, over a day period in March.

4.4. Solar radiation and complete system model

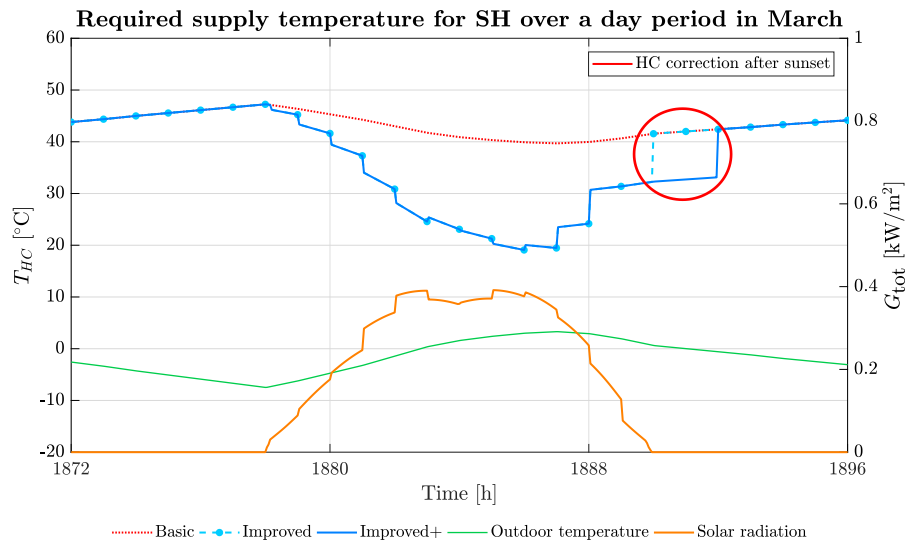


Figure 4.32: On the left-hand side of the y -axis: comparison of the required supply temperature for the space heating, observed in the base case, with the improved control logics and when also the HC correction after sunset is applied. On the right-hand side of the y -axis: total irradiance averaged on the building surfaces, over a day period in March.

Conclusions

The present work is focused on the implementation of smart control strategies applied to a GSHP system, for SH and DHW needs, in a Swedish single-family house. The study is carried out by means of numerical simulations in the TRNSYS[®] software environment. An existing system model (Layout A), developed by Braida and Tomasetig [1], which includes a typical Swedish building, a single-speed GSHP unit coupled with an electrical auxiliary heater, and a stratified storage tank, has been adapted to a different system layout (Layout B). More specifically, the latter is characterised by the direct connection between the heating generation loop and the space heating loop, employing the storage tank for DHW purpose only, differently from the original configuration, where it was used for SH needs as well. The aim of the study is the minimisation of the system energy consumption, while maximising the thermal comfort conditions for both DHW and SH. For the performance evaluation of the developed control strategies, a basic degree-minute on/off controller has been adopted as a benchmark. In particular, the reference controller assumes the heating curve approach for the computation of required supply temperature for the space heating, according to the outdoor temperature value.

After a performance comparison between the two system layouts, in terms of *SPF*, energy saving and thermal comfort, considering both the DHW supply temperature and the indoor temperature, three different rule-based control logics have been implemented, within Layout B, starting from the results achieved in [1]. In particular, they exploit the human behaviour and weather information in order to take into account the internal and external disturbances of the heating system, represented by the DHW consumption, by the internal heat release from people's activity and domestic lighting, and by the solar radiation contribution to the building heating. The control strategies have been applied adopting both a non-predictive and predictive approach, with the assumption of perfect prediction of the considered disturbances, which are provided to the model as input variables. At first, the improved control logic for the DHW heating has been developed, considering a fixed weekly profile of the water draw-offs, and it has been employed in both system layouts for their subsequent comparison over the heating season. Thereafter, the improved control logic that applies the HC correction, based on the internal heat gains, has been tested over the months of January and April, taking into account also the disturbance represented by the DHW consumption, but assuming constant values of the solar radiation. Afterwards, a further improvement has been applied to the control logic based on the solar radiation data, developed in [1], consisting in the HC modulation during a predetermined time interval after the

sunset, in order to compensate the overheating of the indoor environment observed at the end of the day. Eventually, the performance of the complete system model, based on the improved controller, which is characterised by the combination of all the described control logics, has been compared with the performance of the system model that employs the reference controller.

The control strategy for the DHW heating has been tested over the summer season, in order to avoid the influence of the SH request. With the employed parameters of the control logic and the adopted DHW set-point temperature during the Shower mode, the electrical AH is never switched on during the considered period. With respect to the basic controller, it is possible to achieve, over the whole summer season, an energy saving of about 9.3%, with a restricted increase of the DBD_{DHW} parameter.

According to the results obtained from the layout comparison, which has been carried out over the test months of October, January and April, the system model based on the configuration represented by Layout B shows an overall increase of the SPF and of the average COP , with respect to the observed values when Layout A is employed. In particular, the achieved energy saving is in the range of 11–12%, for the months of October and April, while it rises up to 22% in the cold month of January, where a reduction of about 62% is obtained for the AH energy consumption. In Layout B, the employment of the storage tank only for DHW purposes leads to a significant reduction of the DBD_{DHW} parameter of about 96–98%, and to a shorter duration of the DHW mode – with a consequent energy saving –, in which the HP is operating with lower COP values due to higher load temperatures, with respect to the SH mode. However, without the thermal inertia provided by the tank for the space heating, frequent oscillations of the indoor temperature are experienced when Layout B is employed, even though the comfort time during the SH mode is similar in both layouts, in the range of 83–88% of the total hours of the considered months.

The energy saving and the indoor thermal comfort enhancement, achievable with the improved control logic based on the internal gains profile, are in the range of 3.4–4.3%, when a non-predictive approach is used. The latter yields a better performance in terms of indoor thermal comfort, with respect to the predictive logic. Indeed, according to the results obtained from the performed tests, when a prediction horizon of one hour and two hours is employed, in the forecasting of the internal gains, a reduced SH comfort time is experienced, even though an energy saving is always present, in the range of 1–4%.

Moreover, the improvement of the control logic based on the solar radiation data, by means of the HC correction after sunset, leads to an energy saving of 2.5% and to an increase of the SH comfort time of about 5.8%, with respect to the case when the HC correction is applied only until the sundown.

In conclusion, from the simultaneous application of all the described control logics in the complete system model, with respect to the performance of the basic controller, it is possible to achieve an overall 5.4% increase of the SPF and a reduction of 81% and 40% of the DBD_{SH} and DBD_{DHW} parameters, respectively.

Possible future developments

Considering the heating system configuration represented by Layout B, a possible future development of the presented work can be identified, in order to achieve a further improvement of the system performance. In particular, the observed recurring oscillations of the indoor temperature are caused by the frequent on/off cycles of the HP, with a negative impact on the life of its components and on the indoor thermal comfort conditions. Therefore, in order to overcome this issue, a possible solution might be the employment of a variable-speed heat pump, whose capacity is modulated by acting on the compressor frequency, as explained in the literature review. The development of a suited control system model for a variable-speed HP, integrated with the described control strategies, might lead to a further potential energy saving and, more importantly, to a reduced compressor cycling region, with a consequent improved life of the HP components and an increased stability of the indoor temperature.

Appendix A

Adopted scripts

The present appendix reports the adopted scripts for the creation of several profiles of input data, employed within the TRNSYS[®] system model, and for the elaboration of some of the obtained results. In particular, they have been implemented in the VBA[®] and Matlab[®] environments.

A.1 VBA[®] scripts

All the following VBA[®] scripts have been used in the Excel[®] environment for the creation of different macros, in order to obtain as output a data file (".dat") containing the desired profiles over a week period.

By means of the following script [A.1](#), it is possible to obtain the stochastic occupancy profile, employed for the computation of the internal heat release.

Script A.1: Creation of the occupancy profile.

```
1 Attribute VB_Name = "OccScheduleExport"
2 Sub OccScheduleExport()
3     Dim hnd As Long, out As String
4     Dim i As Integer, k As Double
5     Dim fileName As String
6     Dim lastRow As Long
7
8     fileName = ActiveWorkbook.Path & "\" & "Occupancy_week_5min.dat"
9
10    lastRow = shOcc.Cells(shOcc.Rows.Count, "F").End(xlUp).row
11
12    hnd = FreeFile
13    Open fileName For Output As hnd
14
15    'Write #hnd, out
16    For i = 2 To lastRow
17        out = shOcc.Cells(i, "F")
18        If i <> lastRow Then
19            Print #hnd, out
20        Else
21            Print #hnd, out;
22        End If
23
24        k = k + 1
25    Next i
26    'DoEvents
27    Close hnd
28
29
```

```

30     MsgBox CStr(k) & " values written to " & fileName
31
32 End Sub

```

With the following script [A.2](#), instead, it is possible to obtain the DHW schedule, employed in the improved control logic for the DHW heating.

Script A.2: Creation of the DHW schedule.

```

1  Attribute VB_Name = "DHWScheduleExport"
2  Sub DHWScheduleExport()
3      Dim hnd As Long, hnd2 As Long, out As String, out2 As String
4      Dim i As Integer, j As Integer, k As Double
5      Dim kW As Double, H As Double
6      Dim fileName As String, fileName2 As String
7      Dim lastRow As Long, earlyRow As Integer, r As Range, earlyH As Double
8
9      fileName = ActiveWorkbook.Path & "\" & "DHWSchedule.dat"
10     fileName2 = ActiveWorkbook.Path & "\" & "DHWSchedule_slide.dat"
11
12     lastRow = shDHW.Cells(shDHW.Rows.Count, "E").End(xlUp).row
13
14     'Create Slide profile
15     Set r = shDHW.Range("D" & 2 & ":D" & lastRow)
16     earlyH = shDHW.Range("A5")
17     earlyRow = WorksheetFunction.Match(earlyH, r, 1) + 1
18
19     j = 2
20     For i = earlyRow To lastRow
21         shDHW.Cells(j, "F") = shDHW.Cells(i, "E")
22         j = j + 1
23     Next
24     For i = 2 To earlyRow - 1
25         shDHW.Cells(j, "F") = shDHW.Cells(i, "E")
26         j = j + 1
27     Next i
28
29     hnd = FreeFile
30     Open fileName For Output As hnd
31     hnd2 = FreeFile
32     Open fileName2 For Output As hnd2
33     'Write #hnd, out
34     For i = 2 To lastRow
35         out = shDHW.Cells(i, "E")
36         out2 = shDHW.Cells(i, "F")
37         If i <> lastRow Then
38             Print #hnd, out
39             Print #hnd2, out2
40         Else
41             Print #hnd, out;
42             Print #hnd2, out2;
43         End If
44
45         k = k + 1
46     Next i
47     'DoEvents
48     Close hnd
49     Close hnd2
50
51
52     MsgBox CStr(k) & " values written to " & fileName
53
54 End Sub

```

Finally, the profile of the thermal power related to the water draw-offs is at first generated with the script [A.3](#) on the next page, and then it is written into a data file by means of the script [A.4](#) on the facing page.

Script A.3: Generation of the water draw-offs profile.

```

1 Attribute VB_Name = "GenerateDHWprofile1min"
2 Sub GenerateDHWProfile1min()
3     Dim i As Integer, j As Integer, k As Integer
4     Dim peak As Double, kWreq As Double, kW As Double
5     Dim H0 As Integer, E0 As Double
6     Dim H1 As Double, E1 As Double
7     Dim row As Integer, row0 As Integer, r As Range, r1 As Range
8
9     peak = 20 '20 kW max peak allowed
10
11     shDraw.Range("N2") = 0
12     shDraw.Range("N2").Copy
13     shDraw.Range("N3:N3362").PasteSpecial xlPasteValues
14
15
16     For i = 2 To 170
17         H0 = shDraw.Cells(i, 4)
18         E0 = shDraw.Cells(i, 5)
19         E1 = 0
20         If E0 > 0 Then
21             Set r = shDraw.Range("M2:M3362")
22             row = WorksheetFunction.Match(H0 + 1, r, 0) + 1
23             row0 = WorksheetFunction.Match(H0, r, 0) + 1
24
25             Set r1 = shDraw.Range("O" & row0 & ":O" & row)
26
27             H1 = shDraw.Cells(row, "M")
28
29             'Fill "power" in the H1 hour to match E0
30
31             j = row - 1
32
33             While Abs(E1 - E0) / E0 > 0.1
34
35                 kWreq = (E0 - E1) / (shDraw.Cells(j, "M") - shDraw.Cells(j - 1, "
36                     M"))
37
38                 If kWreq > peak Then
39                     kW = peak
40                 Else
41                     kW = kWreq
42                 End If
43
44                 shDraw.Cells(j, "N") = kW
45
46                 E1 = WorksheetFunction.Sum(r1)
47                 j = j - 1 'Going row up
48             Wend
49         End If
50     Next i
51
52 End Sub

```

Script A.4: Writing of the water draw-offs profile into an output data file.

```

1 Attribute VB_Name = "DHWProfileExport"
2 Sub DHWProfileExport()
3     Dim hnd As Long, out As String
4     Dim i As Integer, j As Integer, k As Double
5     Dim kW As Double, H As Double
6     Dim fileName As String
7     Dim lastRow As Long
8
9     fileName = ActiveWorkbook.Path & "\ & "DHWprofile.dat"
10
11     lastRow = shDraw.Cells(shDraw.Rows.Count, "O").End(xlUp).row
12
13     If 1 = 0 Then

```

```

14 out = ""
15 For i = 2 To 1441
16     out = out & vbCrLf & shDraw.Cells(i, "P")
17 Next
18
19 For i = 1 To 365
20     out = out & vbCrLf & out
21 Next i
22 End If
23
24 hnd = FreeFile
25 Open fileName For Output As hnd
26
27 'Write #hnd, out
28 For j = 168 To 8736 Step 168
29     For i = 2 To 3361
30         H = shDraw.Cells(i, "M") + 168 * ((j - 168) / 168)
31         out = shDraw.Cells(i, "N") & " " & H
32         out = Replace(out, ",", ".")
33
34         If i = lastRow And j = 8736 Then
35             Print #hnd, out; 'avoid last empty line
36         Else
37             Print #hnd, out
38         End If
39
40         k = k + 1
41
42     Next i
43
44 Next j
45
46 For i = 2 To 481
47     H = shDraw.Cells(i, "M") + 8736
48     out = shDraw.Cells(i, "N") & " " & H
49     out = Replace(out, ",", ".")
50     If i = 1441 Then
51         Print #hnd, out; 'avoid last empty line
52     Else
53         Print #hnd, out
54     End If
55
56 Next i
57
58 k = k + 480
59
60 Close hnd
61
62 MsgBox CStr(k) & " values written to " & fileName
63
64 End Sub

```

A.2 Matlab[®] scripts

In the improved control logic for the DHW heating, the analyses have been carried out over the whole summer season. The corresponding simulation results have been elaborated with the following script [A.5](#).

Script A.5: Analysis of the simulation results over the summer season.

```

1 %% DHW summer analysis
2 clear
3 close all
4 clc
5
6 ts_h = 1/60;

```

A.2. Matlab® scripts

```
7 % Data Reading - BASIC
8 clc;
9 lines_to_skip = (3624-3600)/ts_h; % Lines skipped to avoid numerical convergence
    period
10
11 FileName = 'C:\Users\Utente\Documents\Marius\POLITO\2. Laurea Magistrale\Tesi (
    Ott 2016-Apr 2017)\Materiale Tesi\Lavoro Marius\1. DHW Mode\Excel Data\
    Simulation Results\DHW_Mode_Basic_out_Summer.txt';
12
13 A = importdata(FileName);
14 Data= A.data;
15
16 B.Time = Data(lines_to_skip:end,1);
17 B.T_node_1 = Data(lines_to_skip:end,2);
18 B.T_node_5 = Data(lines_to_skip:end,3);
19 B.T_node_10 = Data(lines_to_skip:end,4);
20 B.T_supply_HP = Data(lines_to_skip:end,5);
21 B.T_DM_req = Data(lines_to_skip:end,6);
22 B.DM = Data(lines_to_skip:end,7);
23 B.T_tank_avg = Data(lines_to_skip:end,8);
24 B.Schedule_cs = Data(lines_to_skip:end,9);
25 B.CS_shower = Data(lines_to_skip:end,10);
26 B.CS_HP = Data(lines_to_skip:end,11);
27 B.CS_AH_DHW = Data(lines_to_skip:end,12);
28 B.Q_HP_kW = Data(lines_to_skip:end,13);
29 B.P_HP_kW = Data(lines_to_skip:end,14);
30 B.COP = Data(lines_to_skip:end,15);
31 B.Q_AH_DHW_kW = Data(lines_to_skip:end,16);
32 B.Q_DHW_demand_kW = Data(lines_to_skip:end,17);
33 B.m_dot_DHW_actual_kgs = Data(lines_to_skip:end,18);
34 disp(['FileName ' has been imported. OK!']);
35
36 % Data reading - LOGIC
37 FileName = 'C:\Users\Utente\Documents\Marius\POLITO\2. Laurea Magistrale\Tesi (
    Ott 2016-Apr 2017)\Materiale Tesi\Lavoro Marius\1. DHW Mode\Excel Data\
    Simulation Results\DHW_Mode_Logic_out_Summer.txt';
38
39 A = importdata(FileName);
40 Data= A.data;
41
42 L.Time = Data(lines_to_skip:end,1);
43 L.T_node_1 = Data(lines_to_skip:end,2);
44 L.T_node_5 = Data(lines_to_skip:end,3);
45 L.T_node_10 = Data(lines_to_skip:end,4);
46 L.T_supply_HP = Data(lines_to_skip:end,5);
47 L.T_DM_req = Data(lines_to_skip:end,6);
48 L.DM = Data(lines_to_skip:end,7);
49 L.T_tank_avg = Data(lines_to_skip:end,8);
50 L.Schedule_cs = Data(lines_to_skip:end,9);
51 L.CS_shower = Data(lines_to_skip:end,10);
52 L.CS_HP = Data(lines_to_skip:end,11);
53 L.CS_AH_DHW = Data(lines_to_skip:end,12);
54 L.Q_HP_kW = Data(lines_to_skip:end,13);
55 L.P_HP_kW = Data(lines_to_skip:end,14);
56 L.COP = Data(lines_to_skip:end,15);
57 L.Q_AH_DHW_kW = Data(lines_to_skip:end,16);
58 L.Q_DHW_demand_kW = Data(lines_to_skip:end,17);
59 L.m_dot_DHW_actual_kgs = Data(lines_to_skip:end,18);
60 disp(['FileName ' has been imported. OK!']);
61
62 % Analysis
63 disp('Analysis started. ');
64 T_limi = 55;
65 dwo_indexes = find(B.Q_DHW_demand_kW>18);
66
67 % BASIC
68 E_compr_B = sum(B.P_HP_kW*ts_h); %kWh
69 E_ah_dhw_B = sum(B.Q_AH_DHW_kW/0.9*ts_h); %kWh
70 E_tot_B = E_compr_B + E_ah_dhw_B;
71
72 CPP_dwo_B_vect = zeros(1,length(B.T_node_1));
```

```

73 for i = 1: length(B.T_node_1)
74     if (B.T_node_1(i)<T_limi) && (B.Q_DHW_demand_kW(i)>18)
75         CPP_dwo_B_vect(i) = (T_limi-B.T_node_1(i))*ts_h*60;
76     end
77 end
78 CPP_dwo_B = sum(CPP_dwo_B_vect);
79
80 % IMPROVED
81 E_compr_L = sum(L.P_HP_kW*ts_h); %kWh
82 E_ah_dhw_L = sum(L.Q_AH_DHW_kW/0.9*ts_h); %kWh
83 E_tot_L = sum(E_compr_L + E_ah_dhw_L);
84
85 CPP_dwo_L_vect = zeros(1,length(L.T_node_1));
86 for i = 1: length(L.T_node_1)
87     if (L.T_node_1(i)<T_limi) && (L.Q_DHW_demand_kW(i)>18)
88         CPP_dwo_L_vect(i) = (T_limi-L.T_node_1(i))*ts_h*60;
89     end
90 end
91 CPP_dwo_L = sum(CPP_dwo_L_vect);
92 Tot_E_del_B = sum(B.Q_AH_DHW_kW)*ts_h+sum(B.Q_HP_kW)*ts_h;
93 Tot_E_del_L = sum(L.Q_AH_DHW_kW)*ts_h+sum(L.Q_HP_kW)*ts_h;
94 SPF_B = Tot_E_del_B/E_tot_B;
95 SPF_L = Tot_E_del_L/E_tot_L;
96
97 % Output
98 disp('Results - BASIC');
99 disp(['Compressor Energy consumption: ' num2str(E_compr_B) ' kWh']);
100 disp(['DHW Aux Heater Energy consumption: ' num2str(E_ah_dhw_B) ' kWh']);
101 disp(['Total El. Energy consumption: ' num2str(E_tot_B) ' kWh']);
102 disp(['Discomfort parameter (during draw-off): ' num2str(CPP_dwo_B) ' degree-
minute']);
103 disp(['SPF: ' num2str(SPF_B)]);
104
105 disp('Results - IMPROVED');
106 disp(['Compressor Energy consumption: ' num2str(E_compr_L) ' kWh']);
107 disp(['DHW Aux Heater Energy consumption: ' num2str(E_ah_dhw_L) ' kWh']);
108 disp(['Total El. Energy consumption: ' num2str(E_tot_L) ' kWh']);
109 disp(['Discomfort parameter (during draw-off): ' num2str(CPP_dwo_L) ' degree-
minute']);
110 disp(['SPF: ' num2str(SPF_L)]);
111
112 disp('Results - COMPARISON');
113 Energy_sav = (E_tot_L-E_tot_B)/E_tot_B*100;
114 Comfort = (CPP_dwo_B-CPP_dwo_L)/CPP_dwo_L*100;
115
116 disp(['Energy Saving: ' num2str(E_tot_L-E_tot_B) ' kWh']);
117 disp(['Energy Saving,%: ' num2str(Energy_sav) ' %']);
118 disp(['Comfort performance: ' num2str(Comfort) ' %']);
119
120 disp(['T_N_1 AVG BASIC: ' num2str(mean(B.T_node_1)) ' degC']);
121 disp(['T_N_1 MAX BASIC: ' num2str(max(B.T_node_1)) ' degC']);
122 disp(['T_N_1 MIN BASIC: ' num2str(min(B.T_node_1)) ' degC']);
123
124 disp(['T_N_10 AVG BASIC: ' num2str(mean(B.T_node_10)) ' degC']);
125 disp(['T_N_10 MIN BASIC: ' num2str(min(B.T_node_10)) ' degC']);
126
127 disp(['T_N_1 AVG LOGIC: ' num2str(mean(L.T_node_1)) ' degC']);
128 disp(['T_N_1 MAX LOGIC: ' num2str(max(L.T_node_1)) ' degC']);
129 disp(['T_N_1 MIN LOGIC: ' num2str(min(L.T_node_1)) ' degC']);
130
131 disp(['T_N_10 AVG LOGIC: ' num2str(mean(L.T_node_10)) ' degC']);
132 disp(['T_N_10 MIN LOGIC: ' num2str(min(L.T_node_10)) ' degC']);
133
134 disp('Analysis completed.');
```

The creation of the filtered profile of the internal gains, starting from the raw profile, has been carried out by means of the script [A.6](#) on the facing page.

A.2. Matlab® scripts

Script A.6: Creation of the smooth profile of the internal heat gains.

```
1 %%IG profile creation
2 clear
3 close all
4 clc
5
6 FileName = 'C:\Users\Utente\Documents\Marius\POLITO\2. Laurea Magistrale\Tesi (
    Ott 2016-Apr 2017)\Materiale Tesi\Lavoro Marius\2. DHW-SH Mode (IG - HC
    Modulation)\IG computation\Profile filtering\IG_8760_3min_stoch.txt';
7 lines_to_skip = 2;
8 A = importdata(FileName);
9 Data = A.data;
10 IG_P = Data(lines_to_skip:end,2);
11 IG_L = Data(lines_to_skip:end,3);
12 save('IG_data_8760_3min_stoch')
13
14 % Data processing
15 t_start = 0;
16 t_end = 8760;
17 ts = 0.05;
18 x_day = ts:ts:t_end;
19 x_vect = t_start/ts+1:t_end/ts;
20 IG_T_day = IG_P(x_vect)+IG_L(x_vect); %[kJ/h]
21
22 % AVG generation
23 avg_interval = 1; %h
24 IG_T_avg = [];
25 avg_ind = (avg_interval)/ts:avg_interval/ts:t_end/ts;
26 for i =2:length(avg_ind)
27     IG_T_avg = [IG_T_avg;mean(IG_T_day(avg_ind(i-1):avg_ind(i)))];
28 end
29 IG_T_avg = [IG_T_day(1); IG_T_avg];
30
31 %% Profile from data points
32 % This script generates a profile with a chosen time step from interpolating N
    points
33
34 % Input data
35 time_step = ts*60;
36 ord = 1; %Order of the polynomial interpolation
37
38 x = avg_ind*ts;
39 y = IG_T_avg;
40
41 % Initialization
42 N = length(x); %Total number of points in the imported data
43 x_d = (ts:ts:x(end))'; %Discrete x vector
44 y_d = []; %Discrete y vector
45 Nts = length(x_d); %Total number of time steps
46
47 % Polynomial coefficients matrix
48 p = [];
49 for j = 1:N-ord
50     p = [p; polyfit(x(j:j+ord)', y(j:j+ord),ord)];
51 end
52
53 % Discretized vector computation
54 x_d(1) = 0;
55 y_d(1) = y(1);
56 for i = 2:Nts
57     if not isempty(find(x==x_d(i), 1))
58         y_d = [y_d; mean(y(x==x_d(i)))];
59     else
60         ve_mag = find(x > x_d(i));
61         ve_low = find(x < x_d(i));
62         ve_int = find((x<min(x_d(i)+0.5,max(x_d))&(x>max(ts,x_d(i)-0.5)))); %fix
            NaN
63         if isempty(ve_low)
64             ve_low = 0;
65         end

```

```

66     if ve_low(end)>=1
67         y_d = [y_d; max(0,polyval(p(ve_low(end)),:),x_d(i))];
68     else
69         y_d = [y_d; y_d(end)];
70     end
71     if isempty(ve_int)
72         ve_int = ve_mag(1);
73     end
74 end
75 end
76 smooth_factor = 50;
77 IG_T_avg_filtered = y_d;
78 IG_T_smooth = smooth(IG_T_avg_filtered,smooth_factor);
79 %% File writing
80 Profile = IG_T_smooth;
81 fname = 'Week_test_avg1.txt';
82 fileId = fopen(fname,'w');
83 for i = 1:length(Profile)
84     fprintf(fileId,'%3.0f\r\n',Profile(i));
85 end
86 fclose(fileId);
87 disp('File writing completed!');
88 %% Energy comparison
89 en_orig = sum(IG_T_day)*ts/3600;
90 en_avg = sum(IG_T_avg_filtered)*ts/3600;
91 en_smooth = sum(IG_T_smooth)*ts/3600;
92 diff_avg = (en_avg-en_orig)/en_orig*100;
93 diff_smooth = (en_smooth-en_orig)/en_orig*100;
    
```

In conclusion, the following script [A.7](#) computes the hourly average values of the incident solar radiation over the five surfaces of the building, according to the Meteororm[®] data.

Script A.7: Creation of the hourly average profile of the solar radiation.

```

1  %% Radiation hourly avg values
2  clear
3  close all
4  clc
5
6  FileName = 'C:\Users\Utente\Documents\Marius\POLITO\2. Laurea Magistrale\Tesi (
7      Ott 2016-Apr 2017)\Materiale Tesi\Lavoro Altri\Giacomo Work\Data_trnsys\
8      Weather predictions\Annual weather from trnsys output.out';
9
10 A = importdata(FileName);
11 Data= A.data;
12
13 Rad_avg_HO = [];
14 Rad_avg_N = [];
15 Rad_avg_S = [];
16 Rad_avg_E = [];
17 Rad_avg_W = [];
18
19 for i=1:8760
20     Rad_avg_HO = [Rad_avg_HO; mean(Data((i-1)*20+1:i*20,3))]; %kJ/h/m^2
21     Rad_avg_N = [Rad_avg_N; mean(Data((i-1)*20+1:i*20,4))];
22     Rad_avg_S = [Rad_avg_S; mean(Data((i-1)*20+1:i*20,5))];
23     Rad_avg_E = [Rad_avg_E; mean(Data((i-1)*20+1:i*20,6))];
24     Rad_avg_W = [Rad_avg_W; mean(Data((i-1)*20+1:i*20,7))];
25 end
26 %% Save data
27 fileId = fopen('Rad_avg_Annual.txt','w');
28 n = 8760;
29 for i = 1:n
30     fprintf(fileId,'%3.2f\t%3.2f\t%3.2f\t%3.2f\t%3.2f\r\n',...
31         Rad_avg_HO(i),Rad_avg_N(i),Rad_avg_S(i),Rad_avg_E(i),Rad_avg_W(i));
32 end
33 fclose(fileId);
    
```

Bibliography

- [1] Giacomo Braida and Roberto Tomasetig. ‘Preliminary analysis of the potential energy saving achievable with a predictive control strategy of a heat pump for a single-family house’. Polytechnic University of Milan, 2017 (cit. on pp. IX, XI, 2, 21, 25, 26, 30, 31, 41, 42, 46, 55, 58, 82, 87).
- [2] European Environment Agency (EEA). <https://www.eea.europa.eu/signals/signals-2017/articles/energy-and-climate-change> (cit. on p. 1).
- [3] “International Energy Outlook 2017” – U.S. Energy Information Administration (EIA). [https://www.eia.gov/outlooks/ieo/pdf/0484\(2017\).pdf](https://www.eia.gov/outlooks/ieo/pdf/0484(2017).pdf) (cit. on pp. 1, 6).
- [4] Davide Rolando et al. ‘Heat pump system control: the potential improvement based on perfect prediction of weather forecast and user occupancy’. In: *12th IEA Heat Pump Conference, Rotterdam*. 2017 (cit. on p. 2).
- [5] “Energy efficiency indicators - Highlights” – IEA (2017). https://www.iea.org/publications/freepublications/publication/EnergyEfficiencyHighlights_2017.PDF (cit. on pp. 5–7).
- [6] “Directive 2010/31/EU of the European Parliament and of the Council of 19 May 2010 on the energy performance of buildings” – European Parliament Directive (2010). <https://eur-lex.europa.eu/LexUriServ/LexUriServ.do?uri=OJ:L:2010:153:0013:0035:EN:PDF> (cit. on p. 6).
- [7] “Heat Pumps Barometer” – EurObserv’ER (2016). <https://www.eurobserv-er.org/heat-pumps-barometer-2016/> (cit. on pp. 7, 8).
- [8] Burkhard Sanner et al. ‘Current status of ground source heat pumps and underground thermal energy storage in Europe’. In: *Geothermics* 32.4-6 (2003), pp. 579–588 (cit. on pp. 11, 12, 14).
- [9] Signhild Gehlin and Olof Andersson. ‘Geothermal energy use, country update for Sweden’. In: *European Geothermal Congress 2016, Strasbourg*. 2016 (cit. on p. 14).
- [10] Hatef Madani, Joachim Claesson, and Per Lundqvist. ‘Capacity control in ground source heat pump systems part II: Comparative analysis between on/off controlled and variable capacity systems’. In: *International Journal of Refrigeration* 34.8 (2011), pp. 1934–1942 (cit. on pp. 15–18, 34).

- [11] Giacomo Bagarella, Renato Lazzarin, and Marco Noro. ‘Sizing strategy of on–off and modulating heat pump systems based on annual energy analysis’. In: *International journal of refrigeration* 65 (2016), pp. 183–193 (cit. on pp. 16, 19).
- [12] Hatef Madani, Joachim Claesson, and Per Lundqvist. ‘A descriptive and comparative analysis of three common control techniques for an on/off controlled Ground Source Heat Pump (GSHP) system’. In: *Energy and Buildings* 65 (2013), pp. 1–9 (cit. on pp. 17, 19, 20, 43).
- [13] Fredrik Karlsson and Per Fahlén. ‘Capacity-controlled ground source heat pumps in hydronic heating systems’. In: *International Journal of Refrigeration* 30.2 (2007), pp. 221–229 (cit. on p. 18).
- [14] Giacomo Bagarella, Renato Lazzarin, and Biagio Lamanna. ‘Cycling losses in refrigeration equipment: An experimental evaluation’. In: *International Journal of Refrigeration* 36.8 (2013), pp. 2111–2118 (cit. on p. 19).
- [15] Frauke Oldewurtel et al. ‘Use of model predictive control and weather forecasts for energy efficient building climate control’. In: *Energy and Buildings* 45 (2012), pp. 15–27 (cit. on pp. 20, 21).
- [16] Jan Široký et al. ‘Experimental analysis of model predictive control for an energy efficient building heating system’. In: *Applied energy* 88.9 (2011), pp. 3079–3087 (cit. on p. 21).
- [17] Anthony R. Florita and Gregor P. Henze. ‘Comparison of short-term weather forecasting models for model predictive control’. In: *HVAC&R Research* 15.5 (2009), pp. 835–853 (cit. on p. 22).
- [18] Joakim Widén, Annica M Nilsson, and Ewa Wäckelgård. ‘A combined Markov-chain and bottom-up approach to modelling of domestic lighting demand’. In: *Energy and Buildings* 41.10 (2009), pp. 1001–1012 (cit. on pp. 22, 28, 29).
- [19] Aurore Lomet, Frédéric Suard, and David Chèze. ‘Statistical modeling for real domestic hot water consumption forecasting’. In: *Energy Procedia* 70 (2015), pp. 379–387 (cit. on p. 22).
- [20] Markus Sundbrandt. ‘Control of a ground source heat pump using hybrid model predictive control’. Linköping University, Automatic Control, 2011 (cit. on p. 23).
- [21] Bjarne W Olesen and KC Parsons. ‘Introduction to thermal comfort standards and to the proposed new version of EN ISO 7730’. In: *Energy and buildings* 34.6 (2002), pp. 537–548 (cit. on p. 23).
- [22] EPISCOPE and TABULA joint website. <http://episcope.eu/building-typology/country/se/> (cit. on p. 26).
- [23] Meteonorm website. <http://www.meteonorm.com> (cit. on p. 27).
- [24] The Engineering Toolbox – Metabolic Rate. https://www.engineeringtoolbox.com/met-metabolic-rate-d_733.html (cit. on p. 28).
- [25] S. Holst. *TRNSYS–Models for Radiator Heating Systems*. http://trnsys.de/download/en/ts_type_361_362_320_en.pdf (cit. on p. 40).